ELECTROSPINNING OF POLYCAPROLACTONE / BOVINE GELATIN / BOVINE HYDROXYAPATITE BIOMIMETIC COMPOSITE NANOFIBERS

by

Güneş Ece Akalın

B.S., Mechanical Engineering, Istanbul Technical University, 2014

Submitted to the Institute for Graduate Studies in
Science and Engineering in partial fulfillment of
the requirements for the degree of
Master of Science

Graduate Program in Mechanical Engineering

Boğaziçi University

2018

ACKNOWLEDGEMENTS

I would like to thank my advisors Prof. Sabri Altıntaş and Assoc. Prof. Hasan Bedir for their contributions to my academic development. During my studies, Prof. Sabri Altıntaş emphasizes the importance of nano scale for now and atomic scale for near future. The perspective has inspired me for this thesis.

I would also like to thank Prof. Gökhan Baykal, Assoc. Prof. B. Erdem Alaca and Assist. Prof. Gülin Vardar for accepting to be a member of my master's thesis defense committee.

I am grateful to my mother and my father.

ABSTRACT

ELECTROSPINNING OF POLYCAPROLACTONE / BOVINE GELATIN / BOVINE HYDROXYAPATITE BIOMIMETIC COMPOSITE NANOFIBERS

In this study, Polycaprolactone (PCL) / Bovine Gelatin (GE) / Bovine Hydroxyapatite (BHA) biomimetic composite nanofiber scaffolds are manufactured for bone tissue regeneration applications by electrospinning. By controlling BHA concentration and GE concentration in the polymer solutions, the effects of the changes on the manufacturing process and on the nanofiber scaffolds are determined. The physical, morphological, chemical, mechanical and biological properties of PCL/GE/BHA electrospun nanofibers are produced by choosing a non-toxic solvent system. Physical properties of nanofiber scaffolds are recorded by measuring density, viscosity, surface tension and electrical conductivity. Morphological analyses of the nanofiber scaffolds are studied in SEM. Chemical bonds of the nanofiber scaffolds are analyzed by FTIR. Mechanical properties of the scaffolds are determined by using tensile test. Biological properties of the nanofiber scaffolds such as cell viability and attachment are tested by MTT Proliferation Assay and SEM Protocol for 24, 48 and 72 hours. The results of the morphological analyses (SEM) show that the fiber diameters of the nanofiber scaffolds are 119 ± 31 nm, 149 ± 44 nm, 306 ± 68 nm, 241 ± 55 nm and 384 ± 84 nm respectively. The experimental results show that ultimate tensile strength (UTS) of the nanofiber scaffolds are 9.1 ± 0.6 MPa, 15.7 ± 1.4 MPa, 15.8 ± 5.0 MPa, 30.9 ± 16.0 MPa and 15.8 ± 2.3 MPa. Cell attachment and spreading on the samples are observed in SEM. There is no cytotoxicity effect observed by MTT test for 72 hours. As a result of cell proliferation and viability analysis, there are biocompatible samples observed compatible with human osteoblast-like cells and mouse fibroblast cells with statistically significant results.

ÖZET

ELEKTROSPINNING YÖNTEMİ İLE POLİKAPROLAKTON/ SIĞIR JELATİNİ/ SIĞIR HİDROKSİAPATİT KULLANILARAK BİYOMİMETİK KOMPOZİT NANOFİBER ÜRETİMİ

Bu çalışmada elekrospinning yöntemi ile polikaprolakton (PCL)/ sığır jelatini (GE)/ sığır hidroksiapatit (BHA) biyomimetik kompozit nanofiber iskeleleri, kemik doku onarımı uygulamalarında kullanılmak üzere üretilmiştir. Hazırlanan polimer çözeltilerindeki BHA konsantrasyon ve GE konsantrasyon değişiminin, üretim süreci ve nanofiberler üzerine olan etkileri incelendi. Yapılan deneylerde toksik etki yaratmayan çözücü sistemi seçilerek elektrospinnin yöntemi ile üretilmiş PCL/GE/BHA nanofiberlerin fiziksel, morfolojik, kimyasal, mekanik ve biyolojik özelliklerinin incelenmiştir. Üretim esnasında hazırlanan polimer çözeltilerinin fiziksel özellikleri yoğunluk, viskozite, yüzey gerilimi ve elektrik iletkenliği ölçülerek belirlenmiştir. Nanofiber doku iskelelerinin morfolojik analizleri Taramalı Elektron Mikroskobu (SEM) ile yapılmıştır. Elde edilen nanofiberlerin kimyasal bağları Fourier Dönüşümü Kızılötesi Spektroskopisi (FTIR) ile analiz edilmiştir. Üretilen nanofiberlerin maksimum çekme dayanımı (UTS), maksimum çekme dayanımındaki şekil değiştirme ve uzama, kopma gerilmesi gibi mekanik özellikleri mekanik çekme testi ile belirlenmiştir. Nanofiber doku iskelelerinin hücre canlılığı ve tutunması gibi biyolojik özellikleri MTT Hücre Proliferasyonu ve SEM Protokolü uygulanarak test edilmiştir. Morfolojik analiz sonuçları (SEM), nanofiber doku iskelelerinin fiber çapı değerleri sırasıyla 119 ± 31 nm, 149 ± 44 nm, 306 ± 68 nm, 241 ± 55 nm ve 384 ± 84nm olduğunu göstermiştir. Deney sonuçlarına göre, nanofiber doku iskelelerinin maksimum çekme dayanım değerlerinin 9.1± 0.6 MPa, 15.7 ± 1.4 MPa, 15.8 ± 5.0 MPa, 30.9 ± 16.0 MPa ve 15.8 ± 2.3 MPa olduğu tespit edilmiştir. Hücre tutunması SEM ile gözlemlenmiştir. MTT test sonucuna göre, 72 saat boyunca hiçbir numunede sitotoksik etki gözlenmemiştir. Hücre proliferasyonu ve canlılığı test sonuçlarının istatistiksel anlam taşımasıyla birlikte üretilen nanofiber doku iskelelerinin osteoblast benzeri insan hücresi ve fibroblast fare hücresi ile biyouyumlu olduğu gözlemlenmiştir.

TABLE OF CONTENTS

ACKNOWLEDGEMENTS iii

ABSTRACT iv

ÖZET v

LIST OF FIGURES xi

LIST OF TABLES xvii

LIST OF SYMBOLS xx

LIST OF ACRONYMS/ABBREVIATIONS xxi

1. INTRODUCTION 1

1.1. Nanoscience and Nanotechnology 1

1.2. Electrospinning 2

1.3. The Selection Criteria of Biomaterials 3

1.3.1. Polycaprolactone 5

1.3.2. Gelatin 7

1.3.3. Hydroxyapatite 8

1.4. The Selection Criteria of Solvent 9

1.4.1. Acetic Acid 10

1.4.2. Formic Acid 11

2. LITERATURE REVIEW 12

2.1. Patents on Electrospinning Device 12

2.2. Research Areas of Electrospun Polymer Nanofibers 14

2.2.1. Energy and Electronics 14

2.2.2. Environmental Engineering and Biotechnology 15

2.2.3. Defense and Security 15

2.2.4. Bioengineering 15
2.3. Researches on PCL/GE/HA Electrospun Nanofibers 16
3. OBJECTIVES 18
4. METHODOLOGY 19
4.1. Electrospinning Setup 19
4.2. Parameters of Electrospinning 19
4.2.1. Solution Parameters 19
4.2.1.1. The Polymer Molecular Weight. 19
4.2.1.2. Concentration. 21
4.2.1.3. Viscosity 22
4.2.1.4. Electrical Conductivity. 23
4.2.1.5. Surface Tension. 24
4.2.2. Process Parameters 26
4.2.2.1. Feed Rate. 26
4.2.2.2. Applied Voltage. 27
4.2.2.3. Collector. 28
4.2.2.4. Distance Between the Tip of the Needle and the Grounded Collector. 28
4.2.2.5. The Diameter of the Needle. 29
4.2.3. Ambient Parameters 29
5. EXPERIMENT 31
5.1. Materials 31
5.2. Selection of the Solvent System 31
5.3. Preparation of the Solutions 33
5.4. Solution Parameters 33

5.4.1. Concentration 33
5.4.1.1. The Concentration of BHA as a Variable. 33
5.4.1.2. The Concentration of GE as a Variable. 34
5.4.2. Density 34
5.4.2.1. Experiment 1, 2, 3. 34
5.4.2.2. Experiment 1, 4, 5. 35
5.4.3. Viscosity 35
5.4.3.1. Experiment 1, 2, 3 35
5.4.3.2. Experiment 1, 4, 5. 36
5.4.4. Surface Tension 36
5.4.4.1. Experiment 1, 2, 3. 36
5.4.4.2. Experiment 1, 4, 5. 37
5.4.5. Electrical Conductivity 37
5.4.5.1. Experiment 1, 2, 3. 37
5.4.5.2. Experiment 1, 4, 5. 38
5.5. Process Parameters of Electrospinning 39
5.5.1. Experiment 1 39
5.5.2. Experiment 2 40
5.5.3. Experiment 3 40
5.5.4. Experiment 4 41
5.5.5. Experiment 5 42
5.6. Characterization of Electrospun Nanofibers 43
5.6.1. Scanning Electron Microscope (SEM) 43
5.6.2. Fourier Transform Infrared Spectroscopy (FTIR) 45
5.6.3. Mechanical Test 47

5.6.4. Biological Test 50
5.6.4.1. MTT Cell Proliferation Assay 51
5.6.4.2. Cell Attachment. 51
6. RESULTS 53
6.1. Morphological Analysis 53
6.1.1. SEM 53
6.1.1.1. Experiment 1. 53
6.1.1.2. Experiment 2. 55
6.1.1.3. Experiment 3. 58
6.1.1.4. Experiment 4. 60
6.1.1.5. Experiment 5. 63
6.2. Chemical Analysis 65
6.2.1. FTIR 65
6.2.1.1. Experiment 1. 65
6.2.1.2. Experiment 2. 67
6.2.1.3. Experiment 3. 67
6.2.1.4. Experiment 4. 68
6.2.1.5. Experiment 5. 68
6.3. Mechanical Analysis 71
6.3.1. Tensile Test 71
6.3.1.1. Experiment 1. 71
6.3.1.2. Experiment 2. 72
6.3.1.3. Experiment 3. 73
6.3.1.4. Experiment 4. 74
6.3.1.5. Experiment 5. 76

6.4. Biological Analysis..... 77
6.4.1. MTT Cell Proliferation Assay 77
6.4.2. Cell Attachment 80
7. CONCLUSION..... 83
REFERENCES 85

LIST OF FIGURES

Figure 1.1. Scaffold dimensions affects cell binding and spreading [4]. 2

Figure 1.2. Schematic diagram of electrospinning (reproduced [6]). 3

Figure 1.3. Bone tissue configuration [11]. 4

Figure 1.4. Molecular structure of PCL 5

Figure 2.1. The first patented machine as a fundamental concept (reproduced from Cooley (1900) [57]). 12

Figure 2.2. Research category of electrospun polymer nanofibers [67]. 14

Figure 4.1. Electrospinning device. 20

Figure 4.2. Image of viscometer. 23

Figure 4.3. The relationship between the electrical conductivity and the diameter of the electrospun PLLA fibers [84]. 24

Figure 4.4. Image of Electrical Conductivity Meter. 24

Figure 4.5. Schematic representation of the element of surface tension [86]. 25

Figure 4.6. Image of the tensiometer. 26

Figure 4.7. The various geometries of the grounded collector: a) Flat plate, b) Parallel plates /stripes, c) Rotating drum, d) Rotating disk (flat edge), e) Rotating disc (sharp edge), f) Conveyor [99]. 28

Figure 4.8. The surface morphologies of the nanofibers at the different values of humidity: a) below 25%, b) 60-72 % [104]. 30

Figure 5.1. Image of spinnability: a) Nonspinnable solution, b) Spinnable solution. 31

Figure 5.2. The coating process of the samples before SEM: a) Uncoated nanofiber samples, b) Polaron SC7640 Sputter Coater, c) Coated samples on the SEM tab. 43

Figure 5.3. The image of scanning electron microscope (SEM), Philips XL30 ESEM-FEG. 44

Figure 5.4. The magnifications of the SEM images of one of the samples such as 12/1.5/0.5 wt % PCL/GE/BHA: a) x1000, b) x2000, c) x5000, d) x10000, e) x20000, f) x50000 and g) x100000 44

Figure 5.5. The image of Fourier transformation infrared spectroscopy. 46

Figure 5.6. A representation of a specimen during the tensile test [107]. 47

Figure 5.7. The image of the tensile test machine. 49

Figure 5.8. The dimensions of the specimen. 49

Figure 5.9. The image of high-accuracy digimatic micrometer. 50

Figure 5.10. The tensile test images of a sample of 12/0.5/0.5 wt % PCL/GE/BHA at: a) 0 sec , b) 10 sec, c) 50 sec, d) 130.4 sec , e) 130.6 s. 50

Figure 5.11. Equipment of MTT Cell Proliferation Assay kit and SEM protocol. 52

Figure 6.1. SEM image of 12/1/0.5 wt % (PCL/GE/BHA) electrospun nanofibers, Magnitude 20000x. 54

Figure 6.2. SEM image of 12/1/0.5 wt % (PCL/GE/BHA) electrospun nanofibers, Magnitude 100000x. 54

Figure 6.3. Frequency distribution of fiber diameter of 12/1/0.5 wt % (PCL/GE/BHA) electrospun nanofibers. 55

Figure 6.4. SEM image of 12/1/1 wt % (PCL/GE/BHA) electrospun nanofibers, Magnitude 5000x. 56

Figure 6.5. SEM image of 12/1/1 wt % (PCL/GE/BHA) electrospun nanofibers, magnitude 20000x. 56

Figure 6.6. SEM image of 12/1/1 wt % (PCL/GE/BHA) electrospun nanofibers, magnitude 100000x. 57

Figure 6.7. Frequency distribution of fiber diameter of 12/1/1 wt % (PCL/GE/BHA) electrospun nanofibers. 57

Figure 6.8. SEM image of 12/1/2 wt % (PCL/GE/BHA) electrospun nanofibers, Magnitude 5000x. 58

Figure 6.9. SEM image of 12/1/2 wt % (PCL/GE/BHA) electrospun nanofibers, Magnitude 20000x. 59

Figure 6.10. SEM image of 12/1/2 wt % (PCL/GE/BHA) electrospun nanofibers, Magnitude 100000x. 59

Figure 6.11. Frequency distribution of fiber diameter of 12/1/2 wt % (PCL/GE/BHA) electrospun nanofibers. 60

Figure 6.12. SEM image of 12/0.5/0.5 wt % (PCL/GE/BHA) electrospun nanofibers, Magnitude 5000x. 61

Figure 6.13. SEM image of 12/0.5/0.5 wt % (PCL/GE/BHA) electrospun nanofibers, Magnitude 20000x. 61

Figure 6.14. SEM image of 12/0.5/0.5 wt % (PCL/GE/BHA) electrospun nanofibers, Magnitude 100000x. 62

Figure 6.15. Frequency distribution of fiber diameter of 12/0.5/0.5 wt % (PCL/GE/BHA) electrospun nanofibers. 62

Figure 6.16. SEM image of 12/1.5/0.5 wt % (PCL/GE/BHA) electrospun nanofibers, Magnitude 5000x. 63

Figure 6.17. SEM image of 12/1.5/0.5 wt % (PCL/GE/BHA) electrospun nanofibers, Magnitude 20000x. 64

Figure 6.18. SEM image of 12/1.5/0.5 wt % (PCL/GE/BHA) electrospun nanofibers, Magnitude 1000000x. 64

Figure 6.19. Frequency distribution of fiber diameter of 12/1.5/0.5 wt % (PCL/GE/BHA) electrospun nanofibers. 65

Figure 6.20. FTIR analysis of Pure PCL, Pure GE, Pure BHA. 66

Figure 6.21. FTIR analysis of 12/1/0.5 wt % (PCL/GE/BHA) electrospun nanofibers. 69

Figure 6.22. FTIR analysis of 12/1/1 wt % (PCL/GE/BHA) electrospun nanofibers. 69

Figure 6.23. FTIR analysis of 12/1/2 wt % (PCL/GE/BHA) electrospun nanofibers. 70

Figure 6.24. FTIR analysis of 12/0.5/0.5 wt % (PCL/GE/BHA) electrospun nanofibers. 70

Figure 6.25. FTIR analysis of 12/1.5/0.5 wt % (PCL/GE/BHA) electrospun nanofibers. 71

Figure 6.26. Engineering stress-strain curve of 12/1/0.5 wt % (PCL/GE/BHA) electrospun nanofibers. 72

Figure 6.27. Engineering stress-strain curve of 12/1/1 wt % (PCL/GE/BHA) electrospun nanofibers. 73

Figure 6.28. Engineering stress-strain curve of 12/1/2 wt % (PCL/GE/BHA) electrospun nanofibers. 74

Figure 6.29. Engineering stress-strain curve of 12/0.5/0.5 wt % (PCL/GE/BHA) electrospun nanofibers. 75

Figure 6.30. Engineering stress-strain curve of 12/1.5/0.5 wt % (PCL/GE/BHA) electrospun nanofibers. 76

Figure 6.31. MTT Cell Proliferation Assay colorimetric test results and cell viability of all samples from Experiment 1 to Experiment 5 after 24, 48 and 72 hours of cell culture: (a) Initial, (b) 24 hours of 3T3 cell, (c) 48 hours of 3T3 cell, (d) 72 hours of 3T3 cell, (e) 24 hours of Saos-2, (f) 48 hours of Saos-2, (g) 72 hours of Saos-2. 78

Figure 6.32. MTT Proliferation Assay results and cell viability of all samples from Experiment 1 to Experiment 5 after 24, 48 and 72 hours of cell culture:

(a) 24 hours of 3T3 cell, (b) 48 hours of 3T3 cell, (c) 72 hours of 3T3 cell, (d) 24 hours of Saos-2, (e) 48 hours of Saos-2, (f) 72 hours of Saos-2, * P<0.05 indicates the statistical significance. 79

Figure 6.33. SEM images of cell attachment on nanofibers of Experiment 3 after 24, 48 and 72 hours of cell culture: (a-b) 24 hours, (c-d) 48 hours, (e-f) 72 hours. 81

Figure 6.34. SEM images of cell attachment on nanofibers of Experiment 5 after 24, 48 and 72 hours of cell culture: (a-b) 24 hours, (c-d) 48 hours, (e-f) 72 hours. 82

LIST OF TABLES

Table 1.1. Chemical properties of PCL [18- 22]. 5

Table 1.2. The toxicity classification of the solvents [49]. 10

Table 1.3. The parameters of the major solvents of PCL affecting the spinnability of the polymer solution [50]. 11

Table 2.1. Patents on electrospinning. 13

Table 5.1. Parameters of alternate solution systems and the spinnabilities'. 32

Table 5.2. The concentrations of the polymer solutions prepared by changing the ratio of bovine hydroxyapatite. 33

Table 5.3. The concentrations of the polymer solutions prepared by changing the ratio of bovine gelatin. 34

Table 5.4. The density of the solutions prepared by changing the ratio of BHA. 35

Table 5.5. The density of the solutions prepared by changing the ratio of GE. 35

Table 5.6. The viscosity of the solutions prepared by changing the ratio of BHA. 36

Table 5.7. The viscosity of the solution prepared by changing the ratio of GE. 36

Table 5.8. The surface tension of the solutions prepared by changing the ratio of BHA. 37

Table 5.9. The surface tension of the solutions prepared by changing the ratio of GE. 37

Table 5.10. The electrical conductivity of the solutions prepared by changing the ratio of BHA. 38

Table 5.11. The electrical conductivity of the solutions prepared by changing the ratio of GE. 38

Table 5.12. Process parameters of 12/1/0.5 wt % (PCL/GE/BHA) electrospun nanofibers. 39

Table 5.13. Process parameters of 12/1/1 wt % (PCL/GE/BHA) electrospun nanofibers. 40

Table 5.14. Process parameters of 12/1/2 wt % (PCL/GE/BHA) electrospun nanofibers. 41

Table 5.15. Process parameters of 12/0.5/0.5 wt % (PCL/GE/BHA) electrospun nanofibers. 41

Table 5.16. Process parameters of 12/1.5/0.5 wt % (PCL/GE/BHA) electrospun nanofibers. 42

Table 5.17. The group frequencies of functional groups for PCL/GE/BHA [105]. 45

Table 5.18. The group frequencies of functional groups for PCL/GE [69, 106]..... 46

Table 6.1. FTIR analysis and comparison between literature and the experiments. 66

Table 6.2. The tensile test results of PCL/GE/BHA 12/1/0.5 wt % electrospun nanofibers. 72

Table 6.3. The tensile test results of PCL/GE/BHA 12/1/1 wt % electrospun nanofibers. 73

Table 6.4. The tensile test results of PCL/GE/BHA 12/1/2 wt % electrospun nanofibers. 74

Table 6.5. The tensile test results of PCL/GE/BHA 12/0.5/0.5 wt % electrospun nanofibers. 75

Table 6.6. The tensile test results of PCL/GE/BHA 12/1.5/0.5 wt % electrospun nanofibers. 76

LIST OF SYMBOLS

$\Delta\vec{F}$	Capillary force
Δl	Elongation or line on free surface
dl	Unit line element
$\vec{m}$	Normal vector of the unit line element
a	Original radius of the fluid jet
in	Rate of instability of the fluid jet
A_0	Initial area of a specimen
d_f	Diameter of the fiber
E	Young's Modulus
F	Force, Load
l_0	Initial length of a specimen
l_i	Instantaneous length of the specimen
ε	Strain
μ	Dynamic Viscosity
σ	Stress or Surface tension
$\vec{\sigma}$	Stress vector

LIST OF ACRONYMS/ABBREVIATIONS

3T3	Mouse Fibroblast Cell
AA	Acetic acid
ASTM	American Society for Testing and Materials
BfArM	The Federal Institute for Drugs and Medical Devices
BHA	Bovine Hydroxyapatite
BMJV	The Ministry for Consumer Affairs in Germany
CA	Canada
CFDA	China Food and Drug Administration
DCM	Dichloromethane
DE	Germany
DMAC	Dimethylacetamide
DMF	Dimethylformamide
DMSO	Dimethyl sulfoxide
DNA	Deoxyribonucleic acid
EDTA	Ethylenediaminetetraacetic acid
ESB	European Society for Biomaterials
ESEM	Environmental Scanning Electron Microscope
FA	Formic acid
FBS	Fetal bovine serum
FTIR	Fourier transform infrared spectroscopy
GB	Great Britain
GE	Bovine Gelatin
HA	Hydroxyapatite

HFP	Hexafluoro-2- propanol
ICH	International Conference on Harmonisation of Technical Requirements for Registration of Pharmaceuticals For Human Use
MTT	3-(4,5-dimethythiazol- 2-yl)-2,5-diphenyl tetrazolium bromide
PAN-MA	Polyacrylonitrile-co-methylacrylate
PBS	Phosphate buffer saline
PCL	Polycaprolactone
PCLEEP	Poly-caprolactone-co-ethyl ethylene phosphate
PEO	Polyethylene oxide
PLGA	Poly(lactic-co-glycolic acid)
PLLA	Poly (lactic acid)
PSF	Polysulfone
PU	Polyurethane
PVA	Poly (vinyl alcohol)
RGD	Arginine-glycine-aspartic
Saos-2	Human osteogenic sarcoma (human osteoblastic-like cell)
SEM	Scanning electron microscopy
TFE	Trifluoroethanol
THF	Tetrahydrofuran
Ti	Titanium
UK	United Kingdom
USFDA	The United States Food and Drug Administration
UTS	Ultimate tensile strength
UV	Ultraviolet
WHO	World Health Organization

1. INTRODUCTION

1.1. Nanoscience and Nanotechnology

Nanoscience is a discipline of defining mechanisms of atoms, molecules and structure of materials on the nanometer scale. A nanometer is one billionth of a meter, 10^{-9} m. A nanometer is one tenth of hydrogen atom (0.1 nm), and twice of DNA molecule (2 nm), one in ten thousand of white blood cell (10000 nm) whereas a nanometer is approximately one in six thousand of a human hair (60000 nm) [1].

In nanoscience, there is an interaction between physics, chemistry, biology, materials science, mechanical engineering, electronics and medicine because nanoscience is multidisciplinary. The vision of nanoscience is put forward by physicist Richard Feynman at an American Physical Society meeting at the California Institute of Technology (CalTech) on December 29, 1959 [2]. The idea of Richard Feynman is that each individual atom can be manipulated in a controlled manner.

Nanotechnology is the application of nanoscience on designing and manufacturing objects with smaller than 100 nm, one tenth of a micron. In 1974, as a new term of ‘nanotechnology’ is coined by professor Norio Taniguchi, Tokyo Science University and he highlights that " ‘Nano-technology’ mainly consists of the processing of separation, consolidation, and deformation of materials by one atom or one molecule." [3].

Nano-scaled new materials and composites are of great significance in nanotechnology. For instance, as applications in nanomaterials, as shown in Figure 1.1, there are three kinds of scaffold architecture that are micropore scaffold (A), microfiber scaffold (B) and nanofiber scaffold (C) [4]. It indicates that nanofiber scaffold, which is used in tissue regeneration, has more ability to bind cell structures than microfiber scaffold due to its nano- sized dimension and morphology. The reason is that nanofiber scaffold has larger surface area to bind to receptors of cell membrane. Figure 1.1 also points out that nano-sized structure is important for cell compatibility in tissue generation applications.

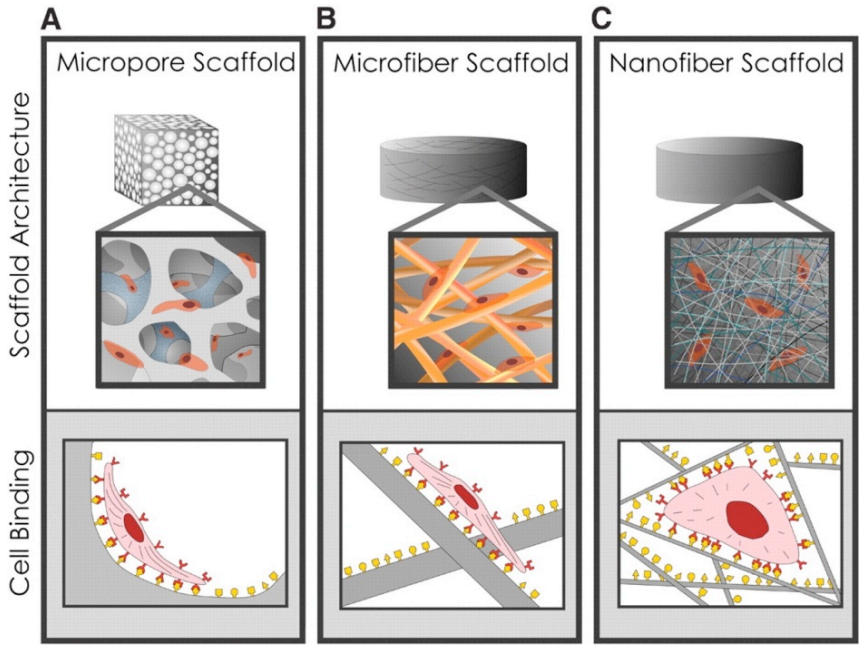

Figure 1.1. Scaffold dimensions affects cell binding and spreading [4].

In nano material technology, there are five kinds of methods known for the manufacture of nanofiber such as drawing, template synthesis, phase separation, self-assembly and electrospinning. The most efficient method is admitted as electrospinning [5].

1.2. Electrospinning

An electrical field is generated by applying a high voltage between two electrodes such as positive electrode and negative electrode. The selected polymer solution is supplied with the aid of a feed pump to form the droplet (Taylor Cone). Due to the electrical field, the electrostatic forces transmit the solution from the positive electrode to the negative electrode (Jet). As a result of the transmission, electrospun nanofibers are formed. This process is called electrospinning. The schematic diagram shown in Figure 1.2 is the original schema of Inovenso NS 24 used in the experiments in this thesis [6].

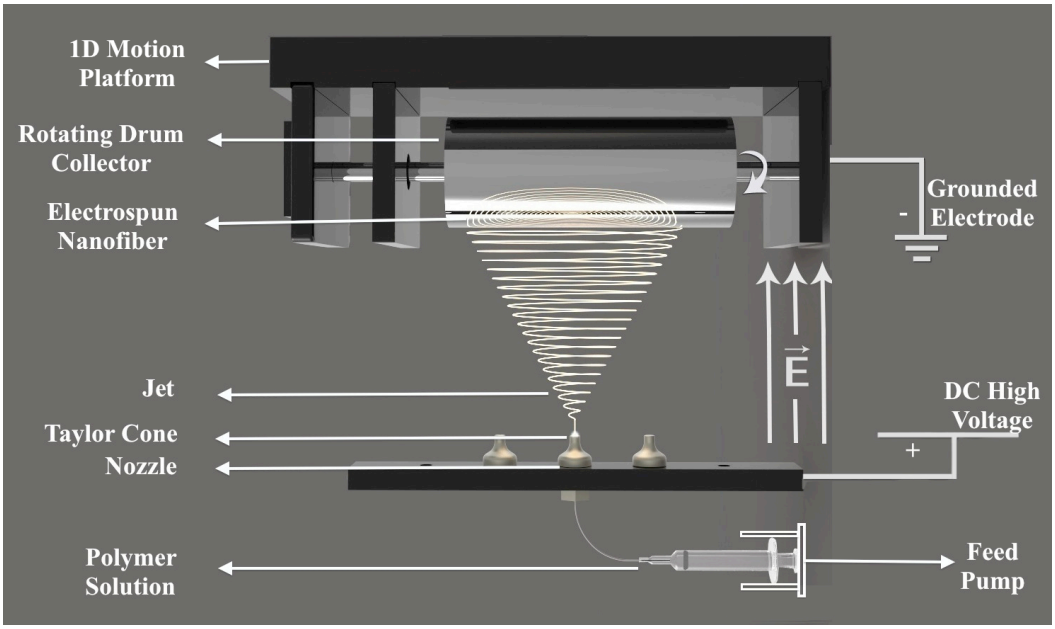

Figure 1.2. Schematic diagram of electrospinning (reproduced [6]).

Electrospinning is the most efficient process to manufacture nanofibers. Compared with the other methods such as drawing, template synthesis, phase separation, self-assembly, it has some advantages. Firstly, long and continuous nanofibers can be manufactured. Secondly, the diameter of nanofiber can be controlled and manipulated. Finally, repeatability of the setup is another advantage of the process at lower cost compared to the others.

1.3. The Selection Criteria of Biomaterials

Biomaterial is defined by the European Society for Biomaterials (ESB) as 'material intended to interface with biological systems to evaluate, treat, augment or replace any tissue, organ or function of the body'. It can be metallic, polymer or ceramic. Titanium (Ti) is a metallic biomaterials. Synthetic polymer biomaterials are Polycaprolactone (PCL), Poly (vinyl alcohol) (PVA), Poly (lactic acid) (PLLA), poly(lactic-co-glycolic acid) (PLGA), Polyurethane (PU). Natural polymer biomaterials are collagen, gelatin, silk, alginate, chitosan, cellulose and starch. Synthetic bioceramics are Alumina based, Zirconia based and Tricalcium phosphate. Hydroxyapatite is a natural bioceramic material.

The interactions between biomaterials with cell are one of the most important issues for tissue engineering. The surface of the biomaterial determines the adhesion of the cell and cell attachment. It is significant to choose the proper combination of biomaterials according to the kinds of tissue such as bone, nerve, skin and blood vessel. For instance, polyacrylonitrile-co-methylacrylate (PAN-MA) and poly-caprolactone-co-ethyl ethylene phosphate (PCLEEP), which are as biomaterial in electrospinning, are used for axons regenerations of rat sciatic nerve and rat tibial nerve [7,8]. Chitin and gelatin are used in skin cell regeneration [9,10].

As shown in Figure 1.3, the schematic diagram of bone indicates that basic bone structure consists of collagen fibrils and hydroxyapatite crystals. To produce more bioactive artificial bone tissue, PCL as a synthetic polymer biomaterial, bovine gelatin as a natural polymer biomaterial, bovine hydroxyapatite as a natural ceramics biomaterial are selected because the structure in Figure 1.3 is the basic reference of the thesis.

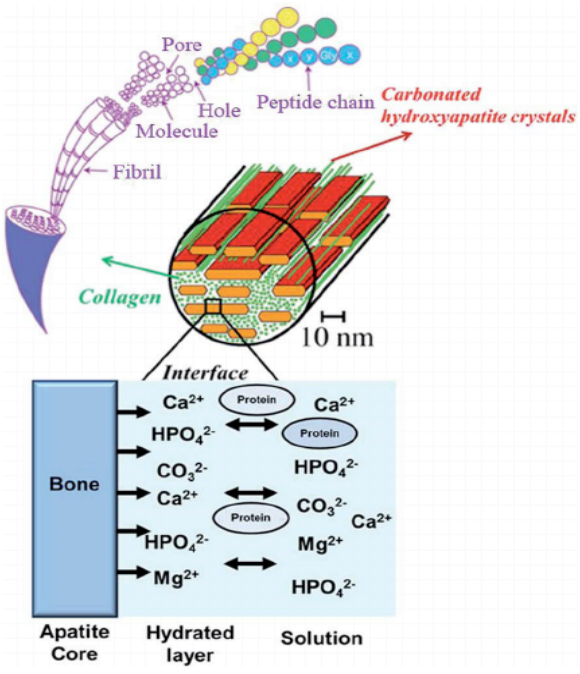

Figure 1.3. Bone tissue configuration [11].

1.3.1. Polycaprolactone

Polycaprolactone (PCL) is a semi crystalline synthetic polymer and an aliphatic polyester. It is linear polymer which is produced by polymerization of ε-caprolactone monomers by applying heat and catalysist [12]. The chemical formula is $(C_6H_{10}O_2)_n$ as shown in Figure 1.4. It is hydrophobic and biodegradable polymer. The chemical properties of PCL are listed in Table 1.1. It is compatible with natural polymers such as collagen, gelatin and silks. As a biomedical material, it is widely used in drug delivery [13], long-term suture [14-16] and tissue regeneration for 3-D scaffolds [17]. It is approved by United States Food and Drug Administration (USFDA) and China Food and Drug Administration (CFDA) for use in human bodies.

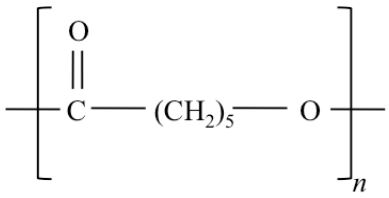

Figure 1.4. Molecular structure of PCL

Table 1.1. Chemical properties of PCL [18- 22].

Chemical Properties of PCL	
Molecular Weight	3,000 to 80,000 g/mol [18]
Density	1.145 g/mL at 25 °C [19] 1.146 g/mL at 25 °C [20]
Glass Transition Temperature	-60°C to -63°C [21-22]
Melting Temperature	60°C [19-20]

In 1932, The Carothers's research group [23] firstly synthesis PCL. By 1970's, the usage of PCL has been increasing in drug delivery [24]. By 1990's and 2000's, the usage

of PCL has been increasing in electrospun scaffold manufacturing because of its adequate rheological properties and relatively economical as compared to the other aliphatic materials [24,25]. Many research groups in electrospinning have achieved the results by dissolving PCL in trifluoroethanol (TFE) [26], tetrahydrofuran (THF), hexafluoro-2-propanol (HFP) [27], toluene [28], dichloromethane (DCM) [29], sodium acetate [30], acetic acid [31,32] and formic acid [33]. It is partly soluable in acetone [34]. It is not solved in dimethylformamide (DMF), alcohols such as ethanol and methanol.

PCL is known as a biodegradable material because its aliphatic ester linkage is sensitive to hydrolysis [35]. However its biodegradation is long- termed such as up to four years [24]. It can be a problem for some applications [36]. Therefore, many researchers aim to do several studies to reduce the biodegradation time of PCL.

One approach is that the molecular weight of PCL is a highly important parameter to see the difference in the biodegradation time. Ester chains increase with increasing molecular weight because the breakage of the chain takes time for the formation of water-soluble monomers [24]. Therefore, the molecular weight of the PCL should be chosen as low as possible while optimizing parameters.

Another approach is adding some materials in the blend of PCL that decreases biodegradation time. For instance, Esperanza Díaz *et al.* [35] pointed out that blending nano hydroxyapatite particles with PCL solution decreases the biodegradation time of the scaffold. The decrease in biodegradation time can be attributed to the decrease in hydrophobicity of PCL. Due to its non-wettability and hydrophobicity, PCL is less linking with cell membrane compared to hydrophilic material. For this reason, altering the surface characteristics of hydrophobic PCL is by combining with natural polymers, such as collagen and gelatin or bioresorbable ceramics, such as calcium phosphate, hydroxyapatite (HA). For example, HA particles within PCL fiber scaffolds could increase mineralization process on the surface and osteoblast proliferation [37].

1.3.2. Gelatin

Gelatin is a protein which is also called a natural polymer. It is derived from collagen by hydrolysis. Collagen is extracted and purified from the tendons, bones, skin or teeth of bovine, porcine or fish. Collagen has triple α-helix structure. By hydrolysis, triple α-helix polypeptide structure of collagen (its molecular weight around 100,000) is divided into single chains which have various molecular weights. If the pretreatment of the hydrolysis of collagen is applied in acidic environment, it is called gelatin Type A. If the pretreatment of the hydrolysis of collagen is applied in alkali environment, it is called gelatin Type B. Each gelatin has own bloom number which identifies the stiffness of gelatin as a mechanical strength. If the extraction temperature during process is decreased, high bloom number is obtained.

Gelatin is approved by the US Food and Drug Administration, World Health Organization (WHO), The Federal Institute for Drugs and Medical Devices (BfArM) and the Ministry for Consumer Affairs in Germany (BMJV) [38].

Gelatin is a significant natural polymer, which has many advantages for bone tissue regeneration. As it indicated in the literature, using gelatin in the scaffold enhances the properties because it is biodegradable, biocompatible, adhesive and low antigenic compared to collagen [39-41]. It has also chain combinations with arginine-glycine-aspartic (RGD) sequences that provide the cell adhesion and recognitions [42].

Whereas gelatin is mostly used in food production and the pharmacology, it is recently used in treatment of degenerative bone disease such osteoarthritis and osteoporosis [38]. Osteoporosis is the reduction of density and mass of bone tissue that is mostly seen in people 35 years and older. The reduction is approximately 1.5% per year. When it comes to osteoarthritis, it is a degenerative joint disease which is seen because of the lack of elasticity of the joint. Therefore, some research groups prove treatment of the diseases by using a mixture of gelatin. For instance, Dr. Seeligmüller, who is a sport medicine specialist in Germany, applied a mixture of gelatin to over 350 patients that is a solution for reducing the feeling of pain and increases the ability of long walking [38].

To enhance the electrospun scaffolds, gelatin can be mixed with ceramics such as hydroxyapatite, $Ca_{10}(PO_4)_6(OH)_2$ and synthetics biopolymers such as Polycaprolactone (PCL) [42], Poly(lactic-co-glycolic acid) (PLGA), Polyethylene oxide (PEO)[43].

1.3.3. Hydroxyapatite

Hydroxyapatite is the main inorganic mineral of natural bone matrix and teeth [44]. Its molecular formula is $Ca_{10}(PO_4)_6(OH)_2$. Around seventy percent of the nature bone matrix consists of hydroxyapatite which has a hexagonal crystalline structure. The crystals are created the bone matrix with the collagen fibrils by aligning along the axis of the collagen fibrils. Thus, the crystals strengthen the collagen matrix to make a very strong and tough composite [45].

Hydroxyapatite can be produced various methods such as derived from natural bone or teeth, obtaining calcium phosphate from egg shells, coral or synthesis with chemicals [46]. The methods of derivation from natural bone or teeth are a deproteinization and calcination methods using calf femur [46,47]. There is also rapid microwave synthesis method [48].

To produce more bioactive artificial tissue for assisting the body in its repair process, research groups use the method of bio mimicking by simulating the bone matrix and teeth time-tested patterns and strategies. Therefore scientific groups have focused on more bioactive and biodegradable materials called biomaterials. Hydroxyapatite (HA) used in elecrospinning as a biomaterial has some advantages. These are being a more robust and stable holding on the bone, providing a strong bond between the implant and bone, helping regular and rapid bone growth at the bone implant interface, prevention of dissolution of metal ions in the body by implant coated with HA, high biocompatibility, chemical similarity to bone, increase of compression strength when tissue engineering applications are considered.

1.4. The Selection Criteria of Solvent

The selection of the solvent during preparing the polymer solution is the most critical parameter that determines the cell viability on the electrospun fiber, the spinnability of the solution and the diameter of the fiber.

In terms of cell viability, the non-toxicity of the electrospun is important. Therefore, it is preferred that the polymers used are non-toxic as well as the solvents are non- toxic. In 2011, the toxicity classification of solvents is revised by ICH Expert Working Group which is in ICH (International Conference on Harmonisation of Technical Requirements for Registration of Pharmaceuticals For Human Use): Q3C guideline for residual solvents (R5) [49]. As shown in Table 1.2, the residual solvents are classified in three classes: Class 1, Class 2 and Class 3. According to ICH, the solvents in Class 1, which are called human carcinogen, cause also environmental hazard that's why it is classified as solvents to be avoided. The solvents in Class 2 are non-genotoxic animal carcinogens or some irreversible toxicity such as neurotoxicity (adverse effect on the nerve system) or teratogenicity (malformation in fetus during pregnancy) that's why it is classified as solvents to be limited. The solvents in Class 3 are low toxic potential to human and there is no health-based exposure limit [49]. In Table 1.2, the most preferred solvents by research groups for electrospinning are selected from the guideline [49].

As shown in Table 1.2, acetic acid and formic acid being also solvents for polycaprolactone, gelatin and hydroxyapatite are identified as Class 3 that's why they are chosen for the thesis work.

In terms of the spinnability of the polymer solution, the electrical conductivity and viscosity of the solvents are significant parameters [50-52]. In electrospinning, dielectric constant of a solvent is highly important for achieving stable jet, the diameter of the fiber and continuous production due to the process in electrostatic field. Increase in dielectric constant and the electrical conductivity of the solvent increases the stability of the jet and decreases the diameter of the electrospun nanofiber.

As shown in Table 1.3, dielectric constant and viscosity of the acetic acid and formic acid, which are favorable compared to the others, are selected for this thesis.

Table 1.2. The toxicity classification of the solvents [49].

Solvent	Structure	Class
Acetic acid	CH_3COOH	Class 3
Acetone	CH_3COCH_3	Class 3
Chloroform	$CHCl_3$	Class 2
Dichloromethane	CH_2Cl_2	Class 2
Dimethylformamide	$HCON(CH_3)_2$	Class 2
Ethanol	CH_3CH_2OH	Class 3
Methanol	CH_3OH	Class 2
Formic acid	HCOOH	Class 3
Toluene	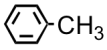	Class 2
Tetrahydrofuran		Class 2

1.4.1. Acetic Acid

Acetic acid is one of the carboxylic acids and organic aliphatic compound [53]. The chemical formula is CH_3COOH. It is colorless with strong vinegar odor. It has antibacterial properties. It is approved by FDA that's why it is used as a solvent in pharmacology such as producing medicines or plastics [54]. As an alternative solvent in electrospinning, acetic acid has just begun to be used. As shown in Table 1.2, it is identified as non-toxic, Class 3 can be preferred in terms of the cell viability on the electrospun nanofiber. It is a solvent for polycaprolactone, gelatin and hydroyapatite. It is selected to be used in the thesis work.

Table 1.3. The parameters of the major solvents of PCL affecting the spinnability of the polymer solution [50].

Solvent	**Boiling Temperature** (°C)	**Dielectric Constant** at 20°C ε	**Electrical Conductivity** at 25°C ($S.m^{-1}$)	**Absolute Viscosity** at 25°C (mPa.s)
Acetic acid	118	6.2	6.0×10^{-7}	1.13
Acetone	56	20.6	5.0×10^{-7}	0.33
Chloroform	61	4.8	$< 1.0 \times 10^{-8}$	0.57
Dichloromethane	40	36.7	4.3×10^{-9}	0.44
Formic acid	100.8	58	6.4×10^{-3}	1. 78 (20°C)
Tetrahydrofuran	66	7.6	4.5×10^{-3}	0.55
H_2O	100	79.7	5.5×10^{-6}	0.89

1.4.2. Formic Acid

Formic acid is the simplest carboxylic acid. It is a organic solvent The chemical formula is HCOOH. It is colorless with penetrating odor [55]. It is used in antioxidants that human body absorbs formic acid and eliminates it into carbon dioxide and water or partly discarded in urine [56]. It is approved by FDA that's why it is used as a solvent in agricultural products and antibacterial products. As shown in Table 1.2, it is identified as non-toxic, Class 3. In addition, it can be seen in Table 1.3 that it has the highest dielectric constant as a solvent of PCL among the listed solvents that's why it is good in terms of the spinnability of the polymer solution. It is also solvent for gelatin and hydroxyapatite as well as polycaprolactone that's why it is also selected to be used with acetic acid in order to achieve an alternate solution system for the materials in the thesis work.

2. LITERATURE REVIEW

2.1. Patents on Electrospinning Device

In 1900, John Francis Cooley, who is an inventor and electrician in City of Boston, is the first inventor of electrospinning machine as the fundamental concept, as shown in Figure 2.1. It is patented in the UK as called GB 06385. The name of the first patent is 'Improved methods of, and apparatus for, electrically separating the relatively volatile liquid component from the component of relatively fixed substances of composite fluids' [57]. He has also two more patents in electrospinning. After Cooley, from 1900 to 1991, there are approximately 55 patents recorded about the development of electrospinning methods. Some of them are listed in Table 2.1.

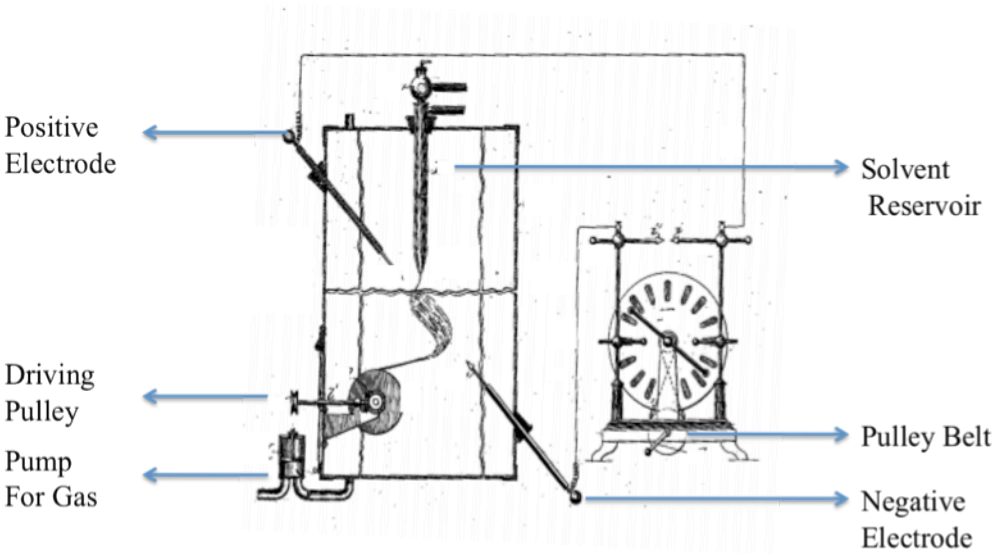

Figure 2.1. The first patented machine as a fundamental concept (reproduced from Cooley (1900) [57]).

In 1934, in terms of a modern electrospinning machine concept, Anton Formhals is a well-known inventor of the electrospinning process with 22 patents in the United States of America, Germany, France and the United Kingdom. He paves the way on the development of the process such as various design of nozzle patent in 1934 [64], removing

rotating fiber emitter design patent in 1938 [65] and producing controlled shorter fibers patent in 1938 [66].

Table 2.1. Patents on electrospinning.

Patent Number	Date	Inventor	Title of Patent
GB 06385	19th May, 1900	J. F. Cooley	Improved methods of, and apparatus for, electrically separating the relatively volatile liquid component from the component of relatively fixed substances of composite fluids [57]
US 705691	29th July, 1902	W. J. Morton	Method of dispersing fluids [58]
CA 293884	8th October, 1929	K. Hagiwara	Process for manufacturing artificial silk and other filaments by applying electric current [59]
US 2077373	13th April, 1937	A. Formhals	Production of artificial fibers [60]
DE 746708C	21st August, 1944	A. Formhals	Vorrichtung zur Herstellung von Fasern und Faserbaendern aus faserbildenden Loesungen mittels Hochspannungselektrizitaet [61] (A device for the production of fibers and fiber carriers from fiber-forming solutions by high-voltage electrics)
US 4552707	12th November, 1985	T.V. How	Synthetic vascular grafts, and methods of manufacturing such grafts [62]
US 4618524	21st October, 1986	D. Groitzsch and E. Fahrbach	Microporous multilayer non-woven material for medical applications [63]

2.2. Research Areas of Electrospun Polymer Nanofibers

Researches in electrospinning create a new wave in the material science in the 21st century in terms of various fields such Energy and Electronics, Environmental Engineering and Biotechnology, Defense and Security and Bioengineering [67]. Sixty percent of the researches in electrospinning are based on the characterization of new electrospun polymer nanofibers and the development of the process as shown in Figure 2.2.

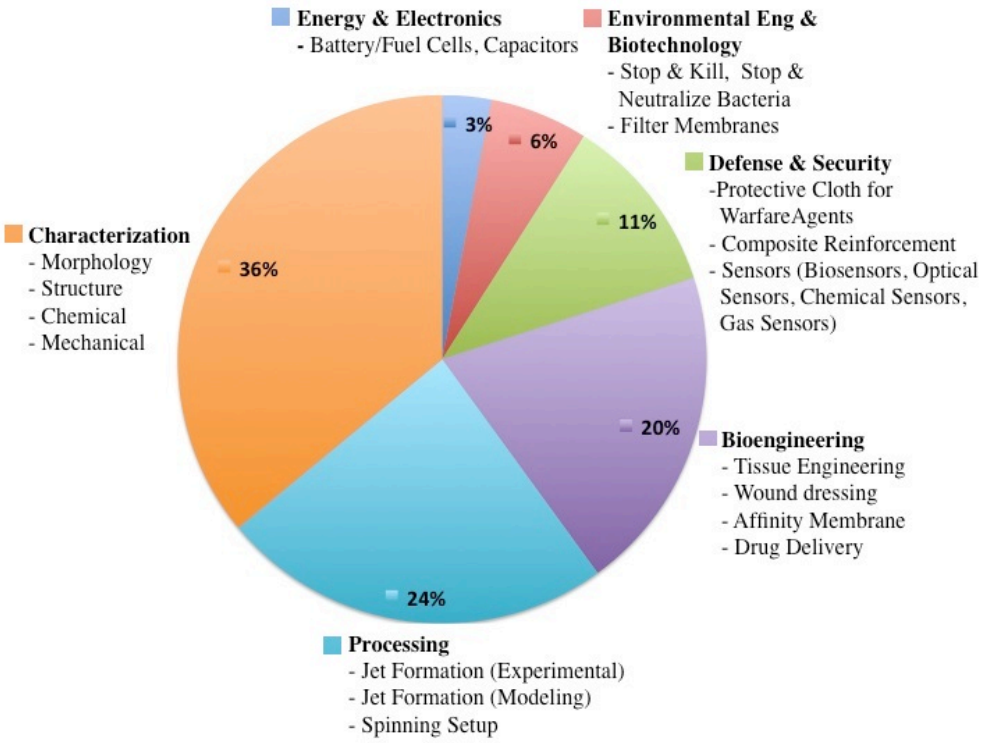

Figure 2.2. Research category of electrospun polymer nanofibers [67].

2.2.1. Energy and Electronics

In terms of energy and electronics, in addition to the increase in energy demand, a new generation energy production is needed because it is aimed at minimizing damage to

the environment. Therefore, electrospinning method creates a new approach to capacitors, fuel cells and the batteries such as polymer battery. Scientists in this field are working on assembling polymer nanofibrous membranes on the battery.

2.2.2. Environmental Engineering and Biotechnology

In terms of environmental engineering and biotechnology, air pollution and water pollution are becoming increasingly problematic day by day. In order to solve this problem, material science continues to be used in order to produce new nano-sized filters. Therefore, the studies are made on the production of polymer nanofibrous membranes filters by electrospinning. These nanofibrous filters prevent spreading toxic gasses and dust from the industrial systems the to the air or deactive bacteria with antibacterial nanofibrous filters.

2.2.3. Defense and Security

In terms of defense and security, there is research on electrospun nanofibers used in protective clothes for warfare agents. The studies are about decreasing impact of both mechanical and chemical damage. In military, gas sensors, optical sensors, chemical sensors are related fields as highly sensitive electrospun sensors. The body of the aircraft consists of micron-sized composites. Mechanically stronger reinforcements can be obtained by using the nano-sized electrospun composite because of its higher surface area.

2.2.4. Bioengineering

In terms of bioengineering, electrospun nanofibers are produced for researches on tissue engineering, wound dressing, affinity membrane and drug delivery. In the treatment of damaged tissues, it was aimed to produce electrospun nanofiber scaffolds by forming different matrices considering the biological similarity of tissue in tissue engineering and wound dressing. The cell attachment and growth in nano-sized electrospun scaffolds are seen much compared to micro-sized scaffolds due to increased surface area contact to be used in the treatment of damaged tissue in the future. In electrospun nanofibers, controlled drug can be placed for drug delivery that can be breakthrough advancement for diabetic

treatments. Today, it is aimed to choose appropriate medication and treatment for each individual patient. With the development of biotechnology, the need for new tools for the more delicate purification of nucleotides, amino acids or other substances has increased in order to achieve electrospun nanofibrous composite for producing affinity membrane due to its high separation capability [68].

2.3. Researches on PCL/GE/HA Electrospun Nanofibers

In tissue engineering, tissue scaffolds are expected to be designed based on various kinds of tissues such as blood vessels, bone, nerve and cartilage. It is expected to choose the appropriate material for the tissue matrix. The attempt to achieve appropriate morphology like real tissue is called as biomimicking.

In terms of biomimicking bone tissue, electrospun scaffold is expected to consist of collagen or gelatin and hydroxyapatite according to physiology of the bone for the recognition of the scaffold by bone cell such as osteoblast.

In 2015, Chong L.H *et al.* published results on electrospinning of PCL/Gelatin nanofibers and defining its antibacterial properties. The work is a good example of using eco-friendly solvent because formic acid is used as a solvent which is identified as Class 3. The diameter of fiber, which is collected by blending 14% w/v of PCL/Gelatin, applying voltage of 18 kV and adjusting flow rate to 0.5 mL/h, is recorded as 547 nm where porcine skin gelatin is used. As a result of the research, the electrospun scaffolds can be used in skin tissue engineering due to its inhibiting bacterial infections. It is noted that there is no mechanical test in the research [69].

In 2016, Yao R *et al.* studied on electrospinning of PCL/Gelatin scaffolds with various mixture ratios of 4:1, 2:1, 1:1, 1:2, 1:4. Gelatin is porcine gelatin. Hexafluoroisopropanol is used as a solvent which is a toxic solvent. The study indicated that the diameter of fibers is around 800-1200 nm and 2:1 PCL/Gelatin sample has highest tensile strength of 3.7 MPa and the highest percentage of elongation of approximately 90% among all. In addition mesenchymal stem cell responses are recorded [70].

In 2016, Rong D. *et al.* worked on electrospinning of of Gelatin/PCL electrospun fiber mat with nano hydroxyapatite and natural bone powder that the cell proliferation and viability on electrospun nanofibers with natural bone is higher than its nano hydroxyapatite. It is recorded that the diameter of fiber is around 600-1200nm with using trifluoroethanol (TFE) as a solvent [71]. Gelatin is porcine gelatin. However it should be given that TFE is identified in Class 2 as a toxic solvent. It is noted that there is no mechanical test in the research.

3. OBJECTIVES

The aim of the thesis is to manufacture electrospun nanofibrous scaffolds for optimal bone tissue regeneration applications by electrospinning. The experimental setup is on the effect of Polycaprolactone (PCL) / Bovine Gelatin (GE) / Bovine Hydroxyapatite (BHA) in the solution investigating the properties and morphological structure of nanofiber scaffolds. By controlling BHA concentration and GE concentration in the polymer solution, the effect on the manufacturing process and the effect on the fiber of the change are examined. The major objectives are below:

(i) To use different combination of biomaterials such as bovine gelatin and bovine hydroxyapatite.
(ii) To select non-hazardous solvent system instead of Trifluoroethanol, Chloroform
(iii) Minimum three hours spinnability for non-hazardous system.
(iv) To decrease the diameter of nanofibers to below 200nm instead of 600 nm.
(v) To increase the mechanical properties (Ultimate Tensile Strenght UTS > 5 MPa)
(vi) The biocompatibility of the composite in terms of the cell viability and attachment.

The physical properties of various composite fibers such as density, viscosity, surface tension and electrical conductivity will be measured in order to determine the differences between the solutions. To determine the morphology of the electrospun nanofibers, Scanning electron microscopy (SEM) will be used. To examine the chemical properties of the electrospun nanofibers, Fourier transform infrared spectroscopy (FTIR) will be used. To identify the mechanical properties of the electrospun nanofibers such as ultimate tensile strength (UTS), mechanical tensile testing will be applied. To define the biocompatibility of the electrospun nanofibrous scaffolds, cell proliferation test (MTT Cell Proliferation Assay) and cell attachment test are applied by using human osteoblast-like cell line and mouse fibroblast cell line.

4. METHODOLOGY

4.1. Electrospinning Setup

As shown in Figure 4.1, the polymer composite solution is ejected by a feed pump from the tip of the positively charged nozzle by creating Taylor Cone to rotating drum grounded electrode. The distance between the metal nozzle tip and rotating drum collector is adjusted to preferable value such as 12 cm. Rotating drum collector can provide the nanofiber mats aligned. Aligned nanofiber scaffolds can be preferable according to the desired morphology. Rotating drum collector is negatively charged and grounded. It has adjustable controller for angular velocity. It is connected to 1D motion platform which is backwards and forwards. Motion of 1D platform is also adjustable as its stroke. A feed pump is connected to the needle with a polyethylene tube and pushed the syringe to provide a stabilized mass flow of the composite solution. Applied voltage is also adjustable in order to achieve stable jet. Fan is used preferably according to stabilizing ambient temperature and humidity. The experiments are at ambient temperature between 25- 28° C and at ambient humidity.

4.2. Parameters of Electrospinning

4.2.1. Solution Parameters

4.2.1.1. The Polymer Molecular Weight. The length of the polymer chains formed by the incorporation of the monomers determines the molecular weight of a polymer. When polymer chain entanglement increases, the molecular weight of polymer increases [72]. The viscosity of the solution prepared with the same percentage of the same polymer (%w/w) in the solution having a different molecular weight of the polymer, even if it is the same kind of polymer, will be different [72]. The reason is that increase in the molecular weight decreases the solubility of the polymer in the solvent [72]. In addition, increase in molecular weight due to polymer chain entanglement increase the concentration of the solution, thus electrospinning is processed in a continuous way without bead formation. However, extra high molecular weight of the polymer is hard to be solved in the solvent

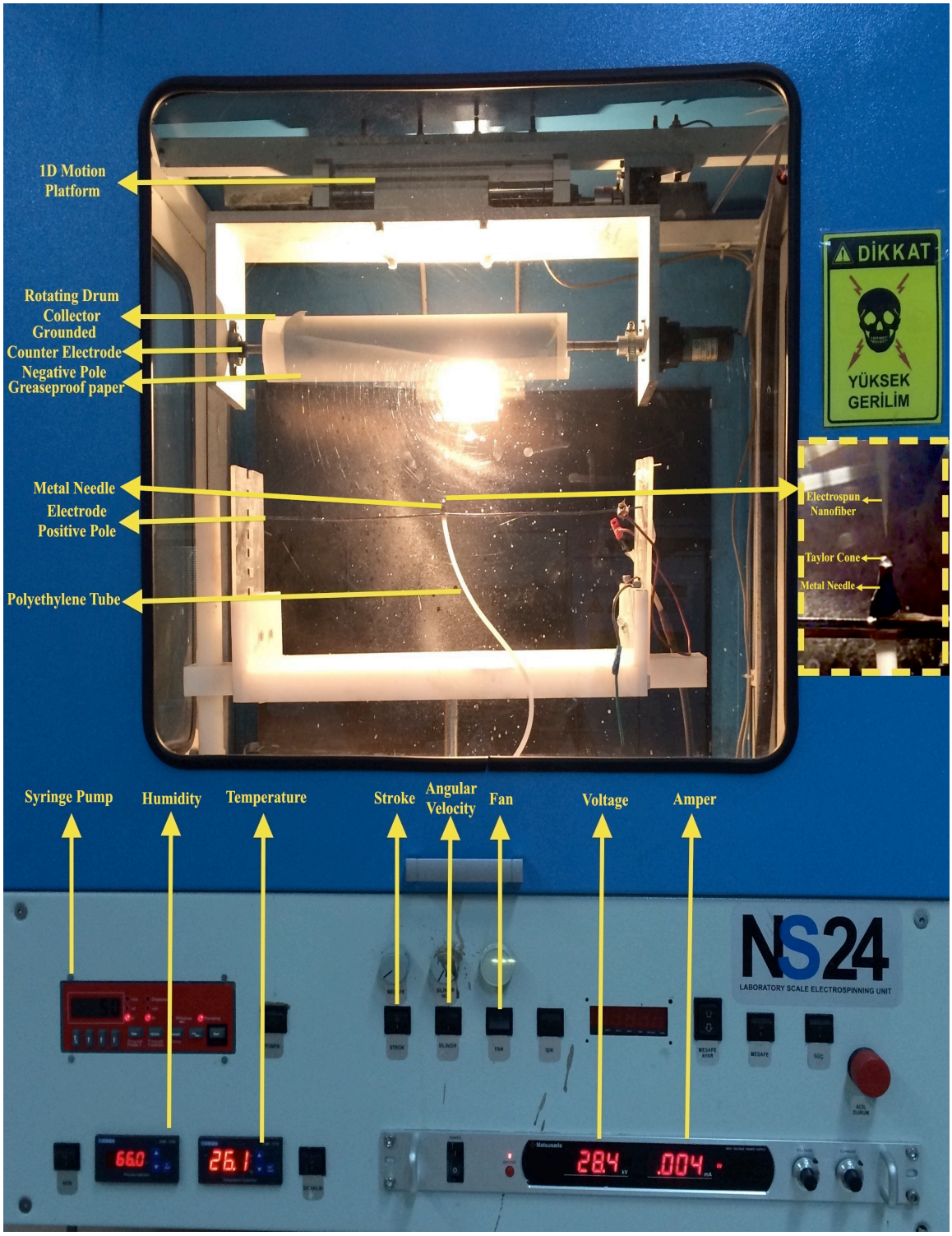

Figure 4.1. Electrospinning device.

making the plumbing of the solution to the nozzle hard due to high viscosity [73-75]. It is also indicated that high viscosity may cause the droplet at the tip of the needle dried, as a result, discontinuity of the jet formation occurs [76].

4.2.1.2. Concentration. The concentration of the solution is one of the major parameters which directly affects the spinnability of the solution, the diameter of the nanofiber, morphology of the scaffold and the ability of cell attachment and viability on the scaffold.

Firstly, when the spinnability of the polymer solution is addressed, the concentration of the solution depends on the molecular weight of the polymer. During the experiments, it is seen that each material has its critical low and high concentration values when considering its interaction with solvent and other dissolved materials. If the polymer concentration of solution is increased, the viscosity increases. Although increase in viscosity make the jet spin more stable, the high value on the viscosity and the concentration cause the droplet at the tip of the needle dried. For this reason, the jet spinning becomes stable when appropriate concentration is achieved.

Secondly, when the diameter of the nanofiber is addressed, the variability of the polymer concentration in the solution affects the fiber diameter [77,78]. As the polymer concentration increases, the fiber diameter increases because when viscosity of the solution increases and the spinning jet at the tip of the needle is avoided from the bending instability. Therefore, the spinning jet is collected in a smaller area by targeting a smaller area. Consequently, the fiber diameter increases [79].

Thirdly, the concentration determines the morphology of the nanofiber scaffold smooth or beaded. If the polymer concentration is below the threshold value, bead formation is detected. If the polymer concentration is suitable such as at threshold value, smooth fibers are detected.

Finally, it is possible to determine the concentration of materials that will assist the reproduction of the cell on the scaffold after certain adjustments have been made.

Therefore, the concentration of materials that will damage the viability of the cell should be optimized and adjusted if necessary.

4.2.1.3. Viscosity. Viscosity of the polymer solution is another prominent parameter which is needed to be adjusted for obtaining consistent and smooth electrospun nanofiber. It is related to the concentration of the polymer solution, the molecular weight of the polymer. There is a relationship between viscosity and the diameter of the fiber. For example, Wang *et al.* found the relationship for electrospinning of polystyrene solutions when flow rate, applied voltage, distance between tip of the needle and the collector, conductivity and surface tension are constant as shown in Equation 4.1 [80],

$$d_f \sim \mu_o^{0.41} \tag{4.1}$$

where d_f is the diameter of the fiber and μ_o is viscosity of polystyrene solutions.

Increase in viscosity of the polymer solution has some consequences. Firstly, if the applied voltage is not increased despite the increase in viscosity, the polymer accumulates and is dried at the tip of the needle [81]. Secondly, increase in viscosity enlarges the diameter of the nanofiber [82, 83]. Finally, increase in viscosity prevent from bead formation [80]

Decrease in viscosity the polymer solution has some consequences. Decrease in viscosity reduces the diameter of the nanofiber. However, if the viscosity is too low, bead formation occurs that's why the electrospun nanofibers are not smooth and consistent [72].

Viscosity is measured by viscometer. In the experiments, DV-E Viscometer (Brookfield AMETEK, Massachusetts, USA) is used as shown in Figure 4.2.

Figure 4.2. Image of viscometer.

4.2.1.4. Electrical Conductivity. Since the basic working principle of electrospinnning is spinning of the polymer solution in the electric field, the electrical conductivity of the polymer solution has an effect on the diameter of the electrospun nanofiber. The ions in the solution are affected and moves from the positive charged electrode to the negatively charged electrode/ grounded collector. Higher conductivity cause narrower fibers due to increase in repulsion associated with electrical forces. Thus, high electrical conductivity of the solution decreases the diameter of the nanofibers as shown in Figure 4.3 [84].

The electrical conductivity of the solution is related to the kind of polymer, the kind of solvent and preferably added salts. If high conductivity is aimed, the salts can be added preferably such as sodium chloride [85].

The electrical conductivity of the solution is measured by an electrical conductivity meter. In the experiment, Cond 3110 SET 1 (Xylem Analytics Germany Sales GmbH & Co. KG, WTW, Weilheim, Germany) is used as shown in Figure 4.4.

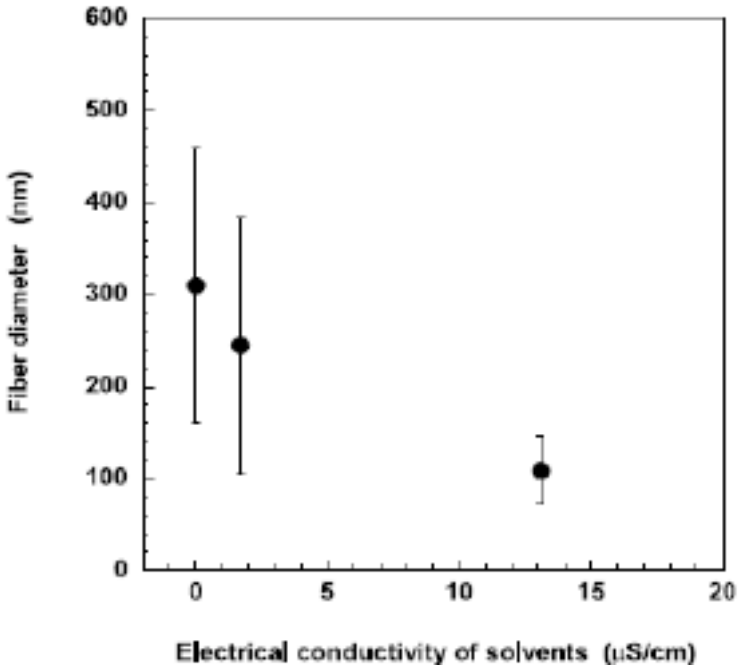

Figure 4.3. The relationship between the electrical conductivity and the diameter of the electrospun PLLA fibers [84].

Figure 4.4. Image of Electrical Conductivity Meter.

4.2.1.5. Surface Tension. From a microscopic point of view, there is a free surface in two kinds of fluid systems or in a system where a liquid interacts with a different environment such gas. The free surface contracts because a molecule on the free surface has imbalance between interaction forces of the neighbor fluid molecules and the outer foreign molecules.

Due to higher attraction forces of the neighbor fluid molecules than the outer foreign molecules, surface tension occurs on the free surface [86, 87].

As a macroscopic view, the capillary force affected on a unit line is given in Equation 4.2 and as shown in Figure 4.5,

$$\Delta\vec{F} = \vec{\sigma}\Delta l \tag{4.2}$$

where $\Delta\vec{F}$ is the capillary force , Δl is line on free surface and $\vec{\sigma}$ is the stress vector of the surface tension which is calculated as shown in Equation 4.3,

$$\vec{\sigma} = \lim_{\Delta l \to 0} \frac{\Delta\vec{F}}{\Delta l} = \frac{d\vec{F}}{dl} \tag{4.3}$$

where dl is the unit line element. $\vec{m}$ is the normal vector of the unit line element as shown in Figure 4.5.

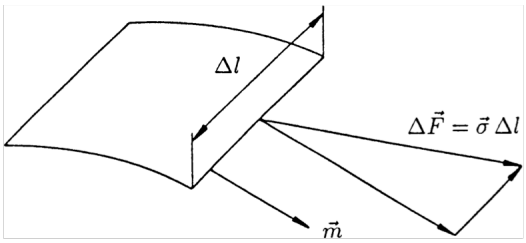

Figure 4.5. Schematic representation of the element of surface tension [86].

Surface tension depends on the polymer and its solvent and temperature. Yang *et al.* [88] pointed out that when all parameters including the concentration of the solution (w/w%) keep constant except the type of the solvent, decrease in surface tension changes the morphology of the fiber from beaded to consistent.

In 1892, Rayleigh investigated a relation between viscosity μ, surface tension σ and the original radius of the fluid jet a with the rate of instability of the fluid jet in, as shown in Equation 4.4 [89, 90].

$$in = \frac{\sigma}{6a\mu} \tag{4.4}$$

In the experiments, surface tension is measured by a tensiometer which is Attension (Biolin Scientific Sigma703/73173 12VDC, Finland) as shown in Figure 4.6.

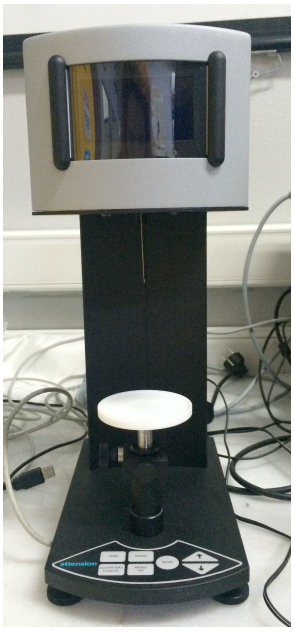

Figure 4.6. Image of the tensiometer.

4.2.2. Process Parameters

4.2.2.1. Feed Rate. Feed rate of the polymer solution is controlled by a syringe pump. It is a significant parameter for adjusting Taylor cone stabilized at the tip of the needle because the challenge of the electrospinning is to obtain homogenized nanofiber mat with consistent diameter.

The change of feed rate of the polymer solution effects directly the morphologies of nanofibers. For instance, Yuan *et al.* [91] pointed out that increase on the flow rate from 0.40 ml/h to 0.66 ml/h make the morphology of nanofibers beads-on-a-string whereas the morphology of nanofibers is smooth at 0.40 ml/h of feed rate.

The feed rate is controlled by manually or a closed loop system. In manual control, the feed rate of the system is adjusted by researchers during the process. In closed loop system, Druesedow *et al.* [92] investigated that feed rate is controlled by a setup with pneumatics and pressure control sensors in order to stabilize the droplet at the tip of the needle.

4.2.2.2. Applied Voltage. The major working principle of electrospinning is based on electric field which provides us convert the polymer solution to nanofiber scaffold with transfering ions from the tip of the needle to the collector. Therefore voltage is an important parameter for manipulating the electric field. To obtain stable spinning and Taylor cone, voltage is adjusted to consistent value which depends on the concentration of the solution, the distance between the tip of the needle and the collector, feed rate and the environmental conditions. When the variability of all these parameters is taken into account, the appropriate voltage is obtained in a narrow scale.

In 1995, Doshi and Reneker [93] highlighted that the applied voltage should be above the threshold value which depends on the surface tension of the polymer solution. If the applied voltage is adjusted to much more higher than the threshold value, spinning is not stable and multi-headed Taylor cone is seen.

The effect of change of the applied voltage on the diameter of the nanofibers is a controversial issue. Some researchers claim that higher voltages increase the size of the fibers. For instance, Demir *et al.* [94] pointed out that increase in applied voltage increase the diameter of the polyurethane fibers. In addition, Coles *et al.* [95] found that increase in applied voltage increase the diameter of the poly (vinyl alcohol) fibers.

Some researchers claim that higher voltage decreases the diameter of the fibers. For instance, Yuan *et al.* [91] found that increase in applied voltage decrease the diameter of the polysulfone (PSF)/DMAC/acetone.

Reneker and Chun [96] claim that the diameter of the fibers is not directly dependent on the applied voltage.

The effect of change of the applied voltage on beads formation is investigated by some research groups that increase in applied voltages can cause the beads formation [94, 97, 98].

4.2.2.3. Collector. Grounded collector is the negative pole of the electrospinning setup. The charged droplet of the polymer solution moves from the tip of the needle to the ground collector. As shown in Figure 4.7, there are various designs for the grounded collector such as rotating drum collector, flat plate, parallel plates /stripes, rotating disk (flat edge), rotating disc (sharp edge) and conveyor [99].

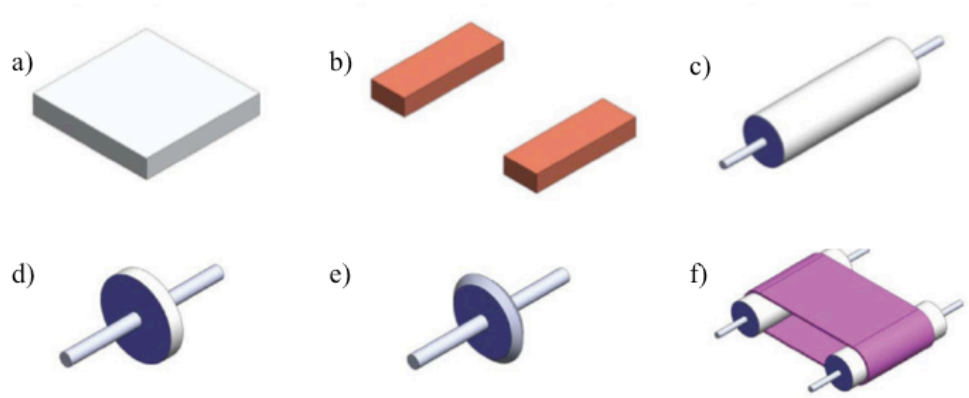

Figure 4.7. The various geometries of the grounded collector: a) Flat plate, b) Parallel plates /stripes, c) Rotating drum, d) Rotating disk (flat edge), e) Rotating disc (sharp edge), f) Conveyor [99].

The nanofibers could be transferred from the collector. Under some conditions, the fibers are not transferred that's why these new geometries of the collector are designed. In addition, the fiber orientation is also effected by the various geometries of the grounded collector.

4.2.2.4. Distance Between the Tip of the Needle and the Grounded Collector. Distance between the tip of the needle and the grounded collector is another parameter for the electric field that's why it affects the morphologies of the nanofibers and the diameters of the nanofibers. If the distance increases, there is bead formation. If the distance decreases, there is no time to formation of the nanofibers and solidify for the polymer solution on the

collector. Yuan *et al.* [91] indicated that increase in distance between the tip of the needle and the grounded collector decreases the diameter of the nanofibers.

4.2.2.5. The Diameter of the Needle. The diameter of the needle is another major parameters for the spinning jet. It affects the fiber diameter and the morphology of the fiber. Firstly, due to viscosity of the polymer solution, there is surface friction in the needle that's why the diameter of the needle should be chosen appropriately. If the diameter of the needle increases, surface tension increases that's why it is necessary to increase the applied voltage of the system to break the surface tension of the droplet [100]. Secondly, some researchers claim that increase on the diameter of the needle increases the diameter of the nanofibers [101, 102]. On the contrary, some researchers cannot find significant correlation between the diameter of the fibers and the diameter of the needle [103].

4.2.3. Ambient Parameters

Environmental conditions also affect the fiber size and morphology as well as process parameters. Temperature and humidity are the major parameters of the ambient parameters.

Firstly, temperature can affect the viscosity of the polymer solution adversely. For example, Mituppatham *et al.* [79] demonstrated that decrease in the ambient temperature increases the diameter of the fibers due to temperature's adverse effect on the viscosity of the polymer solution.

Secondly, humidity affects the surface morphology of the nanofibers. The smooth surface of the fibers becomes porous surface due to increase in humidity. For instance, Casper *et al.* [104] pointed out that smooth nanofibers are obtained in an ambient humidity below 25 % whereas porous nanofibers are obtained in 60-72 % of the ambient humidity as shown in Figure 4.8.

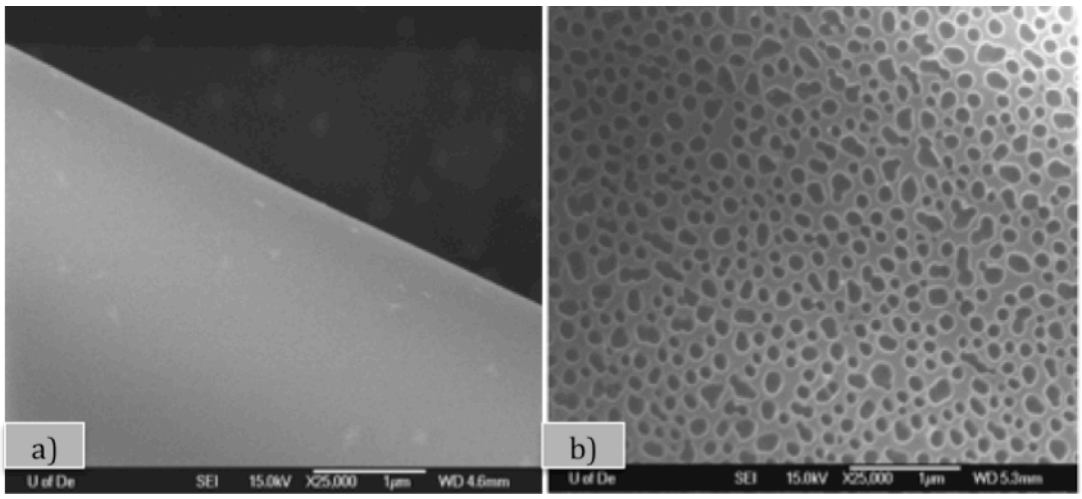

Figure 4.8. The surface morphologies of the nanofibers at the different values of humidity: a) below 25%, b) 60-72 % [104].

5. EXPERIMENT

5.1. Materials

Polycaprolactone PCL (Mn = 80,000 g/mol) is purchased from Sigma–Aldrich, St. Louis, MO, USA. Bovine Gelatin powder Type A (Bloom number: 250) is purchased from Halavet, Istanbul, Turkey. Bovine hydroxyapatite is supplied by the laboratory. Acetic acid (%99) and formic acid (%99) are purchased from Sigma–Aldrich, St. Louis, MO, USA.

5.2. Selection of the Solvent System

One of the aims is to create a non-toxic solvent system for which acetic acid (AA) and formic acid (FA) are selected. To achieve solutions with minimum toxicity for electrospinning and to prepare spinnable solutions for appropriate tests, four solvent systems are prepared such as 0:1 % v/v of AA:FA, 1:0 % v/v of AA:FA, 90:10 % v/v of AA:FA and finally 1:1 % v/v of AA:FA.

The experiments are performed in order to find a appropriate non-toxic solution system such as summarized in Table 5.1 with the statements.

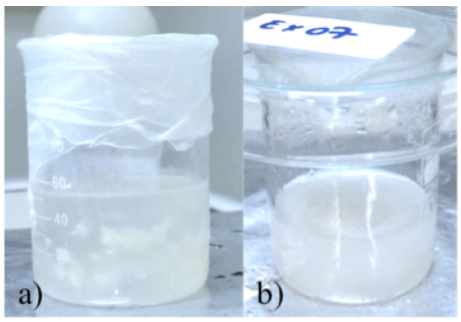

Figure 5.1. Image of spinnability: a) Nonspinnable solution, b) Spinnable solution.

Table 5.1. Parameters of alternate solution systems and the spinnabilities'.

The concentrations of the solution PCL/GE/BHA % w/w in a solvent system	**The concentration of AA:FA solvent system % v/v**	**Statement**	**Spinnability**
12/1/0.5	0:1	High Viscosity	Non-Spinnable
12/1/0.5	1:0	Low solubility of Gelatin with PCL	Inappropriate
12/1/0.5	90:10	High Aggregation of BHA	Inappropriate
12/1/0.5	1:1	Suitable	Spinnable

As it can be seen in Table 5.1, the concentrations of PCL/GE/BHA % w/w in a solvent system are kept constant to find the appropriate solvent system while the ratio of the concentrations of solvent is changed by % v/v. While the concentrations of the solution PCL/GE/BHA is 12/1/0.5 % w/w in 0:1 % v/v AA:FA solvent system, the significant problem is high viscosity of the solution that's why the solution is non-spinnable as can be seen in Figure 5.1.a. When the concentrations of the solution PCL/GE/BHA is 12/1/0.5 % w/w in 1:0 % v/v AA:FA solvent system, the main problem is low solubility of Gelatin with PCL that's why the solution is not adequate for electrospinning. Whilst the concentrations of the solution PCL/GE/BHA is 12/1/0.5 % w/w in 90:10 % v/v AA:FA solvent system, an another major problem is high aggregation of BHA as the solution is not suitable for electrospinning. Table 5.1 shows that the suitable spinnable solvent system is decided as 1:1 % v/v of AA:FA as can be seen in Figure 5.1.b.

5.3. Preparation of the Solutions

The procedures of the adding materials in a solution system are specified according to the experiments. Firstly, PCL is added into the solvent system which is stirred in a 100 ml of beaker on a magnetic stirrer (Wisestir) for 30 min at 60°C. Secondly, bovine gelatin (GE) is added into the same beaker which is stirred at the same magnetic stirrer for 30 min at 500 rev/min and 40°C. Finally, BHA is added into the final solution system which is stirred on the magnetic stirrer at 500 rev/min for 24 hours at room temperature.

5.4. Solution Parameters

5.4.1. Concentration

5.4.1.1. The Concentration of BHA as a Variable. As shown in Table 5.1 and Table 5.2, 12/1/0.5 wt% PCL/GE/BHA is a control group of all experiments in order to investigate the effects of the change in concentrations of bovine hydroxyapatite on the nanofiber scaffolds. Therefore, PCL, Gelatin and AA: FA solvent system is selected as constant, bovine hydroxyapatite is selected as a variable in Table 5.2. The constant values of PCL, Gelatin and AA:FA solvent system are 12 % w/w, 1 % w/w and 1:1 v/v respectively. The concentrations of bovine hydroxyapatite are varied as 0.5 % w/w, 1 % w/w and 2 % w/w.

Table 5.2. The concentrations of the polymer solutions prepared by changing the ratio of bovine hydroxyapatite.

Experiment	The concentration of PCL % w/w	The concentration of Gelatin % w/w	The concentration of BHA % w/w	The Solvent System AA:FA % v/v	The volume of AA:FA mL	Name in the Thesis PCL/GE/ BHA wt %
Experiment 1	12	1	0.5	1:1	25:25	12/1/0.5
Experiment 2	12	1	1	1:1	25:25	12/1/1
Experiment 3	12	1	2	1:1	25:25	12/1/2

5.4.1.2. The Concentration of GE as a Variable. As shown in Table 5.1 and Table 5.3, 12/1/0.5 wt% PCL/GE/BHA is a control group of all experiments in order to investigate the effects of the change in concentrations of gelatin on the nanofiber scaffolds. Therefore, PCL, bovine Hydroxyapatite and AA: FA solvent system is selected as constant, bovine gelatin is selected as a variable in Table 5.3. The constant values of PCL, bovine Hydroxyapatite and AA: FA solvent systems are 12 % w/w, 0.5 % w/w and 1:1 v/v respectively. The concentrations of Bovine gelatin are varied as 0.5 % w/w, 1 % w/w and 1.5 % w/w. The maximum concentration of Bovine Gelatin in the solution is 1.5 % w/w otherwise the sample can not be taken from oily paper foil or aluminum foil so 1.5 % w/w of gelatin in the solution is a limitation for the experiment.

Table 5.3. The concentrations of the polymer solutions prepared by changing the ratio of bovine gelatin.

Experiment	The concentration of PCL % w/w	The concentration of Gelatin % w/w	The concentration of BHA % w/w	The solvent System AA:FA % v/v	The volume of AA:FA mL	Name in the Thesis PCL/GE/ BHA wt %
Experiment 4	12	0.5	0.5	1:1	25:25	12/0.5/0.5
Experiment 1	12	1	0.5	1:1	25:25	12/1/0.5
Experiment 5	12	1.5	0.5	1:1	25:25	12/1.5/0.5

5.4.2. Density

5.4.2.1. Experiment 1, 2, 3. By changing BHA concentration in the polymer solution, its effect on the density of the polymer solutions of the change is listed in Table 5.4. It is observed that increase in BHA concentration in the polymer solution causes slightly increase on the densities.

Table 5.4. The density of the solutions prepared by changing the ratio of BHA.

Experiment	Density (g/ml)	PCL/GE/BHA (wt %)
Experiment 1	1.119	12/1/0.5
Experiment 2	1.119	12/1/1
Experiment 3	1.122	12/1/2

5.4.2.2. Experiment 1, 4, 5. By changing GE concentration in the polymer solution, its effect on the density of the polymer solutions of the change is listed in Table 5.5. It is observed that increase in GE concentration in the polymer solution causes slightly increase on the densities.

Table 5.5. The density of the solutions prepared by changing the ratio of GE.

Experiment	Density (g/ml)	PCL/GE/BHA (wt %)
Experiment 4	1.118	12/0.5/0.5
Experiment 1	1.119	12/1/0.5
Experiment 5	1.119	12/1.5/0.5

5.4.3. Viscosity

5.4.3.1. Experiment 1, 2, 3. By changing BHA concentration in the solution, its effect on the viscosity of the polymer solutions of the change is listed in Table 5.6. Comparing Experiment 1 to Experiment 2, it is observed that when the concentration of BHA in the solution is increased by 0.5%, the viscosity is increased by 7.43 %. Comparing Experiment 1 to Experiment 3, it is observed that when the concentration of BHA in the solution is increased by 1.5 %, the viscosity is increased by 22.82 %.

Table 5.6. The viscosity of the solutions prepared by changing the ratio of BHA.

Experiment	Viscosity (mPa.s)	PCL/GE/BHA (wt %)
Experiment 1	700.6	12/1/0.5
Experiment 2	752.7	12/1/1
Experiment 3	860.5	12/1/2

5.4.3.2. Experiment 1, 4, 5. By changing GE concentration in the polymer solution, its effect on the viscosity of the polymer solutions of the change is listed in Table 5.7. Comparing Experiment 1 to Experiment 5, it is observed that when the concentration of GE in the solution is increased by 0.5%, the viscosity is increased by 71.63 % that's why 1.5 % of gelatin is limitation for the spinnability.

Table 5.7. The viscosity of the prepared by changing the ratio of GE.

Experiment	Viscosity (mPa.s)	PCL/GE/BHA (wt %)
Experiment 4	686.5	12/0.5/0.5
Experiment 1	700.6	12/1/0.5
Experiment 5	1202.5	12/1.5/0.5

5.4.4. Surface Tension

5.4.4.1. Experiment 1, 2, 3. By changing BHA concentration in the solution, its adverse effect on the surface tension of the polymer solutions of the change is listed in Table 5.8. Comparing Experiment 1 to Experiment 2, it is observed that when the concentration of BHA in the solution is increased by 0.5%, the surface tension is decreased by 5.52 %.

Table 5.8. The surface tension of the solutions prepared by changing the ratio of BHA.

Experiment	Surface Tension (mN/m)	PCL/GE/ BHA (wt %)
Experiment 1	30.60	12/1/0.5
Experiment 2	28.91	12/1/1
Experiment 3	29.83	12/1/2

5.4.4.2. Experiment 1, 4, 5. By changing GE concentration in the solution, its adverse effect on the surface tension of the polymer solutions of the change is listed in Table 5.9. Comparing Experiment 1 to Experiment 5, it is observed that when the concentration of GE in the solution is increased by 0.5%, the surface tension is decreased by 0.22 %. Comparing Experiment 4 to Experiment 5, it is observed that when the concentration of GE in the solution is increased by 1%, the surface tension is decreased by 1.35 %.

Table 5.9. The surface tension of the solutions prepared by changing the ratio of GE.

Experiment	Surface Tension (mN/m)	PCL/GE/ BHA (wt %)
Experiment 4	30.95	12/0.5/0.5
Experiment 1	30.60	12/1/0.5
Experiment 5	30.53	12/1.5/0.5

5.4.5. Electrical Conductivity

5.4.5.1. Experiment 1, 2, 3. As shown in Table 5.10, comparing Experiment 1 to Experiment 2, it is observed that when the concentration of BHA in the solution is increased by 0.5%, the electrical conductivity is increased by 32.01 %. Comparing

Experiment 1 to Experiment 3, it is observed that when the concentration of BHA in the solution is increased by 1.5%, the electrical conductivity is increased by 100.37 %.

Table 5.10. The electrical conductivity of the solutions prepared by changing the ratio of BHA.

Experiment	**Electrical Conductivity (µS/cm)**	**PCL/GE/ BHA (wt %)**
Experiment 1	531	12/1/0.5
Experiment 2	701	12/1/1
Experiment 3	1064	12/1/2

5.4.5.2. Experiment 1, 4, 5. As shown in Table 5.11, comparing Experiment 1 to Experiment 5, it is observed that when the concentration of GE in the solution is increased by 0.5%, the electrical conductivity is increased by 17.51 %. Comparing Experiment 4 to Experiment 5, it is observed that when the concentration of GE in the solution is increased by 0.5%, the electrical conductivity is increased by 37.44 %. The difference between Table 5.10 and Table 5.11 shows that BHA particles have higher electrical conductivity than GE.

Table 5.11. The electrical conductivity of the solutions prepared by changing the ratio of GE.

Experiment	**Electrical Conductivity (µS/cm)**	**PCL/GE/ BHA (wt %)**
Experiment 4	454	12/0.5/0.5
Experiment 1	531	12/1/0.5
Experiment 5	624	12/1.5/0.5

5.5. Process Parameters of Electrospinning

The parameters determined during the manufacture of the nanofibers are summarized in Table 5.12 to Table 5.16.

5.5.1. Experiment 1

12/1/0.5 wt % (PCL/GE/BHA) electrospun nanofibers' process parameters are summarized in Table 5.12. The inner diameter of the nozzle is 0.95 mm and the outer diameter of the nozzle is 2.45 mm. The distance between nozzle and the drum collector is adjusted to 12 cm. In the first and second test, feeder pump is adjusted to 100 µl/h and 150 µl/h of feed rate when the applied voltages are attuned at 26.5 kV and 28.4 kV respectively. However, the needle tip is clogged. For this reason, 120 µl/h of flow rate is finally adjusted between the upper and lower values of the flow rates while the applied voltage is set at 28.2 kV so that the stable process could be obtained at 63.3 % of humidity and 27.7 °C of temperature °C.

Table 5.12. Process parameters of 12/1/0.5 wt % (PCL/GE/BHA) electrospun nanofibers.

Test	Diameter of Nozzle Inner-outer (mm)	Distance between nozzle and the drum collector (cm)	Feed Rate (µl/h)	Applied Voltage (kV)	Humidity (%)	Temperature (°C)	Statement
1	0.95 - 2.45	12	100	26.5	63.8	25.8	Needle tip was clogged.
2	0.95 - 2.45	12	150	28.4	63.2	25.9	Needle tip was clogged
3	0.95 - 2.45	12	120	28.2	63.3	27.7	Stable process

5.5.2. Experiment 2

12/1/1 wt % (PCL/GE/BHA) electrospun nanofibers' process parameters are summarized in Table 5.13. The inner diameter of the nozzle is 0.95 mm and the outer diameter of the nozzle is 2.45 mm. The distance between nozzle and the drum collector is adjusted to 12 cm. Feeder pump is adjusted to 129 µl/h of feed rate when the applied voltages is attuned at 26.9 kV so that the stable process could be obtained at 56 % of humidity and 23.8 °C of temperature °C.

Table 5.13. Process parameters of 12/1/1 wt % (PCL/GE/BHA) electrospun nanofibers.

Test	Diameter of Nozzle Inner-outer (mm)	Distance between nozzle and the drum collector (cm)	Feed Rate (µl/h)	Applied Voltage (kV)	Humidity (%)	Temperature (°C)	Statement
1	0.95 - 2.45	12	129	26.9	56	23.8	Stable process

5.5.3. Experiment 3

12/1/2 wt % (PCL/GE/BHA) electrospun nanofibers' process parameters are summarized in Table 5.14. The inner diameter of the nozzle is 0.95 mm and the outer diameter of the nozzle is 2.45 mm. The distance between nozzle and the drum collector is adjusted to 12 cm. In the first test, feeder pump is adjusted to 129 µl/h of feed rate when the applied voltage is attuned at 26.8 kV. However, a splatter of solution on the foil on the rotating drum is occurred as unstable that's why the foil is renewed. In the second test, feeder pump is adjusted to 130 µl/h of feed rate when the applied voltage is attuned at 19.2 kV. However, unstable multi-headed Taylor cone on the needle tip is formed and the needle tip is constantly drying. For this reason, 130 µl/h of flow rate is finally adjusted at the same value while the applied voltage is set at 24.9 kV so that the stable process could be obtained at 65 % of humidity and 26°C of temperature.

5.5.4. Experiment 4

12/0.5/0.5 wt % (PCL/GE/BHA) electrospun nanofibers' process parameters are summarized in Table 5.15. The inner diameter of the nozzle is 0.95 mm and the outer diameter of the nozzle is 2.45 mm. The distance between nozzle and the drum collector is adjusted to 12 cm. Feeder pump is adjusted to 600 µl/h of feed rate when the applied voltages is attuned at 36.9 kV so that the stable process could be obtained at 63.9 % of humidity and 24.8°C of temperature.

Table 5.14. Process parameters of 12/1/2 wt % (PCL/GE/BHA) electrospun nanofibers.

Test	Diameter of Nozzle Inner-outer (mm)	Distance between nozzle and the drum collector (cm)	Feed Rate (µl/h)	Applied Voltage (kV)	Humidity (%)	Temperature (°C)	Statement
1	0.95 - 2.45	12	129	26.8	64.8	21.9	Accumula-tion on paper
2	0.95 - 2.45	12	130	19.2	66.7	22.5	Constantly drying Multi-headed Taylor cone on the needle tip
3	0.95 - 2.45	12	130	24.9	65	26	Stable process

Table 5.15. Process parameters of 12/0.5/0.5 wt % (PCL/GE/BHA) electrospun nanofibers.

Test	Diameter of Nozzle (mm)	Distance between nozzle and the drum collector (cm)	Feed Rate (µl/h)	Applied Voltage (kV)	Humidity (%)	Temperature	Statement
1	0.95 - 2.45	15	600	36.9	63.9	24.8	Stable process

5.5.5. Experiment 5

12/1.5/0.5 wt % (PCL/GE/BHA) electrospun nanofibers' process parameters are summarized in Table 5.16. The inner diameter of the nozzle is 0.95 mm and the outer diameter of the nozzle is 2.45 mm. The distance between nozzle and the drum collector is adjusted to 12 cm. In the first test, feeder pump is adjusted to 500 µl/h of feed rate when the applied voltage is attuned at 26.6 kV. However, overflowed of the solution on the needle tip is occurred that's why the Taylor cone is unstable. In the second test, feeder pump is adjusted to 100 µl/h of feed rate when the applied voltage is attuned at 18 kV. However, solution does not come to the tip of the needle and the needle tip is constantly drying because of low feed rate. For this reason, 200 µl/h of flow rate is finally adjusted by increasing the previous value of feed rate while the applied voltage is set at 19.7 kV so that the stable process could be obtained at 61.7 % of humidity and 23.9°C of temperature.

Table 5.16. Process parameters of 12/1.5/0.5 wt % (PCL/GE/BHA) electrospun nanofibers.

Test	Diameter of Nozzle Inner-outer (mm)	Distance between nozzle and the drum collector (cm)	Feed Rate (µl/h)	Applied Voltage (kV)	Humidity (%)	Temperature	Statement
1	0.95 - 2.45	12	500	26.6	58.3	21.7	Overflowed on the needle tip
2	0.95 - 2.45	12	100	18	59.8	23	Low feed rate Solution does not come to the tip of the needle
3	0.95 - 2.45	12	200	19.7	61.7	23.9	Stable process

5.6. Characterization of Electrospun Nanofibers

5.6.1. Scanning Electron Microscope (SEM)

The morphological characterization of the nanofibers is investigated by using a scanning electron microscope (SEM). SEM is used to monitor high-resolution texture, orientation and crystalline structure of objects by a focused beam of high-energy electrons as a working principle. The sample preparations are necessary before using SEM. The preparations are simple or complex according to the samples' characteristics and the requested information. Commonly carbon, gold, platinum etc. are used to coat the sample.

In this study, platinum coating is suitable for high resolution imaging. The nanofiber samples are coated by Polaron SC7640 Sputter Coater as shown in Figure 5.2. Chamber pressure is adjusted to 0.2 mbar before coating process. The coating voltage and plasma current are adjusted to 18 kV and 18mA respectively. The coating time is 90 seconds. Orientation of nanofibers and diameter of the each fiber are examined.

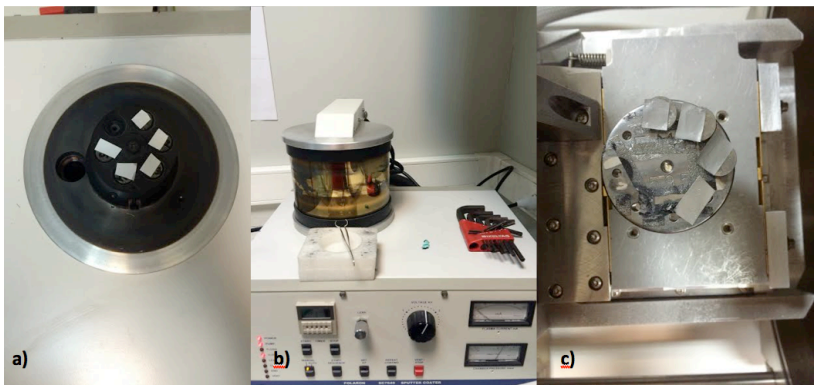

Figure 5.2. The coating process of the samples before SEM: a) Uncoated nanofiber samples, b) Polaron SC7640 Sputter Coater, c) Coated samples on the SEM tab.

As shown in Figure 5.3, each of the nanofiber samples is monitored by scanning electron microscope (SEM), Philips XL30 ESEM-FEG. The magnifications of the SEM images are x1000, x2000, x5000, x10000, x20000, x50000 and x100000 for each of the samples as can be seen in Figure 5.4.

Figure 5.3. The image of scanning electron microscope (SEM), Philips XL30 ESEM-FEG.

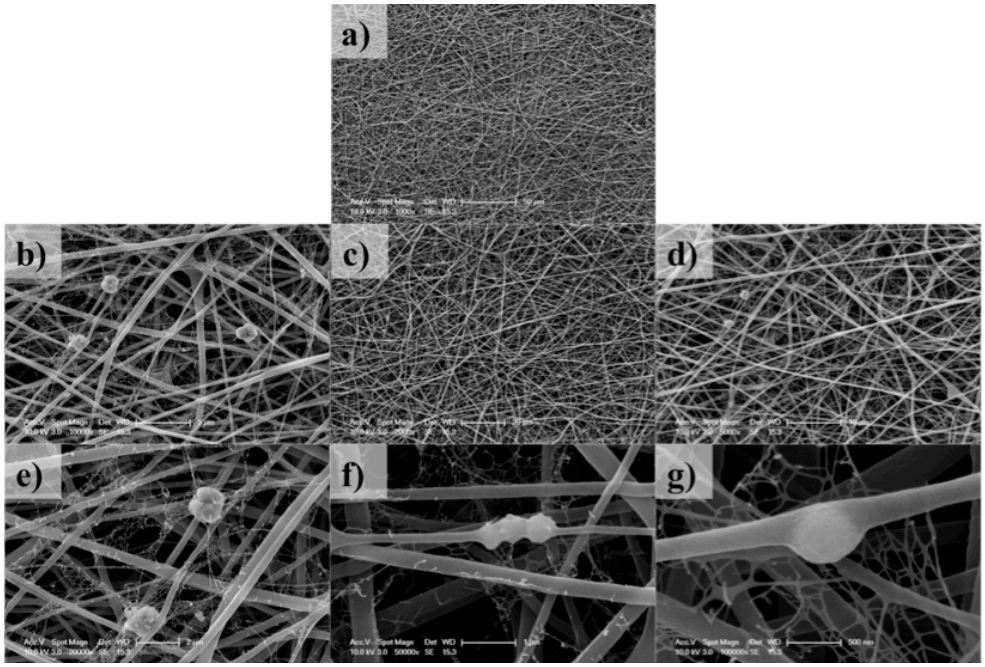

Figure 5.4. The magnifications of the SEM images of one of the samples such as 12/1.5/0.5 wt % PCL/GE/BHA: a) x1000, b) x2000, c) x5000, d) x10000, e) x20000, f) x50000 and g) x100000 .

5.6.2. Fourier Transform Infrared Spectroscopy (FTIR)

Transform Infrared Spectroscopy (FTIR) detect chemical bonds such as covalent bonds and functional groups of the electrospun nanofibers by generating an infrared absorption spectrum at a wavenumber range of 400- 4000 cm^{-1} . In Encyclopedia of Analytical Chemistry, John Coates is listed the frequency of all functional groups.

To characterize the nanofibers, it is necessary to know the specific chemical bonds of each material. In Table 5.17, the frequency of PCL's, gelatin's and hydroxyapatite's functional groups are summarized based on John Coates's [105]. PCL has specifically chemical bonds to be considered such as asymmetric Methylene (CH_2) C-H stretching, the symmetric Methylene (CH_2) C-H stretching, C-O C-C carbonyl stretching and asymmetric C-O-C stretching. Gelatin has specifically chemical bonds to be considered such as Amide I and Amide II. Hydroxyapatite has specifically resonances of the ions to be considered such as phosphate ion $(PO_4)^-$ and carbonate ion (CO_3).

Table 5.17. The group frequencies of functional groups for PCL/GE/BHA [105].

Group frequency (cm^{-1})	**Functional group**
1490 – 1410 (intense) 880 – 860 (weak)	Carbonate ion
1100–1000	Phosphate ion
2935 – 2915	Asymmetric Methylene C-H stretching
2865 – 2845	Symmetric Methylene C-H stretching
1320 – 1210	Carbonyl stretching C-O
1680 – 1630	Amide I

These chemical bonds are examined at a wavenumber range of 400- 4000 cm-1 by Fourier Transformation Infrared Spectroscopy (JASCO FT/IR-4700 Spectrometer) as shown in Figure 5.5. In Table 5.18, the group frequencies of functional groups are

summarized for the electrospun nanofibers of the similar materials such as the different types of gelatin blended with PCL [71, 106]. The data are compared in the section of the results of the thesis.

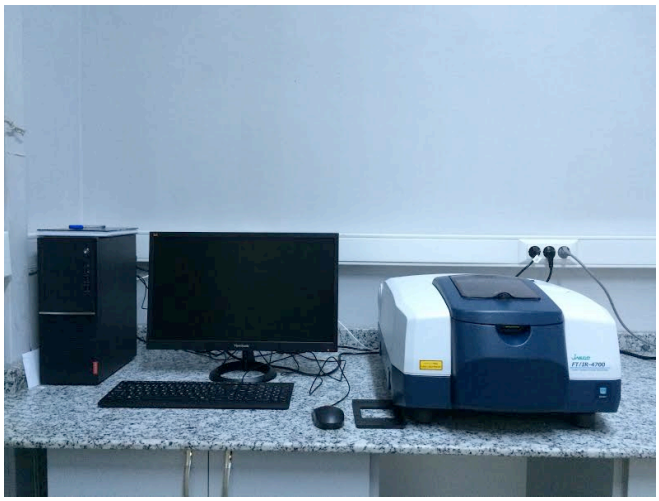

Figure 5.5. The image of Fourier transformation infrared spectroscopy.

Table 5.18. The group frequencies of functional groups for PCL/GE [69, 106].

Group frequency (cm $^{-1}$)		**Functional group**
Chong *et al.* [69]	Rather *et al.* [106]	
PCL/GE	PCL/GE	
2949	2943	Asymmetric Methylene C-H stretching
2865	2865	Symmetric Methylene C-H stretching
1293	Undefined	Carbonyl stretching C-O
1240	Undefined	Asymmetric C-O-C stretching
1650	1640	Amide I C=O
1540	1540	Amide II N—H

5.6.3. Mechanical Test

As used for defining the mechanical properties of metals, the mechanical properties of polymers are also identified with some of the identical parameters, which are modulus of elasticity, yield stress and ultimate tensile strength [107]. The simple stress–strain test is utilized for the specification of some of the tensile properties of many polymers or their composites [108].

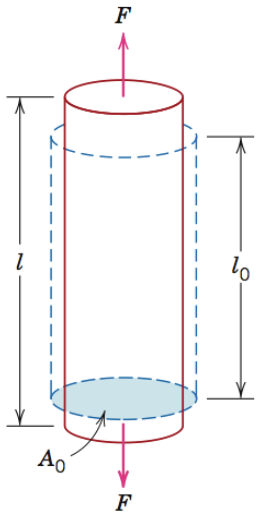

Figure 5.6. A representation of a specimen during the tensile test [107].

As shown in Figure 5.6, blue dashed lines refer to the specimen's initial sizes with the initial length l_0 and the initial area A_0 before the tensile testing. F is instantaneous load. After F load is applied, l or l_i is the instantaneous length of the specimen. Elongation due to deformation, Δl, refers to l_i - l_0. Figure 5.6 shows that the strain is positive in the uniaxial tensile test [107].

When the specimen is positioned at the holding grips of the tensile test machine, load F and elongation Δl are measured by a tensile test machine by running a its software. The force – elongation data depend on the specimen's dimension. During the test, area of the specimen changes. However, if there is not a sensor to define the instantaneous area of the specimen, engineering stress σ and engineering strain ε are calculated for specifying the mechanical properties of the material. In order to reduce size factors, force and elongation

are normalized to engineering stress σ and engineering strain because engineering stress σ and engineering strain ε are calculated from the specimen's initial dimensions [107]. Engineering stress σ is calculated as Equation 5.1.

$$\sigma = \frac{F}{A_0} \tag{5.1}$$

F is instantaneous load or force which is applied from the center of the specimen' cross-sectional area to outside and perpendicular to the cross-sectional area of the specimen. In SI unit system, Newton N is the unit of force F. A_0 is the initial area before the tensile testing. The unit of A_0 *is* m^2. The unit of engineering stress σ is megapascals, MPa (10^6 Pa = 10^6 N/m^2).

Engineering strain ε is calculated as Equation 5.2.

$$\varepsilon = \frac{l_i - l_0}{l_0} = \frac{\Delta l}{l_0} \tag{5.2}$$

l_i is the instantaneous length of the specimen, l_0 is the initial length of specimen, the unit is meter, m. Δl is elongation due to deformation which is written as the units of meter, m. ε is engineering strain which is unitless because of m/m. It can be preferably used in percentage where ε is multiplied by 100.

Ultimate tensile strength (UTS), Young's Modulus (E), strain at UTS, load at UTS, elongation at UTS, tensile stress at fracture are significant data for defining the reliability of artificial bone tissue. For the reason, the mechanical properties of the nanofiber samples are tested by Instron 4411 Tensile Strength Tester in Figure 5.7.

As can be seen in Figure 5.8, the samples are cut from three different sites of each scaffold by a hammer and a rectangular size of 50 mm x 10 mm metal mold (Figure 5.8.a) in order to obtain the tensile test specimens (Figure 5.8.b).

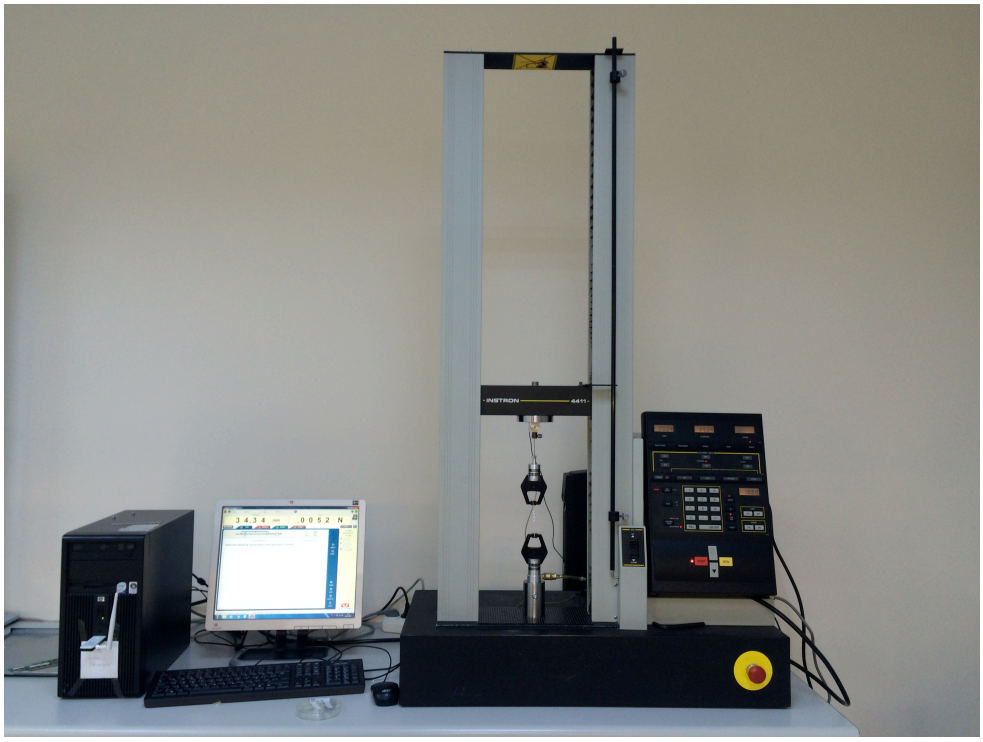

Figure 5.7. The image of the tensile test machine.

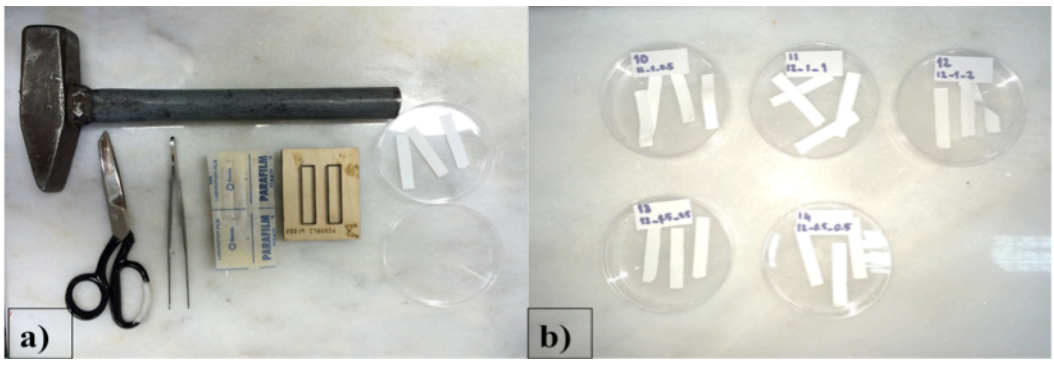

Figure 5.8. The dimensions of the specimen.

After the samples are cut into 50 mm x 10 mm size [109-113], the thicknesses of the specimens are measured by high-accuracy digimatic micrometer (Mitutoyo's 0.1μm resolution ABS (absolute) rotary sensor) as shown in Figure 5.9. The strain rate of universal tensile test machine is adjusted to 10 mm/min. The tensile test is performed at 20°C. The test is performed according to American Society for Testing and Materials (ASTM), Standard Test Method for Tensile Properties of Thin Plastic Sheeting (ASTM D882) [113]. As shown in Figure 5.10, the tensile testing is applied on a sample of

12/0.5/0.5 wt % PCL/GE/BHA. Initial image of the sample without load is seen in Figure 5.10.a. At 50 sec, necking is clearly seen. In Figure 5.10.b, At 130.6 sec, fracture is clearly seen in Figure 5.10.e.

Figure 5.9. The image of high-accuracy digimatic micrometer.

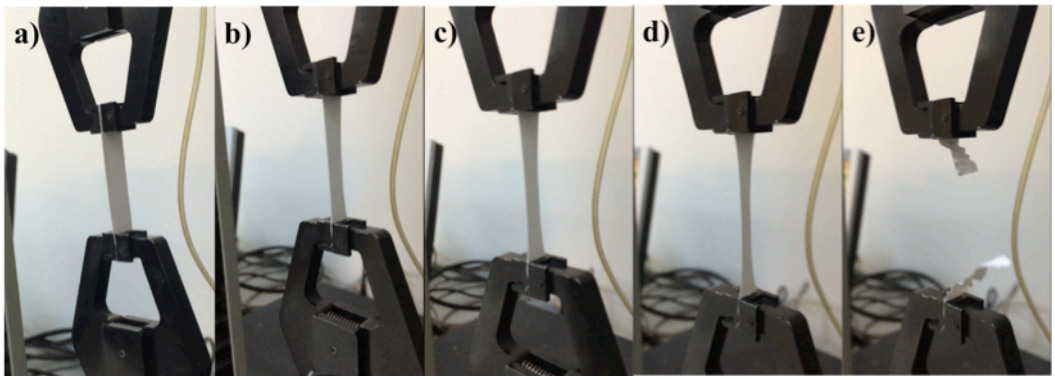

Figure 5.10. The tensile test images of a sample of 12/0.5/0.5 wt % PCL/GE/BHA at: a) 0 sec , b) 10 sec, c) 50 sec, d) 130.4 sec , e) 130.6 s.

5.6.4. Biological Test

In order to examine the cell viability on the samples, biological tests are applied such as MTT Cell Proliferation Assay Protocol and Cell Attachment SEM Protocol.

Human osteogenic sarcoma (human osteoblastic-like Saos-2 cell line) and mouse fibroblast (3T3 cell line) are obtained from ATCC. Cells are cultured in Dulbecco's modified Eagle medium (DMEM, Gibco) with 10% Fetal bovine serum (FBS, Gibco) and 1% penicillin/streptomycin in a humidified air 5% CO_2/95% air incubator. Culture incubation is fixed at 37^oC. When the cells are reached approximately 80% confluency, they are washed with phosphate buffer saline (PBS). They are trypsinized with 0.25% Trypsin/EDTA for each passage and each seed. The confluent cells are used in cell growth.

5.6.4.1. MTT Cell Proliferation Assay. Mossman's MTT Cell Proliferation Assay [114] procedure is applied. After the 5 mm x 10 mm samples are sterilized for 2 hours with UV, 3T3 cells and Saos-2 cells are seeded on the samples. MTT assay is performed in 96-well plates in Figure 5.11. Approximately 10^5 cells are seeded per well. The seeded samples are incubated for 24 hours, 48 hours, and 72 hours.

MTT Assay is a colorimetric assay [109]. When yellow colored 3-(4,5-dimethythiazol- 2-yl)-2,5-diphenyl tetrazolium bromide (MTT) enters the cell, mitochondria of the active cells produce dark purple-blue formazan which is partially soluble in the medium. The production of dark purple-blue formazan shows viable cell number and the degree of cytotoxicity. It is incubated in dark for 3.5- 4 hours at a humidified air 5% CO_2/95% air incubator at 37^oC. After 4 hours of incubation, the mixture is removed and 100 μL of dimethyl sulfoxide (DMSO) per well is added in order to make formazan soluble and homogenous in the medium. The optical density of formazan dye is recorded using microplate spectrophotometer (Kayto RT-2100C) at wavelength of 570 nm. The cell viability charts are plotted by GraphPad Prism 5.

5.6.4.2. Cell Attachment. To define the cell attachment and adhesion on the samples, SEM protocol is applied. After the 5 mm x 10 mm samples are sterilized for 2 hours with UV, 3T3 cells are seeded on the samples in the 6-well cell culture plates. The seeded samples are incubated for 24 hours, 48 hours, and 72 hours at in a humidified 5% CO_2/95% air incubator at 37^oC. Fixation of the cell is important for SEM that's why the samples are fixed with 3% volume fraction of glutaraldehyde, dehydrated in graded alcohol (30-100%) and kept at -20^oC.

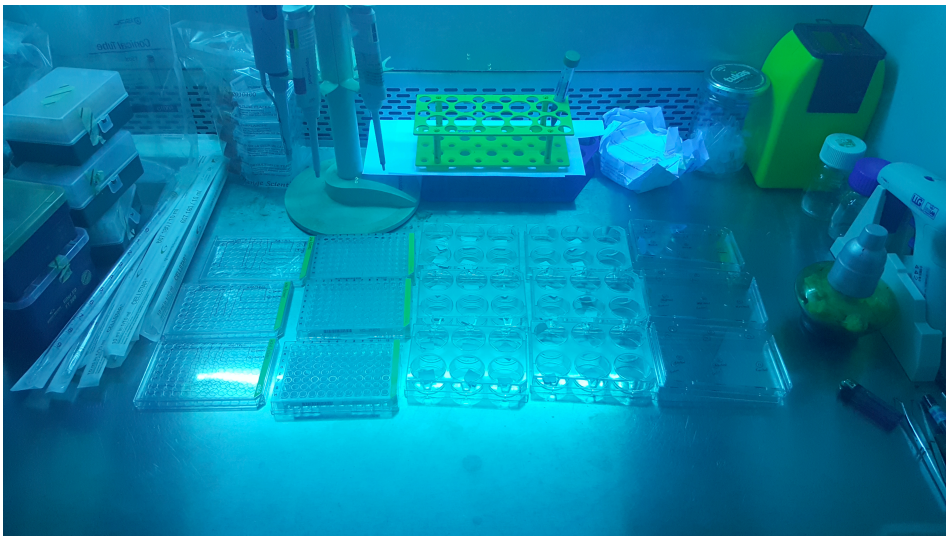

Figure 5.11. Equipment of MTT Cell Proliferation Assay kit and SEM protocol.

6. RESULTS

6.1. Morphological Analysis

6.1.1. SEM

The morphologies of PCL/GE/BHA nanofibers with various concentrations are indicated in Scanning electron microscope (The Philips XL30 ESEM-FEG/EDAX). Before the ESEM monitoring of the nanofibers, the samples are coated with platinum. This process takes 90 minutes with 18 mV.

The aim of SEM images is to be figured out the effect of gelatin concentration change on morphology, the effect of BHA concentration change on morphology, the size of the fibers and whether beads formation occurs on fibers or not.

6.1.1.1. Experiment 1. Figure 6.1 and Figure 6.2 show the morphologies of 12/1/0.5 wt % (PCL/GE/BHA) electrospun nanofibers which is produced under the defined conditions such as feed rate of 120 µl/h, voltage of 28.2kV, humidity of %63.3, temperature of 23°C. As shown in Figure 6.3, the average size of the diameter is 119 ± 31 nm. BHA particles added for the purpose of increasing osteoblast vialibity are seen to be attached to the fibers in the structure. In Figure 6.2, it is pointed out that BHA's nanoparticle size is 356 nm approximately. It is also significant to examine that there is no bead formation on nanofibers corresponding to density of 1.119 g/ml, electrical conductivity of 531 µS/cm, viscosity of 700.655 mPa.s, surface tension of 30.60 mN/m.

.

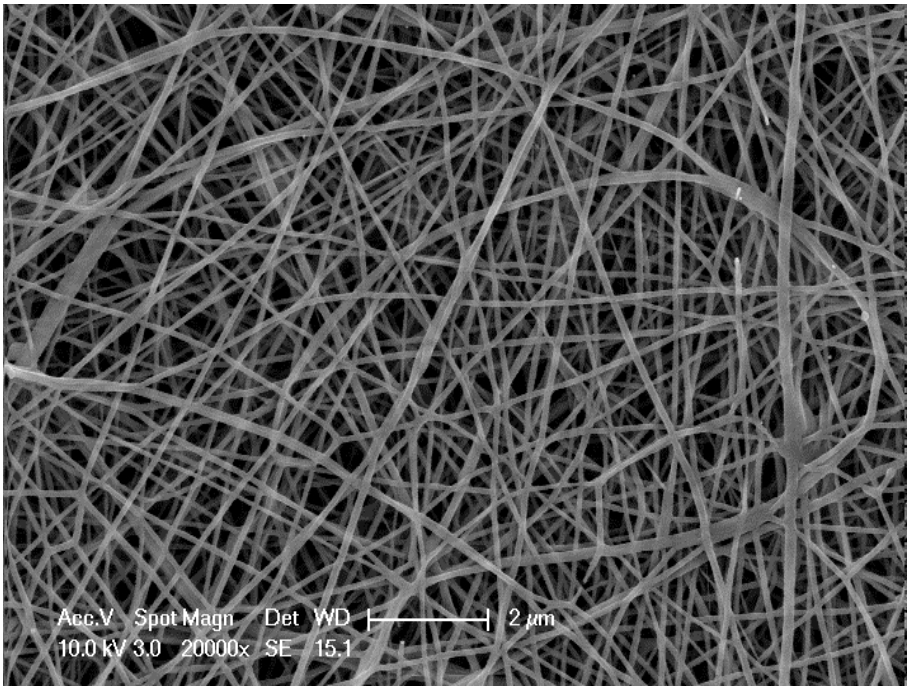

Figure 6.1. SEM image of 12/1/0.5 wt % (PCL/GE/BHA) electrospun nanofibers, Magnitude 20000x.

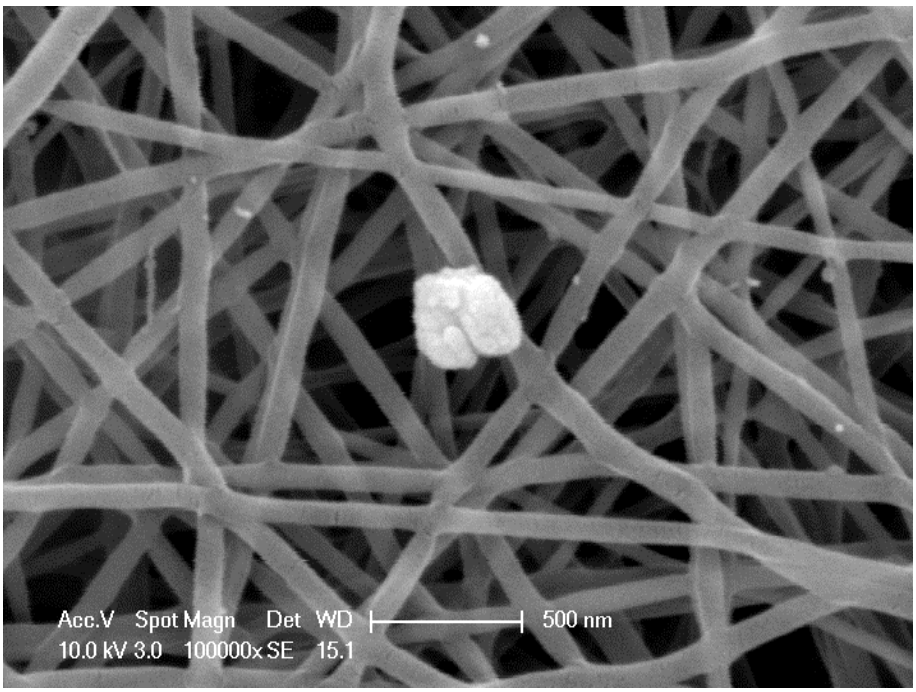

Figure 6.2. SEM image of 12/1/0.5 wt % (PCL/GE/BHA) electrospun nanofibers, Magnitude 100000x.

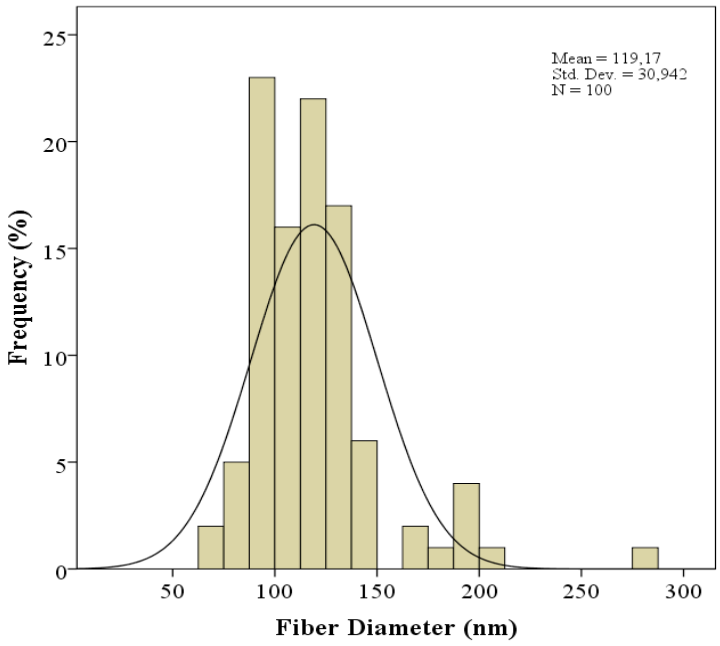

Figure 6.3. Frequency distribution of fiber diameter of 12/1/0.5 wt % (PCL/GE/BHA) electrospun nanofibers.

6.1.1.2. Experiment 2. Figure 6.4, Figure 6.5 and Figure 6.6 show the morphologies of 12/1/1 wt % (PCL/GE/BHA) electrospun nanofibers which is produced under the defined conditions such as feed rate of 129 µl/h, voltage of 26.9 kV, humidity of %56, temperature of 23.8 °C. It is observed the increase in the number of BHA particles in Figure 6.5 by doubling the concentration of BHA from wt 0.5% to wt 1% while the percentages of the PCL and gelatin are constant. Bovine hydroxyapatite particles added for the purpose of increasing osteoblast vialibity are seen to be attached to the fibers in the structure. Figure 6.6 points out the increase in the concentration of BHA on this sample. As shown in Figure 6.7, the average size of the diameter is 149 ± 44 nm . BHA's nanoparticle size is 356 nm approximately. It is also significant to examine that there is no bead formation on nanofibers corresponding to density of 1.112 g/ml, electrical conductivity of 701 µS/cm, viscosity of 752.75 mPa.s, surface tension of 28.91 mN/m.

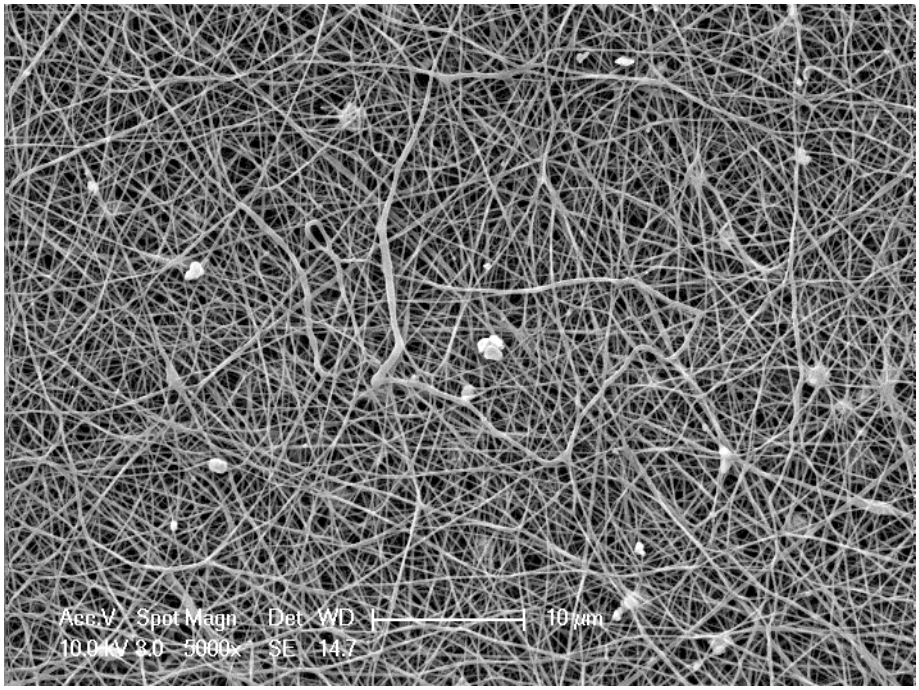

Figure 6.4. SEM image of 12/1/1 wt % (PCL/GE/BHA) electrospun nanofibers, Magnitude 5000x.

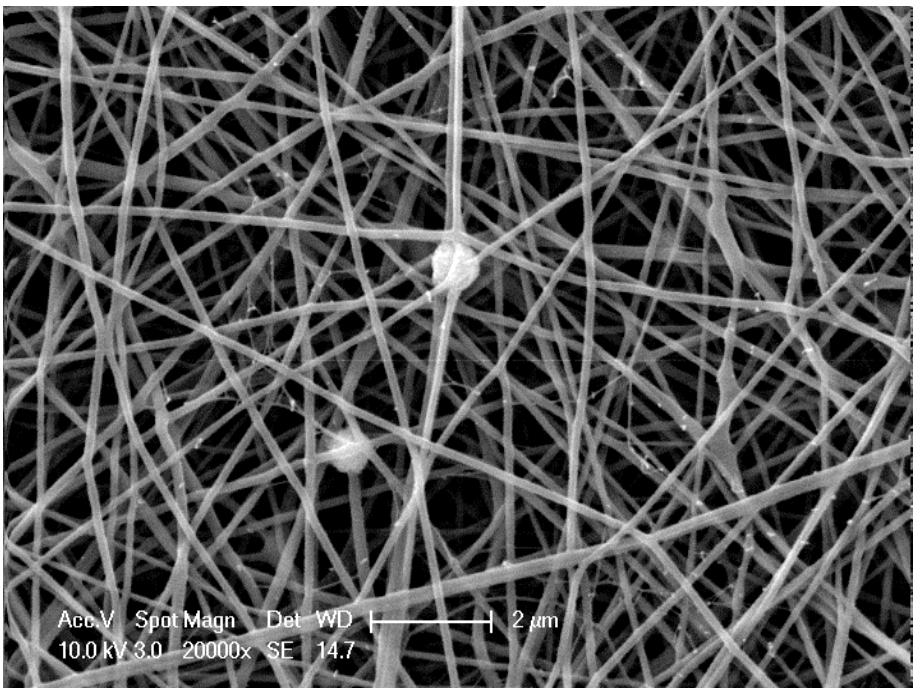

Figure 6.5. SEM image of 12/1/1 wt % (PCL/GE/BHA) electrospun nanofibers, magnitude 20000x.

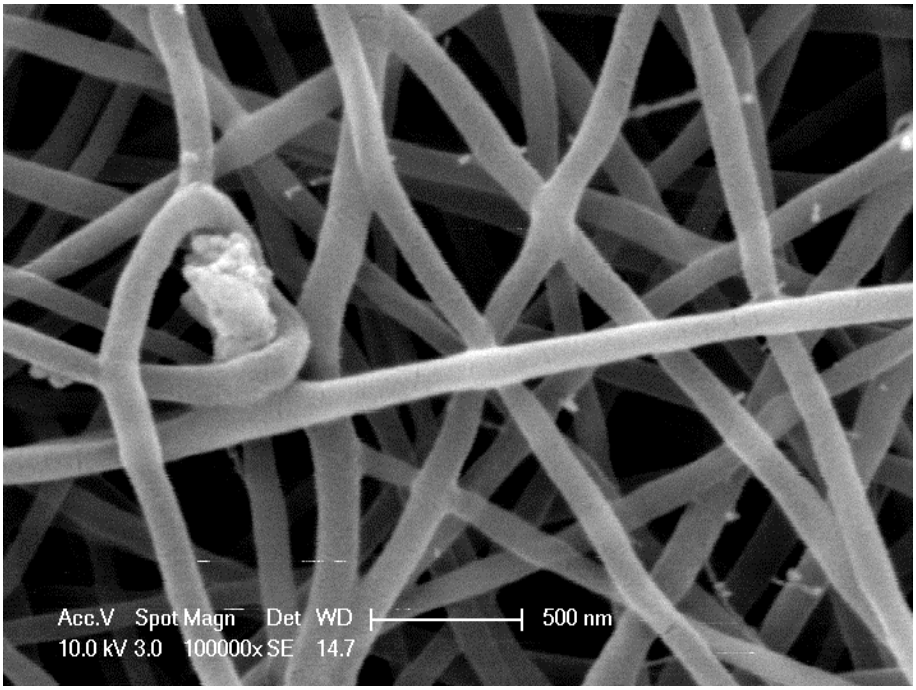

Figure 6.6. SEM image of 12/1/1 wt % (PCL/GE/BHA) electrospun nanofibers, magnitude 100000x.

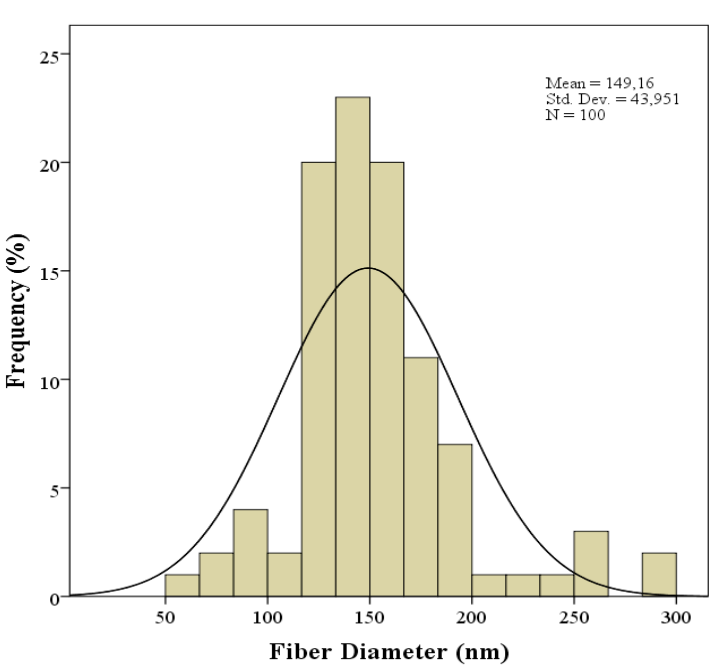

Figure 6.7. Frequency distribution of fiber diameter of 12/1/1 wt % (PCL/GE/BHA) electrospun nanofibers.

6.1.1.3. Experiment 3. Figure 6.8, Figure 6.9 and Figure 6.10 show the morphologies of 12/1/2 wt % (PCL/GE/BHA) electrospun nanofibers which is produced under the defined conditions such as feed rate 130 µl/h, voltage 24.9 kV, humidity %65, temperature 26°C. It is observed the increase in the number of BHA particles in Figure 6.9 by doubling the concentration of BHA from wt 0.1% to wt 2% while the percentages of the PCL and gelatin are constant. As shown in Figure 6.11, the average size of the diameter is 306 ± 68 nm. In Figure 6.10, BHA's nanoparticle size is 500 nm approximately. It is also significant to examine that there is no bead formation on nanofibers corresponding to density 1.122 g/ml, electrical conductivity 1064 µS/cm, viscosity 860.5 mPa.s, surface tension 29.83 mN/m.

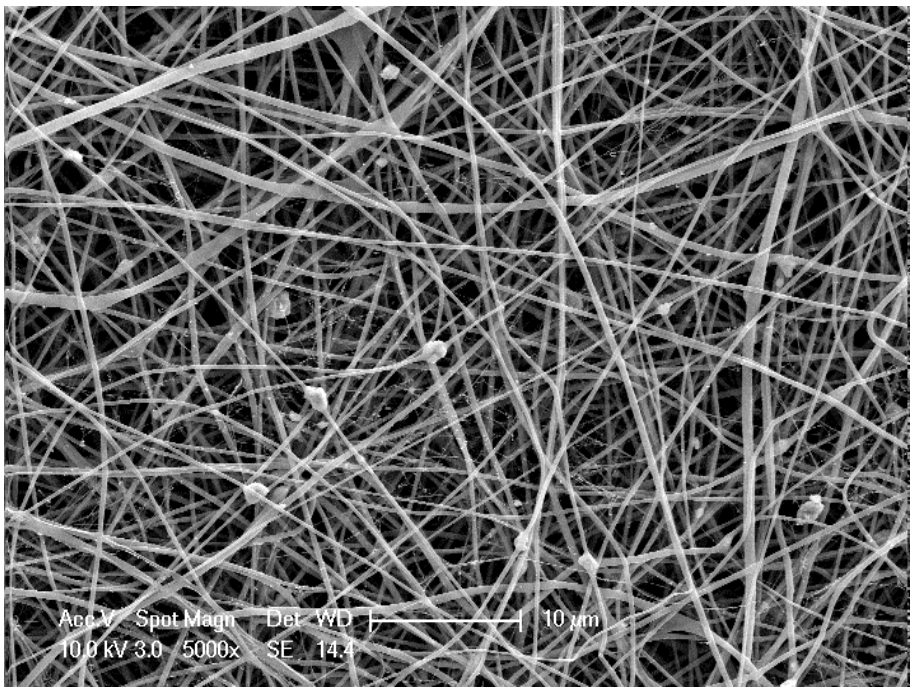

Figure 6.8. SEM image of 12/1/2 wt % (PCL/GE/BHA) electrospun nanofibers, Magnitude 5000x.

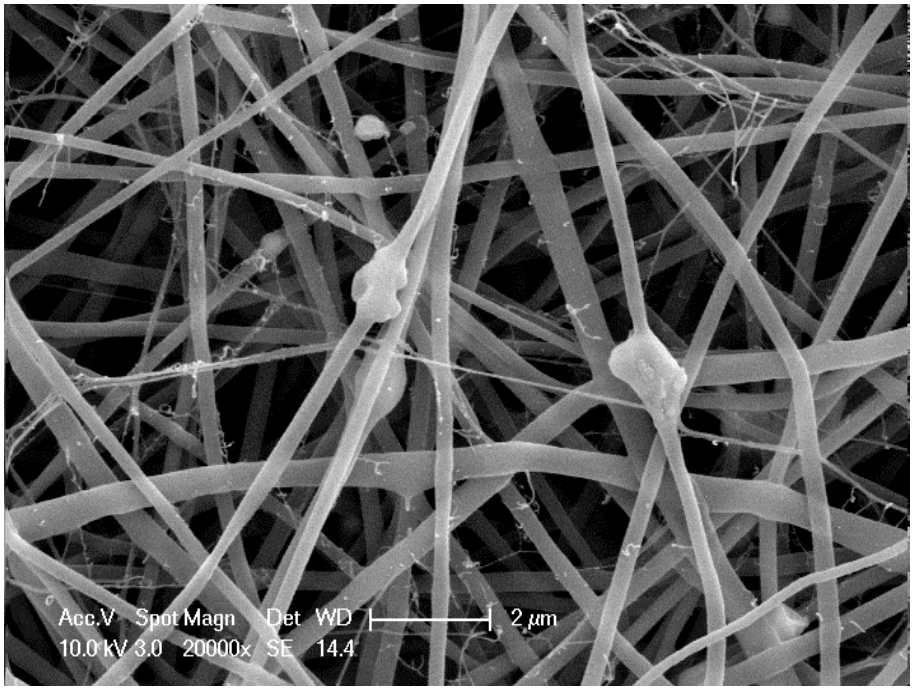

Figure 6.9. SEM image of 12/1/2 wt % (PCL/GE/BHA) electrospun nanofibers, Magnitude 20000x.

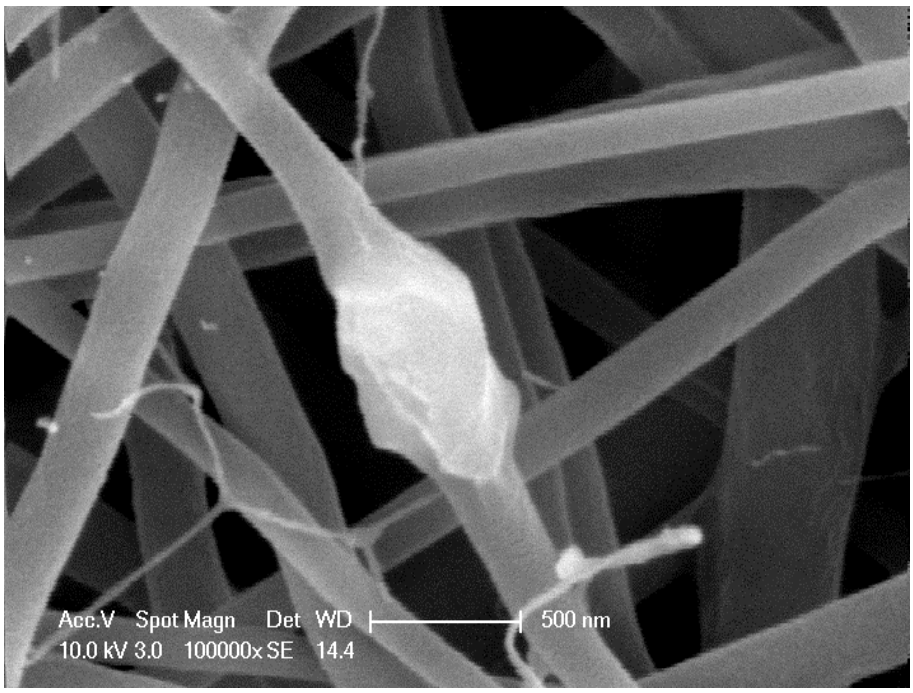

Figure 6.10. SEM image of 12/1/2 wt % (PCL/GE/BHA) electrospun nanofibers, Magnitude 100000x.

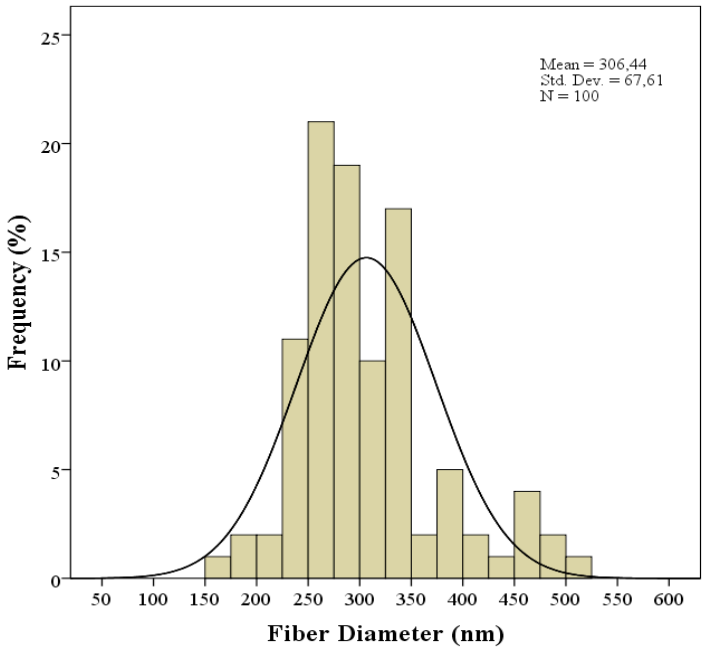

Figure 6.11. Frequency distribution of fiber diameter of 12/1/2 wt % (PCL/GE/BHA) electrospun nanofibers.

6.1.1.4. Experiment 4. Figure 6.12, Figure 6.13 and Figure 6.14 show the morphologies of 12/0.5/0.5 wt % (PCL/GE/BHA) electrospun nanofibers which is produced under the defined conditions such as feed rate 600 µl/h, voltage 36.9 kV, humidity %63.9, temperature 24.8°C. In Figure 6.15, the average size of the diameter is 241 ± 55 nm. BHA particles added for the purpose of increasing osteoblast vialibity are seen to be attached to the fibers in the structure. It is also significant to examine that there is no bead formation on nanofibers corresponding to density 1.118 g/ml, electrical conductivity 454 µS/cm, viscosity 686.5 mPa.s, surface tension 30.95 mN/m.

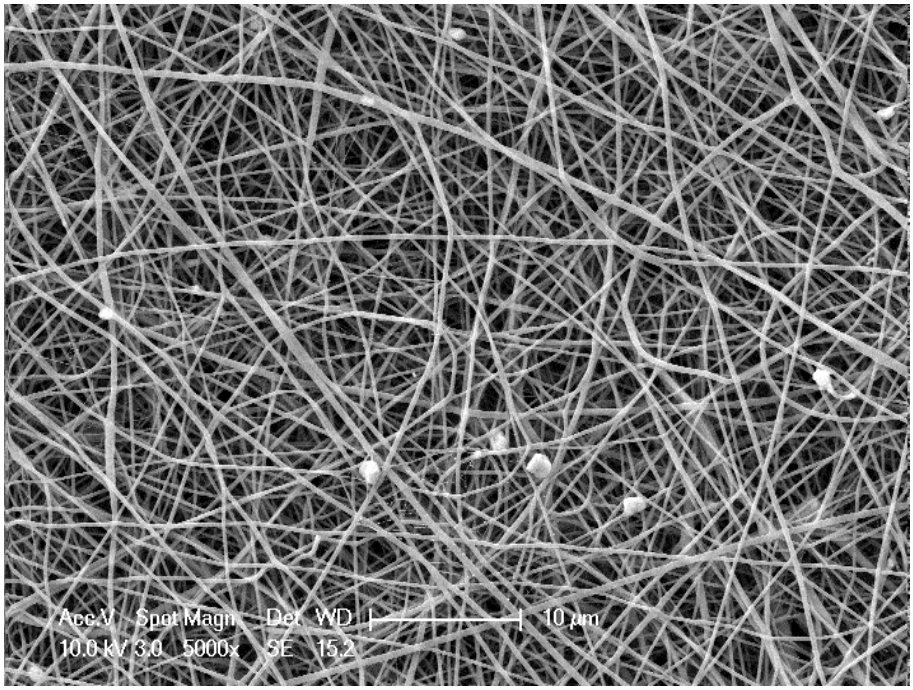

Figure 6.12. SEM image of 12/0.5/0.5 wt % (PCL/GE/BHA) electrospun nanofibers, Magnitude 5000x.

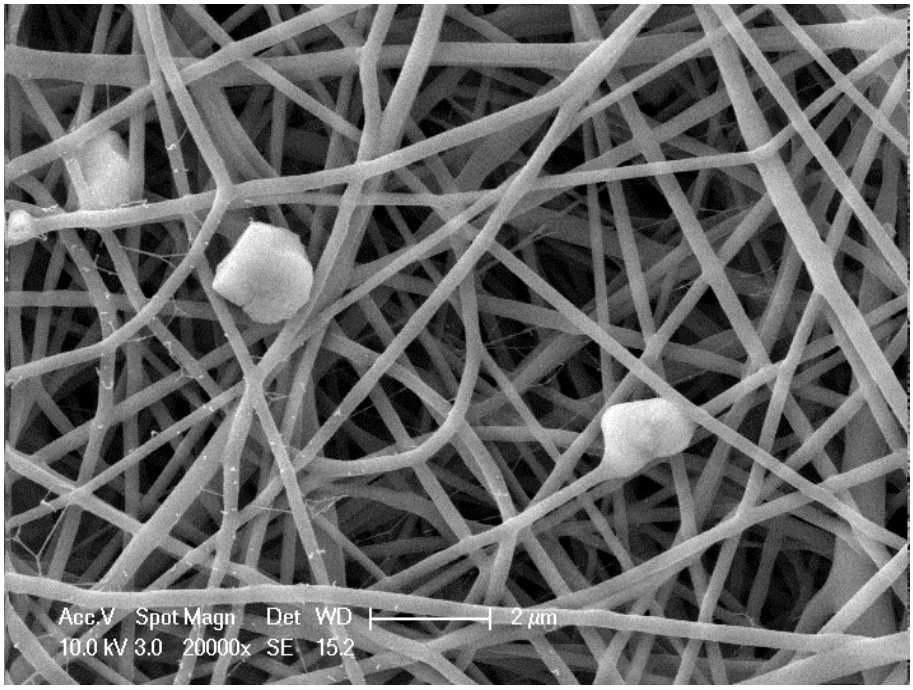

Figure 6.13. SEM image of 12/0.5/0.5 wt % (PCL/GE/BHA) electrospun nanofibers, Magnitude 20000x.

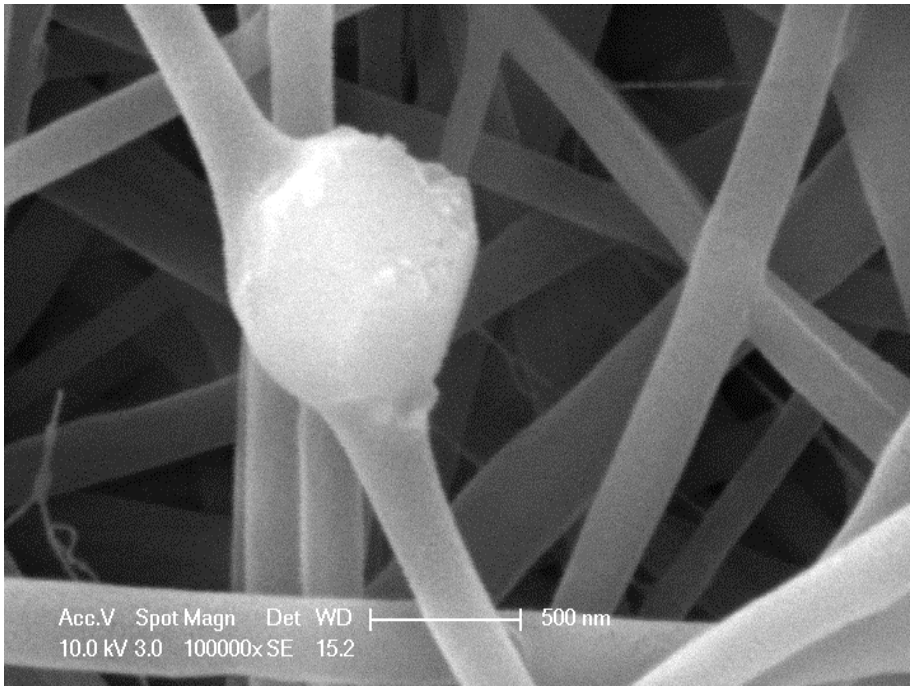

Figure 6.14. SEM image of 12/0.5/0.5 wt % (PCL/GE/BHA) electrospun nanofibers, Magnitude 100000x.

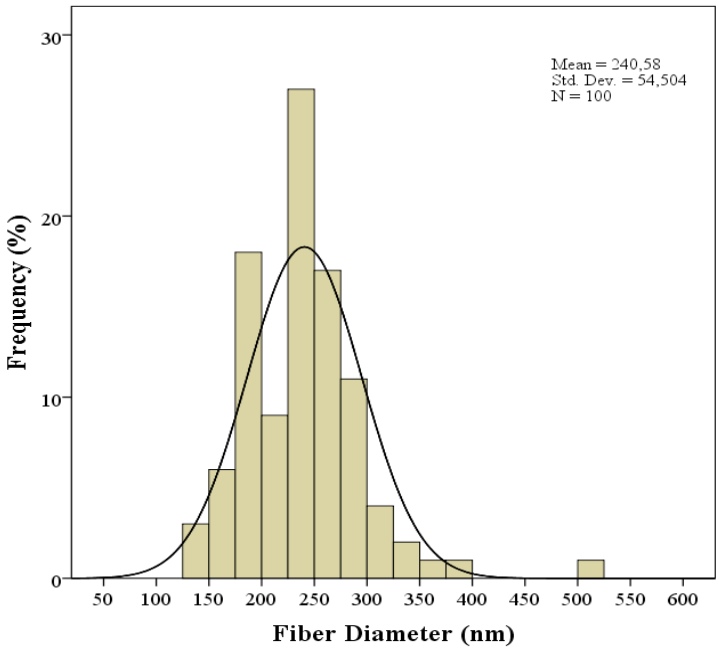

Figure 6.15. Frequency distribution of fiber diameter of 12/0.5/0.5 wt % (PCL/GE/BHA) electrospun nanofibers.

6.1.1.5. Experiment 5. Figure 6.16, Figure 6.17 and Figure 6.18 show the morphologies of 12/1.5/0.5 wt % (PCL/GE/BHA) electrospun nanofibers which is produced under the defined conditions such as feed rate 200 µl/h, voltage 19.7 kV, humidity %61.7, temperature 23.9°C. It is observed the increase in web formation in Figure 6.17 and Figure 6.18 by tripling the concentration of gelatin from wt 0.5% to wt 1.5 % while the percentages of the PCL and BHA are constant. As shown in Figure 6.19, the average size of the diameter is 384 ± 84 nm. Figure 6.18, BHA's nanoparticle size is 500 nm approximately. It is also significant to examine that there is no bead formation on nanofibers corresponding to density 1.116 g/ml, electrical conductivity 624 µS/cm, viscosity 1202.5 mPa.s, surface tension 30.53 mN/m.

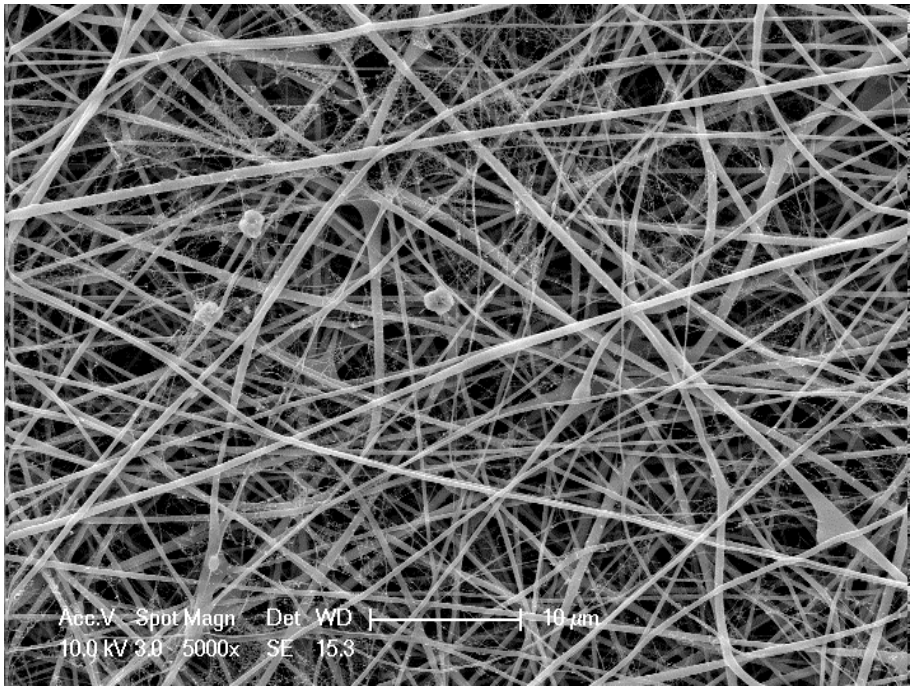

Figure 6.16. SEM image of 12/1.5/0.5 wt % (PCL/GE/BHA) electrospun nanofibers, Magnitude 5000x.

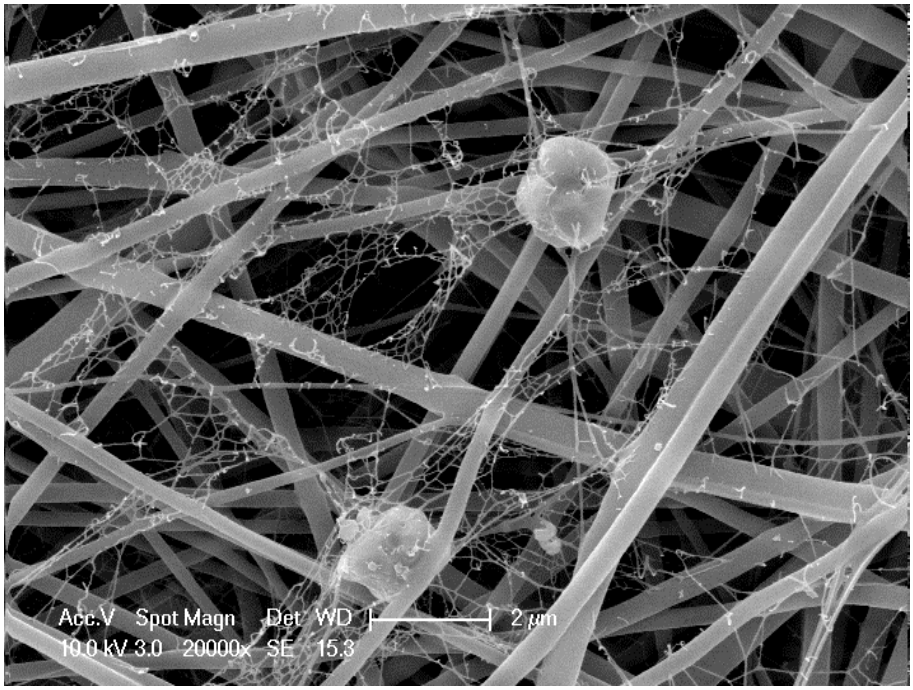

Figure 6.17. SEM image of 12/1.5/0.5 wt % (PCL/GE/BHA) electrospun nanofibers, Magnitude 20000x.

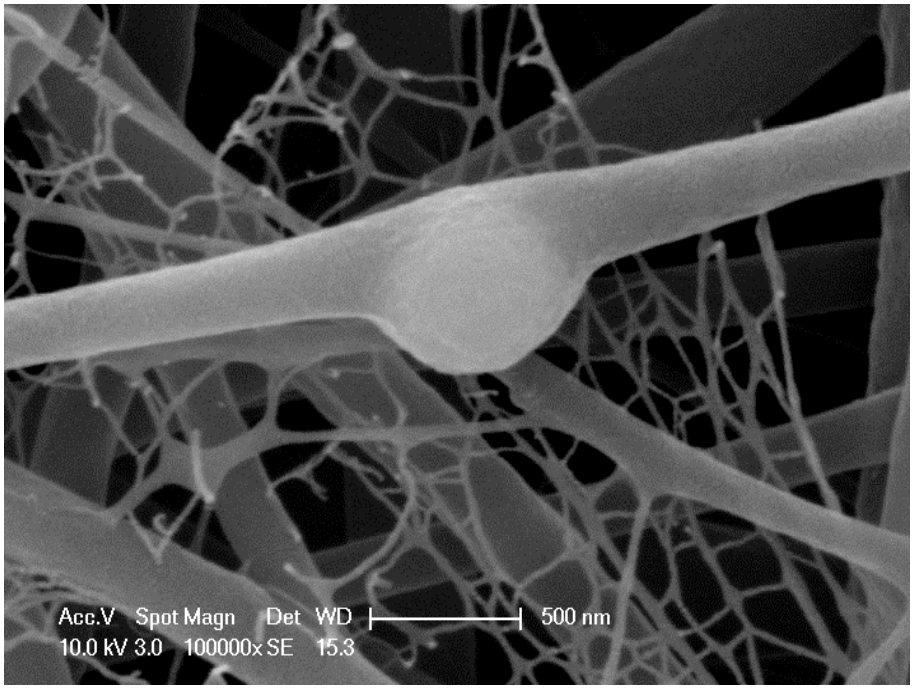

Figure 6.18. SEM image of 12/1.5/0.5 wt % (PCL/GE/BHA) electrospun nanofibers, Magnitude 1000000x.

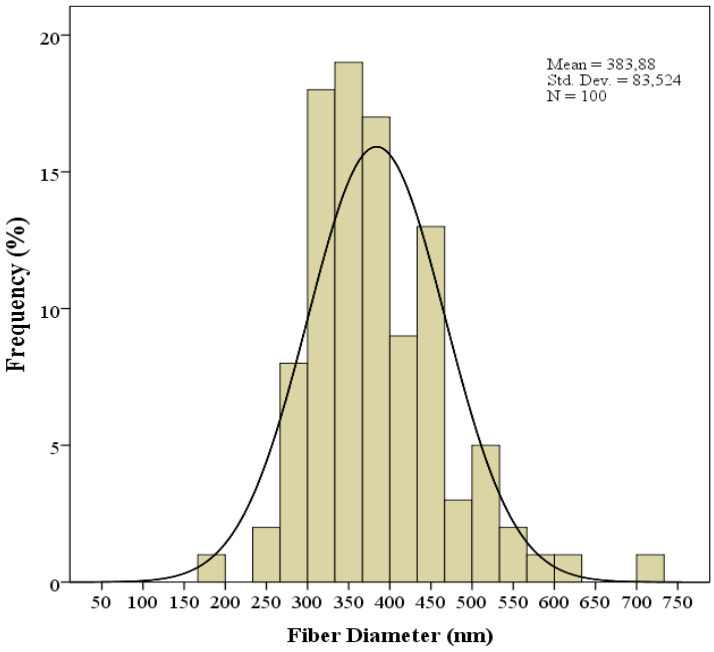

Figure 6.19. Frequency distribution of fiber diameter of 12/1.5/0.5 wt % (PCL/GE/BHA) electrospun nanofibers.

6.2. Chemical Analysis

6.2.1. FTIR

The chemical bonds are examined at a wavenumber range of 400- 4000 cm^{-1} by Fourier Transformation Infrared Spectroscopy (JASCO FT/IR-4700 Spectrometer). The samples with different concentrations are analyzed in detail. FTIR analysis of pure PCL, GE, BHA is shown in Figure 6.20. FTIR analysis and comparison between literature and the experiments is given in Table 6.1.

6.2.1.1. Experiment 1. Figure 6.21 provides the characteristic of 12/1/0.5 wt % (PCL/GE/BHA) electrospun nanofibers. The peak appeared at 2944 cm^{-1} (intensity of 96.6404 %) shows the presence of asymmetric H-C-H stretching which is the characteristic value of PCL. In addition of the indicating of the presence of PCL, there are three more

peaks at 2866 cm^{-1}, 1293 cm^{-1} and 1239 cm^{-1}which prove the symmetric H-C-H stretching, C-O C-C carbonyl stretching and asymmetric C-O-C stretching.

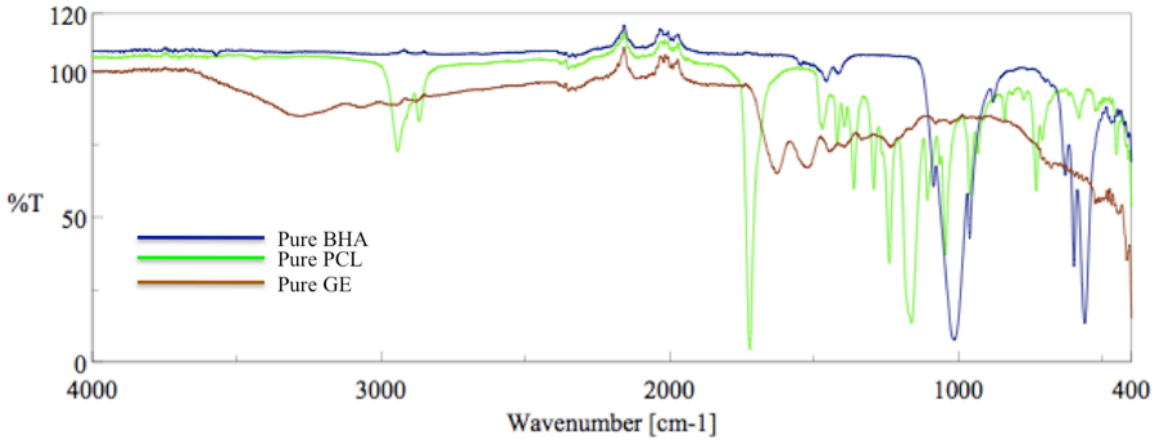

Figure 6.20. FTIR analysis of Pure PCL, Pure GE, Pure BHA.

Table 6.1. FTIR analysis and comparison between literature and the experiments.

	Literature		The Experiment Results of PCL/GE/BHA					
	Chong et al. [69] PCL/GE (cm^{-1})	Rather et al. [106] PCL/GE (cm^{-1})	Pure PCL (cm^{-1})	12/1/0.5 (cm^{-1})	12/1/1 (cm^{-1})	12/1/2 (cm^{-1})	12/0.5/0.5 (cm^{-1})	12/1.5/0.5 (cm^{-1})
Asymmetric Methylene C-H stretching	2949	2943	2942	2944	2944	2944	2944	2944
Symmetric Methylene C-H stretching	2865	2865	2867	2866	2866	2866	2866	2866
Carbonyl C-O stretching	1293	Undefined	1293	1293	1293	1293	1293	1293
Asymmetric C-O-C stretching	1240	Undefined	1239	1239	1239	1240	1239	1239
Amide I C=O	1650	1640	-	1655	1655	1656	1655	1655
Amide II N—H	1540	1540	-	1544	1543	1543	1543	1543

The main difference of pure PCL and PCL/GE/BHA composite in FTIR analysis, by comparing Table 6.1 with Figure 6.21, is seen at 1655 cm^{-1} (Amide I) and 1544 cm^{-1} (Amide II) where the presence of an amide group (NH_2) in PCL/GE/BHA composite. The amide group of gelatin has an ability to create a hydrogen bond with H_2O that's why it decreases the hydrophobic interactions of PCL [69]. With the appearance of the amide

group in the 12/1/0.5 wt % (PCL/GE/BHA) electrospun nanofibers, it demonstrates the presence of gelatin in the composites and PCL binds with gelatin.

6.2.1.2. Experiment 2. Figure 6.22 shows the characteristic of 12/1/1 wt % (PCL/GE/BHA) electrospun nanofibers. The peak observed at 2944 cm^{-1} shows the existence of asymmetric H-C-H stretching which is the characteristic value of PCL. In addition of the indicating of the presence of PCL, there are three more peaks at 2866 cm^{-1}, 1293 cm^{-1} and 1239 cm^{-1} which verify the symmetric H-C-H stretching, C-O C-C carbonyl stretching and asymmetric C-O-C stretching.

The main distinction of pure PCL and PCL/GE/BHA composite in FTIR analysis, by comparing Table 6.1 with Figure 6.22, is clearly observed at 1655 cm^{-1} (Amide I) and 1543 cm^{-1} (Amide II) where the existence of an amide group (NH_2) in PCL/GE/BHA composite. With the appearance of the amide group in the 12/1/1 wt % (PCL/GE/BHA) electrospun nanofibers, it demonstrates the presence of gelatin in the composites and PCL binds with gelatin.

6.2.1.3. Experiment 3. Figure 6.23 shows the characteristic of 12/1/2 wt % (PCL/GE/BHA) electrospun nanofibers. The peak observed at 2944 cm^{-1} shows the existence of asymmetric H-C-H stretching which is the characteristic value of PCL. In addition of the indicating of the presence of PCL, there are three more peaks at 2866 cm^{-1}, 1293 cm^{-1} and 1240 cm^{-1} which verify the symmetric H-C-H stretching, C-O C-C carbonyl stretching and asymmetric C-O-C stretching.

The main distinction of pure PCL and PCL/GE/BHA composite in FTIR analysis, by comparing Table 6.1 with Figure 6.23, is clearly observed at 1656 cm^{-1} (Amide I) and 1543 cm^{-1} (Amide II) where the existence of an amide group (NH_2) in PCL/GE/BHA composite. With the appearance of the amide group in the 12/1/2 wt % (PCL/GE/BHA) electrospun nanofibers, it demonstrates the presence of gelatin in the composites and PCL binds with gelatin.

6.2.1.4. Experiment 4. Figure 6.24 shows the characteristic of 12/0.5/0.5 wt % (PCL/GE/BHA) electrospun nanofibers. The peak observed at 2944 cm^{-1} shows the existence of asymmetric H-C-H stretching which is the characteristic value of PCL. In addition of the indicating of the presence of PCL, there are three more peaks at 2866 cm^{-1}, 1293 cm^{-1} and 1239 cm^{-1} which verify the symmetric H-C-H stretching, C-O C-C carbonyl stretching and asymmetric C-O-C stretching.

The main distinction of pure PCL and PCL/GE/BHA composite in FTIR analysis, by comparing Table 6.1 with Figure 6.24, is clearly observed at 1655 cm^{-1} (Amide I) and 1543 cm^{-1} (Amide II) where the existence of an amide group (NH_2) in PCL/GE/BHA composite. With the appearance of the amide group in the 12/0.5/0.5 wt % (PCL/GE/BHA) electrospun nanofibers, it demonstrates the presence of gelatin in the composites and PCL binds with gelatin.

6.2.1.5. Experiment 5. Figure 6.25 shows the characteristic of 12/1.5/0.5 wt % (PCL/GE/BHA) electrospun nanofibers. The peak observed at 2944 cm^{-1} shows the existence of asymmetric H-C-H stretching which is the characteristic value of PCL. In addition of the indicating of the presence of PCL, there are three more peaks at 2866 cm^{-1}, 1293 cm^{-1} and 1239 cm^{-1} which verify the symmetric H-C-H stretching, C-O C-C carbonyl stretching and asymmetric C-O-C stretching.

The main distinction of pure PCL and PCL/GE/BHA composite in FTIR analysis, by comparing Table 6.1 with Figure 6.25, is clearly observed at 1655 cm^{-1} (Amide I) and 1543 cm^{-1} (Amide II) where the existence of an amide group (NH_2) in PCL/GE/BHA composite. With the appearance of the amide group in the 12/1.5/0.5 wt % (PCL/GE/BHA) electrospun nanofibers, it demonstrates the presence of gelatin in the composites and PCL binds with gelatin.

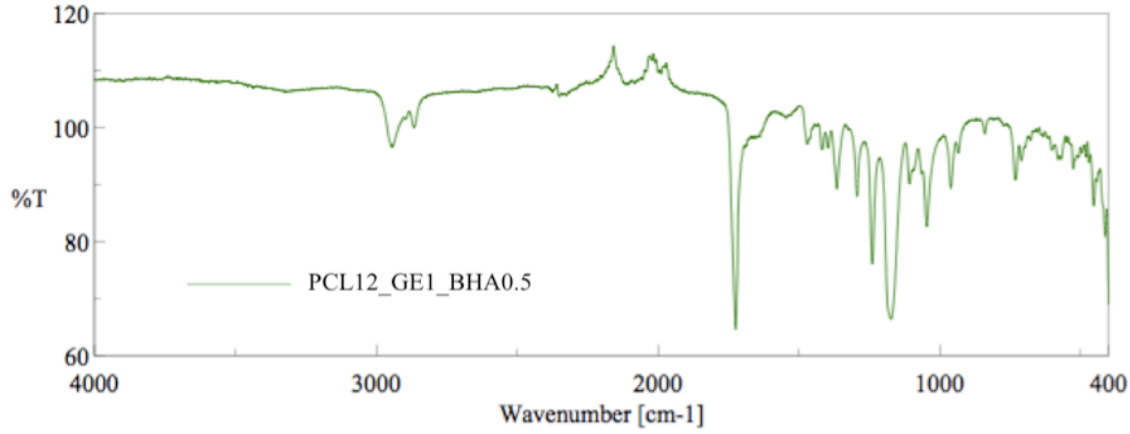

Figure 6.21. FTIR analysis of 12/1/0.5 wt % (PCL/GE/BHA) electrospun nanofibers.

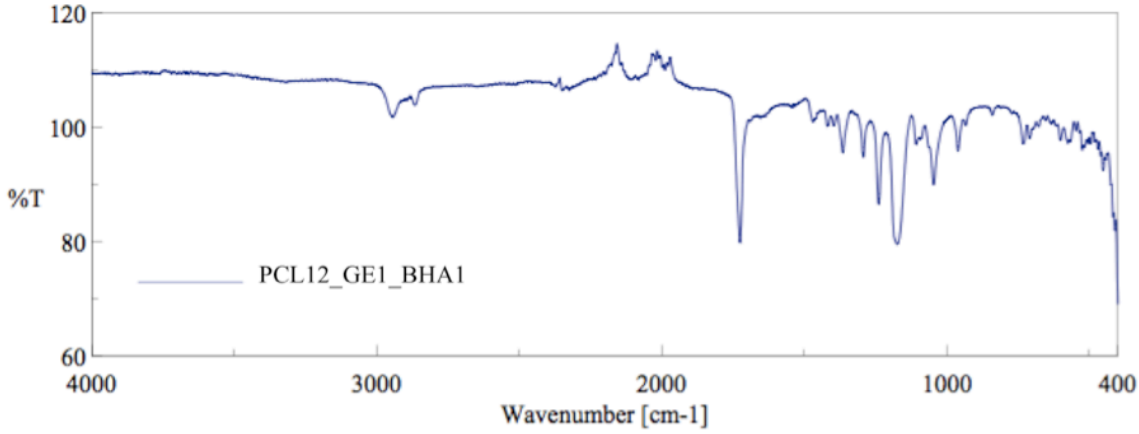

Figure 6.22. FTIR analysis of 12/1/1 wt % (PCL/GE/BHA) electrospun nanofibers.

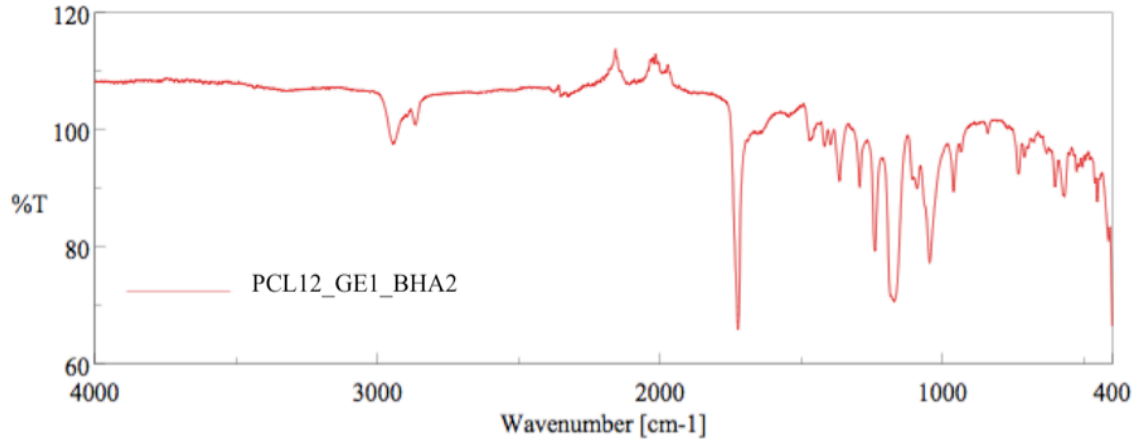

Figure 6.23. FTIR analysis of 12/1/2 wt % (PCL/GE/BHA) electrospun nanofibers.

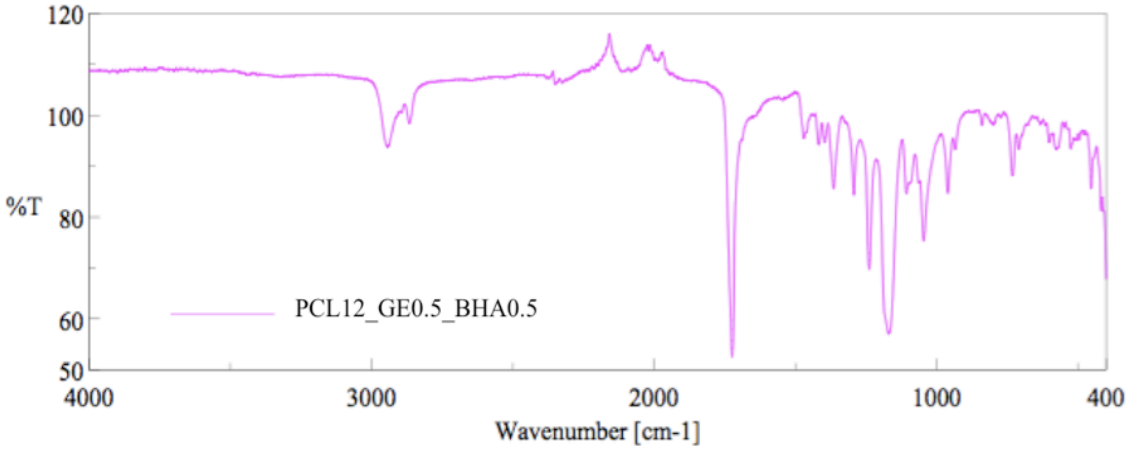

Figure 6.24. FTIR analysis of 12/0.5/0.5 wt % (PCL/GE/BHA) electrospun nanofibers.

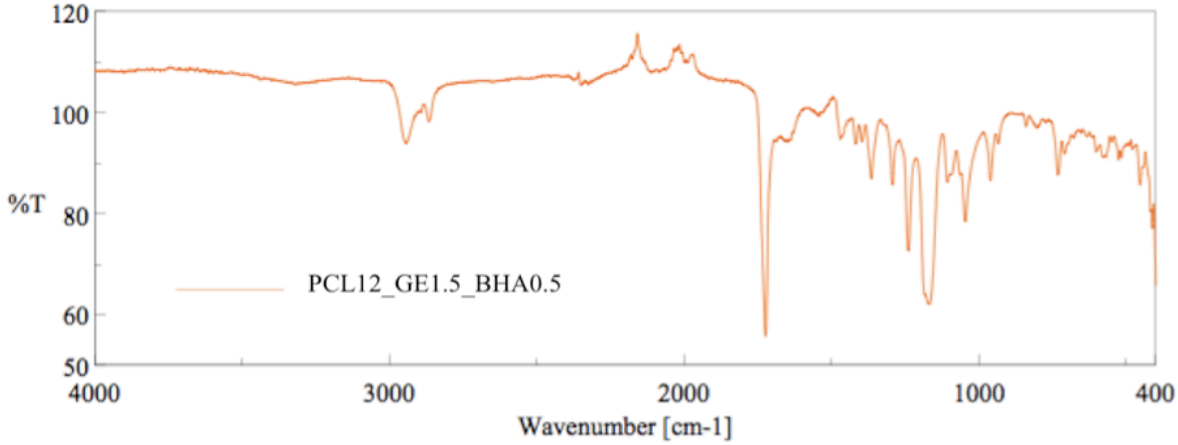

Figure 6.25. FTIR analysis of 12/1.5/0.5 wt % (PCL/GE/BHA) electrospun nanofibers.

6.3. Mechanical Analysis

6.3.1. Tensile Test

6.3.1.1. Experiment 1. As shown in Figure 6.26, there is an engineering tensile stress - strain diagram of 12/1/0.5 wt % (PCL/GE/BHA) electrospun nanofibers. The average thicknesses of sample 1, sample 2 and sample 3 are 0.039, 0.028 and 0.027 mm respectively. As shown in Table 6.2, the ultimate tensile strength (UTS) of the samples are 9.8 MPa at 21.4 of tensile strain, 8.6 MPa at 18.9 of strain and 9.0 MPa at 23.1 of strain respectively. The average value of UTS is 9.1 ± 0.6 MPa. The value of strain at UTS is 21.1 ± 2.2 %.

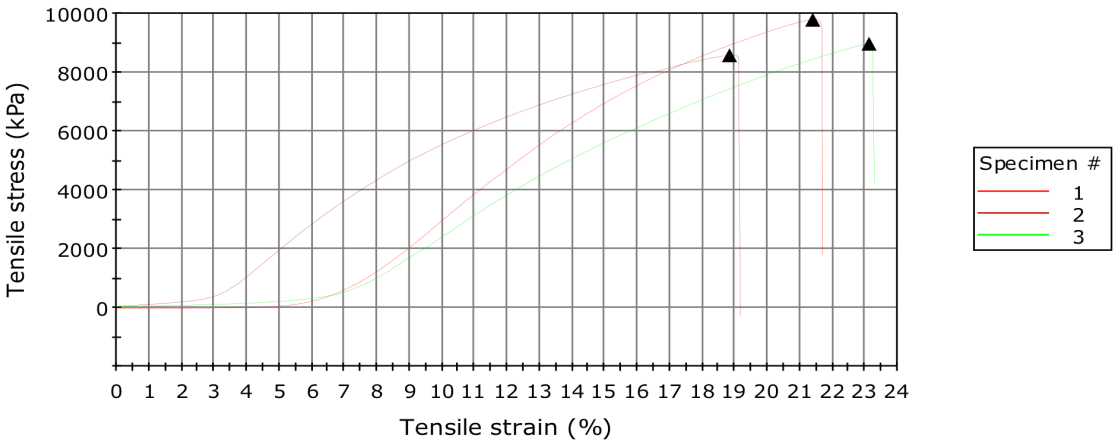

Figure 6.26. Engineering stress-strain curve of 12/1/0.5 wt % (PCL/GE/BHA) electrospun nanofibers.

Table 6.2. The tensile test results of PCL/GE/BHA 12/1/0.5 wt % electrospun nanofibers.

Sample	UTS (MPa)	Strain at UTS (%)	Load at UTS (N)	Elongation at UTS (mm)	Tensile stress at Fracture (kPa)
Sample 1	9.8	21.4	2.67	6.41	0.00
Sample 2	8.6	18.9	2.34	5.65	72.3
Sample 3	9.0	23.1	2.44	6.93	48.2
Mean of the samples	9.1	21.1	2.48	6.33	40.2
Standard deviation	0.6	2.2	0.17	0.65	36.8

6.3.1.2. Experiment 2. As shown in Figure 6.27, there is an engineering tensile stress - strain diagram of 12/1/1 wt % (PCL/GE/BHA) electrospun nanofibers. The thicknesses of sample 1, sample 2 and sample 3 are 0.012, 0.012 and 0.012 mm respectively. As a result of the testing, Table 6.3 shows that the ultimate tensile strength (UTS) of the samples are 15.8 MPa at 38.3 of tensile strain, 14.2 MPa at 42.2 of strain and 17.0 MPa at 46.2 of strain respectively. The average value of UTS is 15.7 ± 1.4 MPa. The value of strain at UTS is 42.2 ± 4.0 %.

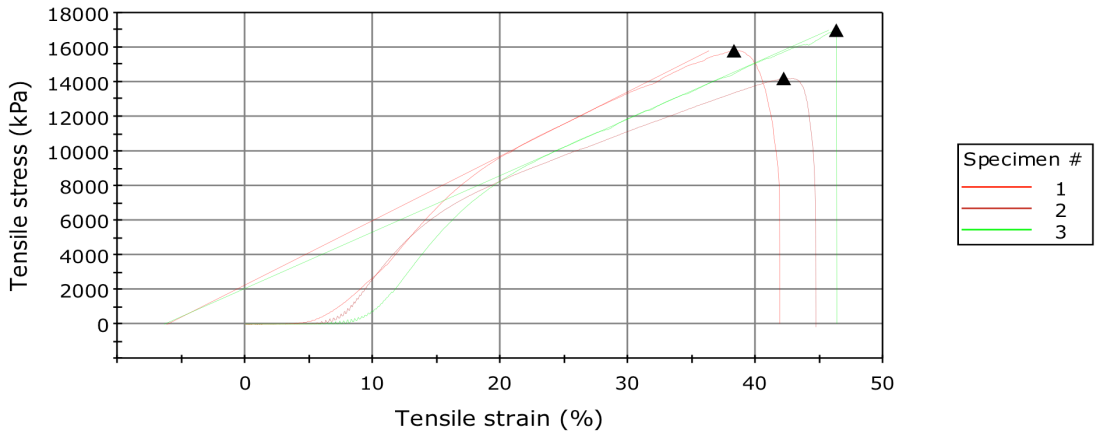

Figure 6.27. Engineering stress-strain curve of 12/1/1 wt % (PCL/GE/BHA) electrospun nanofibers.

Table 6.3. The tensile test results of PCL/GE/BHA 12/1/1 wt % electrospun nanofibers.

Sample	UTS (MPa)	Strain at UTS (%)	Load at UTS (N)	Elongation at UTS (mm)	Tensile stress at Fracture (kPa)
Sample 1	15.8	38.3	1.8	11.48	32.2
Sample 2	14.2	42.2	1.69	12.65	----
Sample 3	17.0	46.2	2.02	13.88	32.6
Mean of the samples	15.7	42.2	1.86	12.67	32.4
Standard deviation	1.4	4.0	0.17	1.20	0.3

6.3.1.3. Experiment 3. As shown in Figure 6.28, there is an engineering tensile stress - strain diagram of 12/1/2 wt % (PCL/GE/BHA) electrospun nanofibers. The thicknesses of sample 1, sample 2, sample 3 and sample 4 are 0.008, 0.004, 0.004 and 0.004 mm respectively. As a result of the testing, Table 6.4 shows that the ultimate tensile strength (UTS) of the samples are 11.5 MPa at 107.3 of tensile strain, 21.6 MPa at 79.4 of strain,

18.3 MPa at 91.0 of strain and 11.6 MPa at 68.4 of strain respectively. The average value of UTS is 15.8 ± 5.0 MPa. The value of strain at UTS is 86.5 ± 16.6 %.

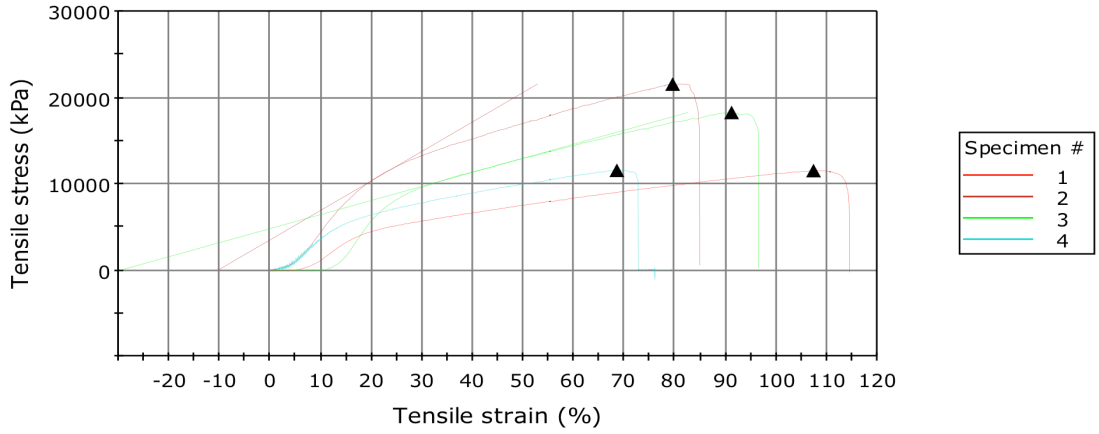

Figure 6.28. Engineering stress-strain curve of 12/1/2 wt % (PCL/GE/BHA) electrospun nanofibers.

Table 6.4. The tensile test results of PCL/GE/BHA 12/1/2 wt % electrospun nanofibers.

Sample	UTS (MPa)	Strain at UTS (%)	Load at UTS (N)	Elongation at UTS (mm)	Tensile stress at Fracture (kPa)
Sample 1	11.5	107.3	0.92	32.18	31.9
Sample 2	21.6	79.4	0.81	27.31	68.3
Sample 3	18.3	91.0	0.68	27.31	68.3
Sample 4	11.6	68.4	0.43	20.53	105.1
Mean of the samples	15.7	86.5	0.71	26.83	68.4
Standard deviation	5.0	16.6	0.21	4.79	29.9

6.3.1.4. Experiment 4. As shown in Figure 6.29, there is an engineering tensile stress - strain diagram of 12/0.5/0.5 wt % (PCL/GE/BHA) electrospun nanofibers. The thicknesses

of sample 1, sample 2 and sample 3 are 0.017, 0.017 and 0.008 mm respectively. As a result of the testing, Table 6.5 shows that the ultimate tensile strength (UTS) of the samples are 23.4 MPa at 87.7 of tensile strain, 20.0 MPa at 72.5 of strain, 49.3 MPa at 117.1 of strain respectively. The average value of UTS is 30.9 ± 16.0 MPa. The value of strain at UTS is 92.5 ± 22.7 %.

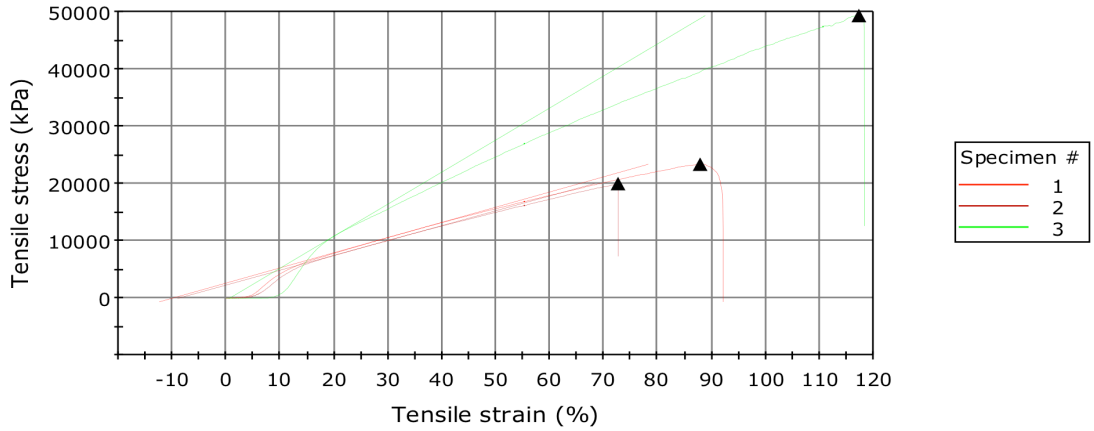

Figure 6.29. Engineering stress-strain curve of 12/0.5/0.5 wt % (PCL/GE/BHA) electrospun nanofibers.

Table 6.5. The tensile test results of PCL/GE/BHA 12/0.5/0.5 wt % electrospun nanofibers.

Sample	UTS (MPa)	Strain at UTS (%)	Load at UTS (N)	Elongation at UTS (mm)	Tensile stress at Fracture (kPa)
Sample 1	23.4	87.7	3.91	26.32	86.2
Sample 2	20.0	72.5	3.35	21.76	31.1
Sample 3	49.3	117.1	3.94	35.14	65
Mean of the samples	30.9	92.5	3.73	27.74	60.7
Standard deviation	16.0	22.7	0.34	6.80	27.8

6.3.1.5. Experiment 5. As shown in Figure 6.30, there is an engineering tensile stress - strain diagram of 12/1.5/0.5 wt % (PCL/GE/BHA) electrospun nanofibers. The thicknesses of sample 1, sample 2 and sample 3 are 0.007, 0.007 and 0.007 mm respectively. As a result of the testing, Table 6.6 shows that the ultimate tensile strength (UTS) of the samples are 14.0 MPa at 104.3 of tensile strain, 15.1 MPa at 120.4 of strain, 18.3 MPa at 147.3 of strain respectively. The average value of UTS is 15.8 ± 2.2 MPa. The value of strain at UTS is 124.0 ± 21.7 %.

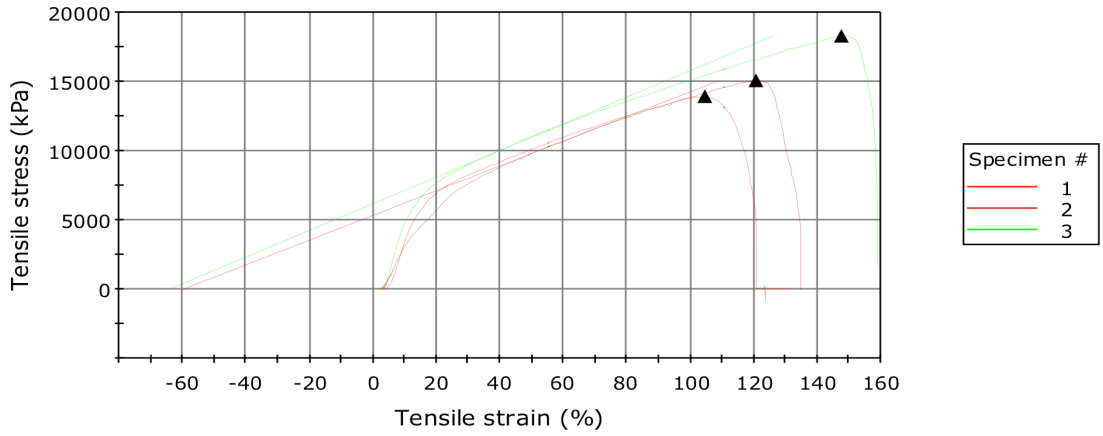

Figure 6.30. Engineering stress-strain curve of 12/1.5/0.5 wt % (PCL/GE/BHA) electrospun nanofibers.

Table 6.6. The tensile test results of PCL/GE/BHA 12/1.5/0.5 wt % electrospun nanofibers.

Sample	UTS (MPa)	Strain at UTS (%)	Load at UTS (N)	Elongation at UTS (mm)	Tensile stress at Fracture (kPa)
Sample 1	14.0	104.3	0.95	31.29	37.5
Sample 2	15.1	120.4	1.03	36.13	57.7
Sample 3	18.3	147.3	1.24	44.18	37.5
Mean of the samples	15.8	124.0	1.07	37.20	44.2
Standard deviation	2.2	21.7	0.15	6.51	11.7

6.4. Biological Analysis

Saos-2 cell line is human osteosarcoma cell line and bone tumors with abnormal activities. It is also called human osteoblastic-like cell. It should be indicated that although research groups are used Saos-2 for analyzing biocompatibility of the materials, it is still a difference between human osteoblast cell line and osteosarcoma cell line in terms of extracellular matrix [115]. In this study, Saos-2 cell line (human osteoblastic-like) is found in Faculty of Medicine at Istanbul University because of the lack of osteoblast cell in some research laboratories. In addition, mouse fibroblast 3T3 cells with normal activities are also used for analyzing biocompatibility of the materials.

6.4.1. MTT Cell Proliferation Assay

To examine the cell viability, proliferation and cytotoxicity of the samples from Experiment 1 to Experiment 5, MTT Cell Proliferation Assay is applied by seeding 3T3 and Saos-2 on all samples for 24, 48 and 72 hours as shown in Figure 6.31. MTT test is a colorimetric test that's why yellow colors at initial wells are expected to turn into purple color (formazan) in order to indicate viable cell number and the degree of cytotoxicity as shown in Figure 6.31.

It can be seen in Figure 6.32.a, Figure 6.32.b and Figure 6.32.c, there is no cytotoxicity of the samples for 3T3 cells and all samples are biocompatible for 72 hours. At 24 and 48 hours after exposure, the results for cell viability on all samples from Experiment 1 to Experiment 5 are statistically significant for all samples ($*P<0.05$), however there is no cell proliferation any of them for 24 hours. It can be a result of the adaptation period. When it comes to 72 hours after exposure, Figure 6.32.c indicates that cell proliferation occurs in Experiment 3, 4 and 5 with statistically significant, $*P<0.05$. Consequently, Experiment 3, 4 and 5 are more biocompatible and cytocompatible compared to Experiment 1 and 2 for 72 hours.

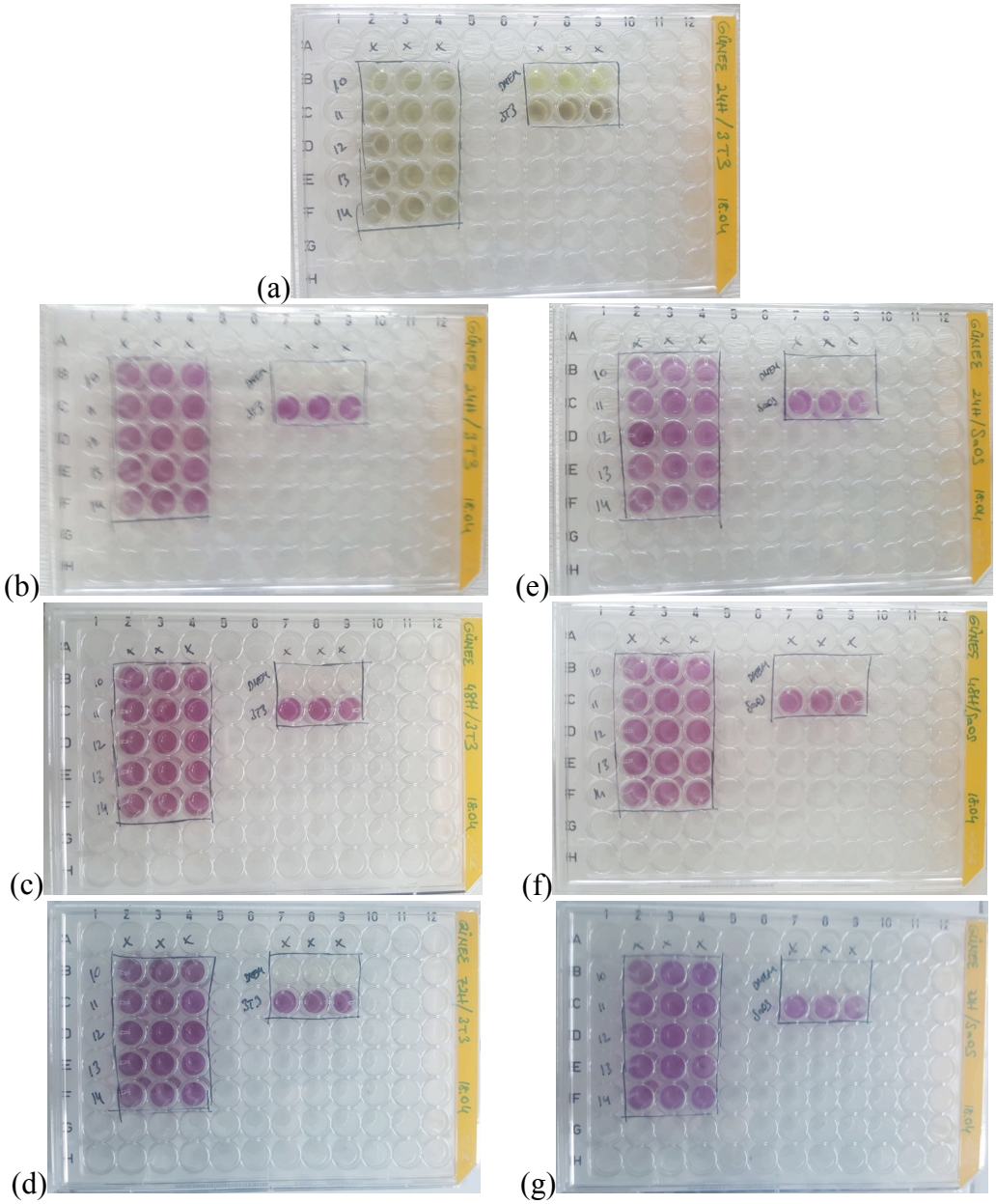

Figure 6.31. MTT Cell Proliferation Assay colorimetric test results and cell viability of all samples from Experiment 1 to Experiment 5 after 24, 48 and 72 hours of cell culture: (a) Initial, (b) 24 hours of 3T3 cell, (c) 48 hours of 3T3 cell, (d) 72 hours of 3T3 cell, (e) 24 hours of Saos-2, (f) 48 hours of Saos-2, (g) 72 hours of Saos-2.

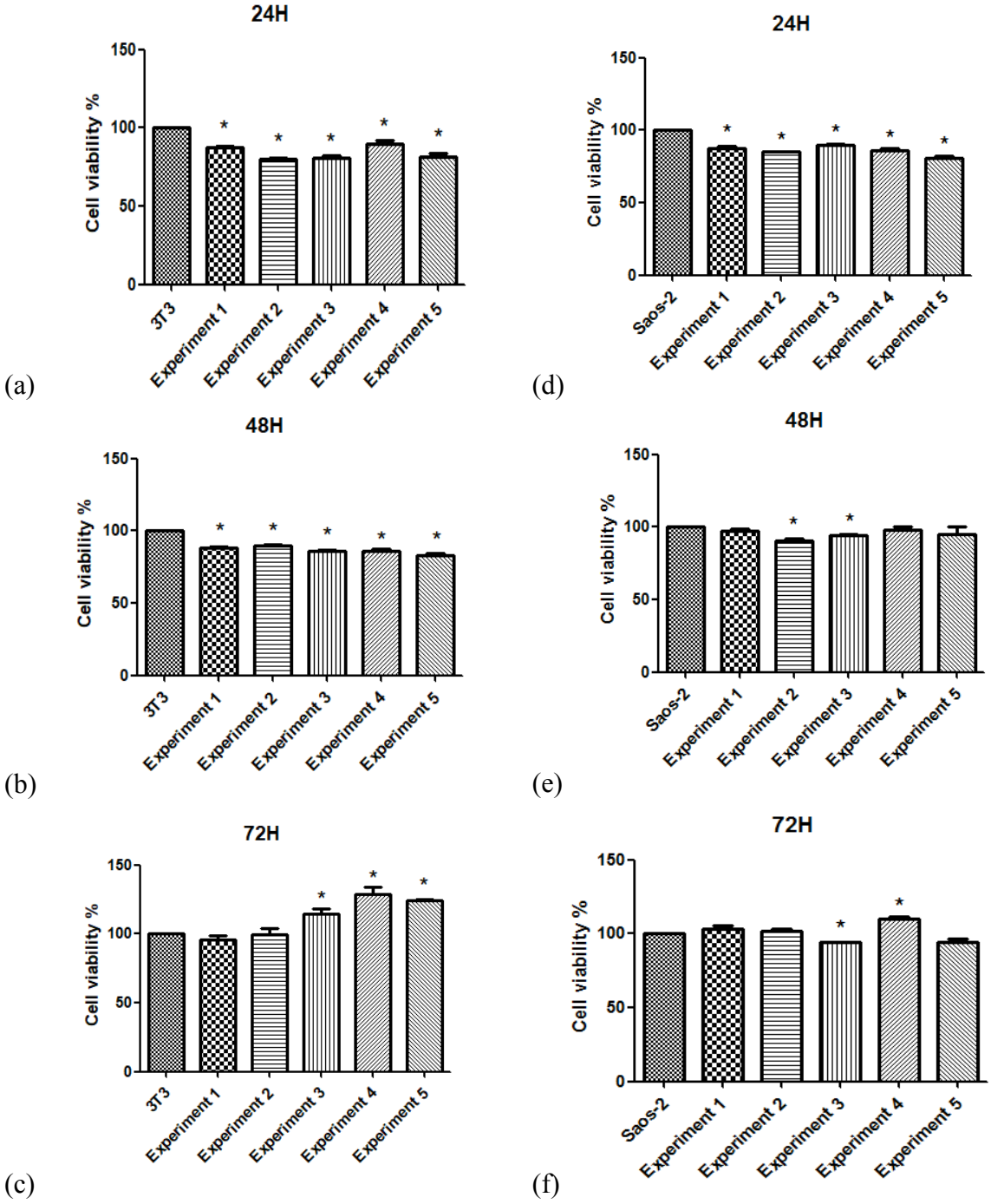

Figure 6.32. MTT Proliferation Assay results and cell viability of all samples from Experiment 1 to Experiment 5 after 24, 48 and 72 hours of cell culture: (a) 24 hours of 3T3 cell, (b) 48 hours of 3T3 cell, (c) 72 hours of 3T3 cell, (d) 24 hours of Saos-2, (e) 48 hours of Saos-2, (f) 72 hours of Saos-2, * $P<0.05$ indicates the statistical significance.

It can be seen in Figure 6.32.d, Figure 6.32.e and Figure 6.32.f, there is no cytotoxicity of the samples for Saos-2 and all samples are biocompatible for 72 hours. At 24 hours after exposure, the results for cell viability on all samples from Experiment 1 to Experiment 5 are statistically significant for all samples (*P<0.05), however there is no cell proliferation any of them for 24 hours. It can be a result of the adaptation period. At 48 hours and 72 hours after exposure, there is seen that cell proliferation increases as shown in Figure 6.32.e and Figure 6.32.f. When it comes to 72 hours after exposure, Figure 6.32.f indicates that cell proliferation occurs in Experiment 4 with statistically, *P<0.05. It can be said that Experiment 4 is more biocompatible and cytocompatible compared to the others for 72 hours.

6.4.2. Cell Attachment

Cell adhesion and spreading on the samples are studied in SEM as shown in Figure 6.33. In vitro cell attachment is important for the biocompatibility of the samples and the behavior of cells on the samples. Cell moves on the nanofiber scaffolds or when the samples start to biodegrade, cell can tend to move into the fibers.

According to the results for 3T3 cells of MTT Cell Proliferation assay in Figure 6.32, Experiment 3 and 5 are selected for SEM because they are more biocompatible and cytocompatible compared to Experiment 1 and 2 for 72 hours.

As shown in Figure 6.33, in vitro cell attachment on Experiment 3 is clearly visible. It is seen that cell spreading on the sample of Experiment 3 has increased over time compared with Figure 6.33.e to Figure 6.33.a.

Figure 6.34 indicates that cell attachment on Experiment 5 is visible. At the end of 24 hours, the cells have been attached but have not been spread too much as shown in Figure 6.34.a, whereas at the end of 72 hours it is observed that the cell has begun to spread on the scaffold by attaching to the nanofibers as shown in Figure 6.34.e.

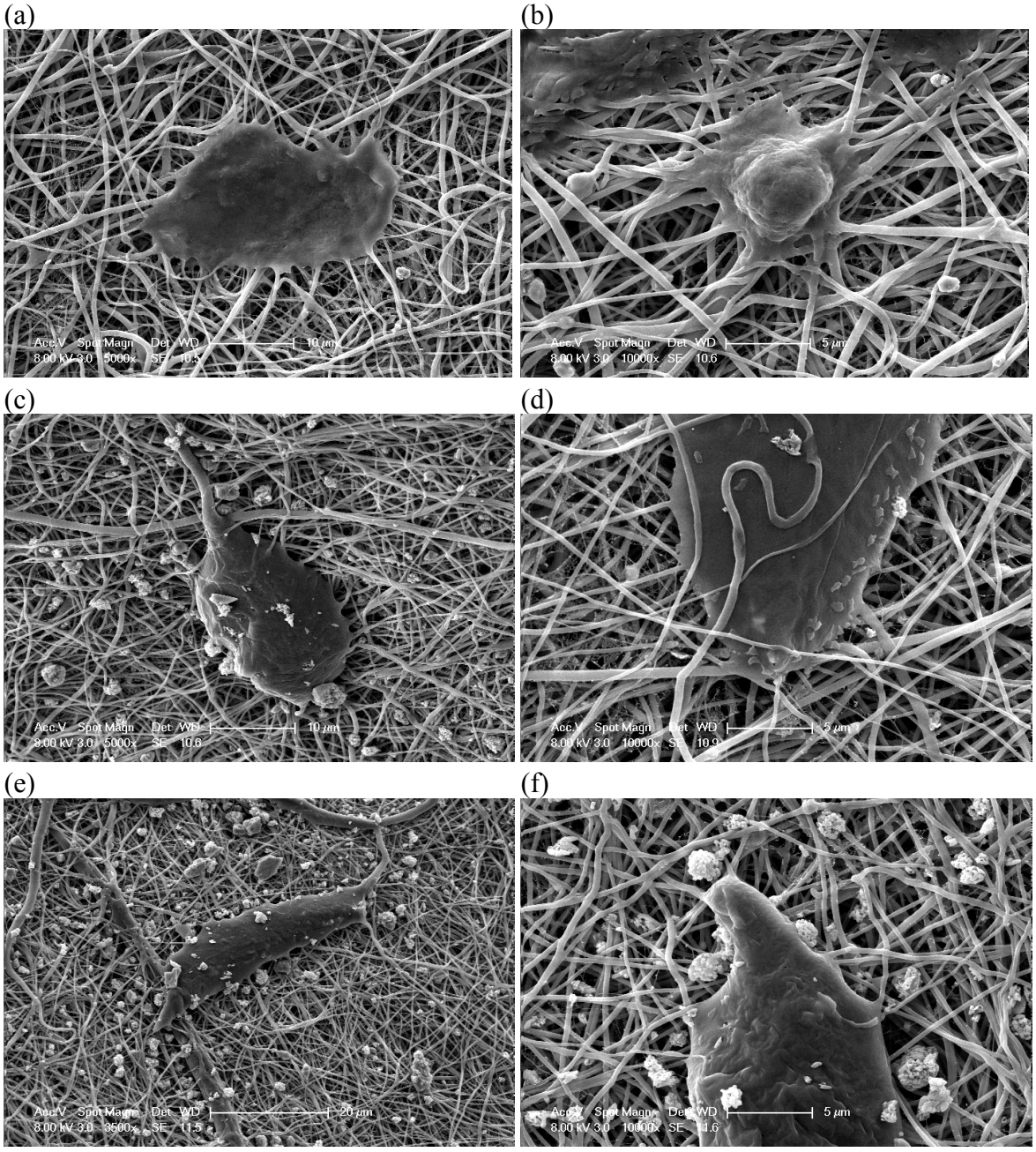

Figure 6.33. SEM images of cell attachment on nanofibers of Experiment 3 after 24, 48 and 72 hours of cell culture: (a-b) 24 hours, (c-d) 48 hours, (e-f) 72 hours.

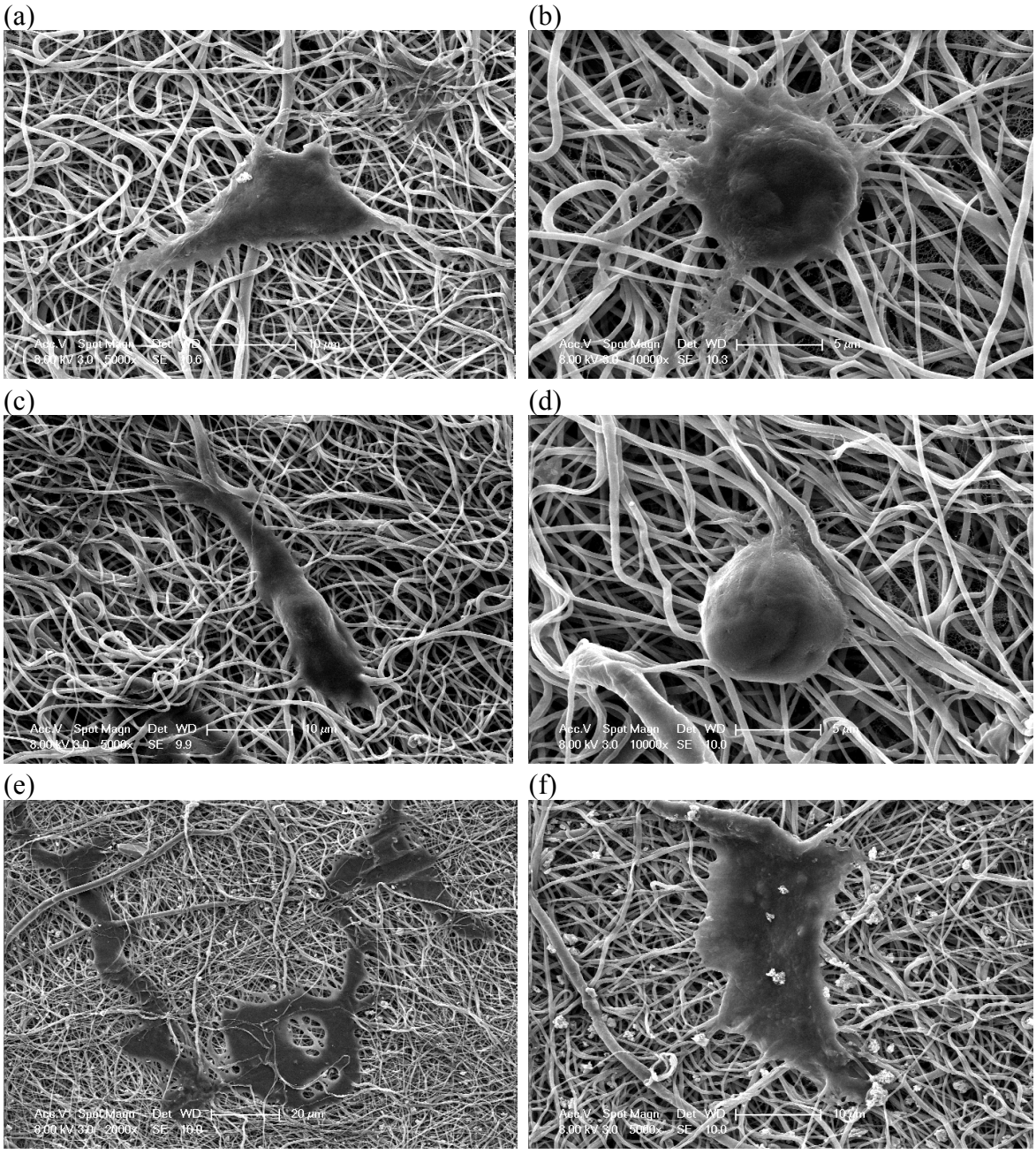

Figure 6.34. SEM images of cell attachment on nanofibers of Experiment 5 after 24, 48 and 72 hours of cell culture: (a-b) 24 hours, (c-d) 48 hours, (e-f) 72 hours.

7. CONCLUSION

In this thesis, Polycaprolactone (PCL) / Bovine Gelatin (GE) / Bovine Hydroxyapatite (BHA) electrospun nanofibrous scaffolds are manufactured for optimal bone tissue regeneration applications by electrospinning.

The experimental setup is to examine the effect of Polycaprolactone (PCL) / Bovine Gelatin (GE) / Bovine Hydroxyapatite (BHA) in the selected non-hazardous solvent system (acetic acid and formic acid) on physical, morphological, chemical, mechanical, and biological properties of nanofiber scaffolds.

Physical properties of nanofiber scaffolds are recorded by measuring density, viscosity, surface tension and electrical conductivity. Morphological analyses of nanofiber scaffolds are studied in SEM. Chemical bonds of the nanofiber scaffolds are analyzed by FTIR. Mechanical properties of the scaffolds are determined by mechanical tensile test. Biological properties of nanofiber scaffolds such as cell viability and attachment are determined by MTT Proliferation Assay and SEM Protocol.

In Experiment 1, 2 and 3, by controlling BHA concentration in the polymer solution, its effect of the change on the nanofibers is examined. In Experiment 1, 4 and 5, by controlling GE concentration in the polymer solution its effect of the change on the nanofibers is examined.

It is observed that the feed rate of the process by controlling the BHA concentration (0.5%, 1%, 2% w/w in PCL / GE / BHA) is needed to be increased with the increase of the concentration of BHA in the solution. The increase of the concentration of BHA in the solution increases the electrical conductivity of the solution that’s why the applied voltage of the process by controlling the BHA concentration is needed to be decreased with the increase of the concentration of BHA in the solution.

In terms of the morphological analysis (SEM) of the nanofiber scaffolds, it is observed that the diameter of the nanofiber scaffolds produced by controlling the BHA concentration (0.5%, 1%, 2% w/w in PCL / GE / BHA) increases with the increase of the concentration of BHA in the solution, 119 ± 31 nm, 149 ± 44 nm and 306 ± 68 nm respectively. In terms of the mechanical analysis (tensile testing) of the nanofiber scaffolds, it is observed that ultimate tensile strength (UTS) of the nanofiber scaffolds produced by controlling the BHA concentration (0.5%, 1%, 2% w/w in PCL / GE / BHA) increases with the increase of the concentration of BHA in the solution, 9.1 ± 0.6 MPa, 15.7 ± 1.4 MPa and 15.8 ± 5.0 MPa respectively.

In terms of the morphological analysis (SEM) of the nanofiber scaffolds, it is observed that the diameter of the nanofiber scaffolds produced by controlling the GE concentration such as 0.5%, 1%, 1.5% w/w in PCL/GE/BHA are 241 ± 55 nm, 119 ± 31 nm and 384 ± 84 nm respectively. In terms of the mechanical analysis (tensile testing) of the nanofiber scaffolds, it is observed that ultimate tensile strength (UTS) of the nanofiber scaffolds produced by the GE concentration such as 0.5%, 1%, 1.5% w/w in PCL/GE/BHA are 30.9 ± 16.0 MPa, 9.1 ± 0.6 MPa and 15.8 ± 2.2 MPa respectively.

In terms of the biological analysis, cell attachment on the samples is observed in SEM. It is observed at the end of 72 hours that cell spreading on the samples has increased over time. There is no cytotoxicity effect observed by MTT test for 72 hours. As a result of cell proliferation and viability analysis, there are biocompatible samples observed compatible with human osteoblast-like cells and mouse fibroblast cells with statistically significant results.

REFERENCES

1. Edwards, S. A., *The Nanotech Pioneers*, Wiley-VCH Verlag GmbH & Co. KGaA, Weinheim, Germany, 2006.

2. Feynman, R. P., "There's Plenty of Room at the Bottom", *Caltech Engineering and Science*, Vol. 23, No. 5, pp. 22-36, 1960.

3. Taniguchi, N., "On the Basic Concept of 'Nano-Technology'", Proceedings of the International Conference on Production Engineering Tokyo, Part II, *Japan Society of Precision Engineering*, 1974.

4. Place, E.S., J. H. George, C. K. Williams and M. M. Stevens, "Synthetic polymer scaffolds for tissue engineering", *Chemical Society Reviews*, Vol. 38, No.4, pp.1139-1151, 2009.

5. Ramakrishna, S., *An introduction to electrospinning and nanofibers*, Hackensack, NJ, World Scientific, 2005.

6. "Electrospinning to Produce Polymer Based Nanofibers", Inovenso, July 2011, http://inovenso.com/wp-content/uploads/2011/07/nanofiber_production_Electrospinning.jpg, accessed at February 2018.

7. Chew, S. Y., R. Mi, A. Hoke and K.W. Leong, "Aligned Protein-Polymer Composite Fibers Enhance Nerve Regeneration: A Potential Tissue-Engineering Platform", *Advanced Functional Materials*, Vol. 17, No. 8, pp. 1288–1296, 2007.

8. Kim Y-T., V.K. Haftel, S. Kumar and R.V. Bellamkonda, "The role of aligned polymer fiber based constructs in the bridging of long peripheral nerve gaps", *Biomaterials*, Vol. 29, No. 21, pp. 3117–3127, 2008.

9. Noh, H. K., S. W. Lee, J. -M. Kim, J. -E. Oh, K. -H. Kim, C. -P. Chung, S. -C. Choi, W. H. Park and B-M. Min, "Electrospinning of chitin nanofibers: Degradation behavior and cellular response to normal human keratinocytes and fibroblasts", *Biomaterials*, Vol. 27, No. 21,2006, pp. 3934–3944, 2006.

10. Powell, H. M. and S.T. Boyce, "Fiber density of electrospun gelatin scaffolds regulates morphogenesis of dermal-epidermal skin substitutes", *Journal of Biomedical Materials Research Part A*, Vol. 84, No. 4, pp. 1078–1086, 2008.

11. Peng, H. –S., X. Liu, R. Wang, F. Jia, L. Dong and Q. Wang, "Emerging Nanostructured Materials for Musculoskeletal Tissue Engineering", *Journal of Materials Chemistry B,* Vol. 2, No. 38, pp. 6435-6461, 2014.

12. Vroman, I. and L. Tighzert, "Biodegradable Polymers", *Materials*, Vol. 2, No. 2, pp.307–344, 2009.

13. Goodson, J. M., D. Holborow, R. L. Dunn, P. Hogan and L. Dunham, "Monolithic tetracycline containing fibers for controlled delivery to periodontal pockets", *Journal of Periodontol*, Vol. 54, pp. 575-579, 1983.

14. Nakamura, T., Y. Shimizu, T. Matsui, N. Okumura, S. H. Hyon, and K. Nishiya, "A novel bioabsorbable monofilament surgical suture made from (caprolacton, L Lactide) copolymer", *Degradation Phenomena on Polymeric Biomaterials*, Springer: Berlin, pp. 153-162, 1992.

15. Tomihata, K., M. Suzuki, T. Oka and Y. Ikada, "A new resorbable monofilament suture", *Polymer Degrad.Stability*, Vol.59, pp. 13-18, 1998.

16. Hutmacher, D. W., T. Schantz, I. Zein, K. W. Ng, S. W. Teoh and K. C. Tan, "Mechanical properties and cell cultural response of polycaprolactone scaffolds designed and fabricated via fused deposition modeling", *Journal of Biomed Material Research*, Vol. 55, pp. 203-216, 2001.

17. Bezwada, R. S., D. D. Jamiolkowski, I. Y. Lee, V. Agarwal, J. Persivale, M. Erneta, S. Trenka- Benthin, J. Suryadevara, A. Yang and S. Liu, "Monocryl suture, a new ultra-pliable absorbable monofilament suture", *Biomaterials*, Vol. 16, pp. 1141-1148, 1995.

18. Hayash, T., "Biodegradable polymers for biomedical uses", *Progress in Polymer Science*, Vol.19, pp. 663-702, 1994.

19. "Polycaprolactone 440752", Sigma-Aldrich, 2018, https://www.sigmaaldrich.com/catalog/product/aldrich/440752?lang=en&region=TR, accessed at March 2018.

20. "Polycaprolactone 440744", Sigma-Aldrich, 2018, https://www.sigmaaldrich.com/catalog/product/aldrich/440744?lang=en&region=TR, accessed at March 2018.

21. Corradini, E., L. H. C. Mattoso, C. G. F. Guedes and D. S. Rosa, "Mechanical, thermal and morphological properties of poly(e-caprolactone)/zein blends", *Polymer Advance Technology*, Vol. 15, No. 6, pp. 340-345, 2004.

22. Hubbell, D. S. and Cooper, S. L., "The physical properties and morphology of poly-e-caprolactone polymer blends", *Journal of Applied Polymer Science*, Vol. 21, pp. 3035-3061, 1977.

23. Carothers, W. H., G. L. Dorough and F. J. Van Natta, "Polymerization and ring formation reversible polymerization of six-membered cyclic esters", *Journal of American Chemical Society*, Vol. 54, No. 5, pp. 761–72, 1932.

24. Bano, K., R. Pandey, J. E. Fatima and Roohi, "New advancements of bioplastics in medical applications", *International Journal of Pharmaceutical Sciences Research*, Vol. 9, No. 2, pp. 402-416, 2018.

25. Lee, K. H., H. Y. Kim, M. S. Khil, Y. M. Ra and D. R. Lee, "Characterization of nano-structured poly (epsilon caprolactone) non-woven mats via electro spinning", *Polymer*, Vol. 44, No. 4, pp. 1287–1294, 2003.

26. Yang, F., J. G. C. Wolke and J. A. Jansen, "Biomimetic calcium phosphate coating on electrospun poly (e-caprolactone) scaffolds for bone tissue engineering", *Chemical Engineering Journal*, Vol. 137, No. 1, pp. 154–161, 2008.

27. Huang, Y., S. Agarwal and J. Lannutti, "Materials selection and residual solvent retention in biodegradable electrospun fibers", *Journal of Applied Polymer Science*, Vol. 107, No. 3, pp. 1547–1554, 2008.

28. Pal, J., S. Sharma, S. Sanwaria, R. Kulshreshtha, B. Nandan and R. K. Srivastava, "Conducive 3D porous mesh of poly(ε-caprolactone) made via emulsion electrospinning", *Polymer*, Vol. 55, No.16, pp. 3970–3979, 2014.

29. Erisken, C., D. M. Kalyon and H. Wang, "Functionally graded electrospun polycaprolactone and β-tricalcium phosphate nanocomposites for tissue engineering applications", *Biomaterials*, Vol. 29, No. 30, pp. 4065-4073, 2008.

30. Lawson, C., A. Stanishevsky, M. Sivan, P. Pokorny and D. Lukáš, "Rapid fabrication of poly(ε- caprolactone) nanofibers using needleless alternating current electrospinning", *Journal of Applied Polymer Science*, Vol. 133, No. 13, 43232, 2016.

31. Ferreira, J. L., S. Gomes, C. Henriques, J. P. Borges and J. C. Silva, "Electrospinning polycaprolac- tone dissolved in glacial acetic acid: fiber production, nonwoven characterization, and in vitro evaluation", *Journal of Applied Polymer Science*, Vol. 131, No. 22, 41086, 2014.

32. Chakrapani, V. Y., A. Gnanamani, V. R. Giridev, M. Madhusoothanan and G. Sekaran, "Electrospinning of type I collagen and PCL nanofibers using acetic acid", *Journal of Applied Polymer Science*, Vol. 125, No. 4, pp. 3221–3227, 2012.

33. Da Silva, G. R., T. H. Lima, R. L. Oréfice, G. M. Fernandes-Cunha, A. Silva-Cunha, M. Zhao and F. Behar-Cohen, "In vitro and in vivo ocular biocompatibility of electrospun poly(ε-caprolactone) nanofibers", *European Journal of Pharmaceutical Sciences*, Vol. 73, pp. 9–19, 2015.

34. Bosworth, L. A. and S. Downes, "Acetone, a Sustainable Solvent for Electrospinning Poly (ε-Caprolactone) Fibers: Effect of Varying Parameters and Solution Concentrations on Fibre Diameter", *Journal of Polymers and the Environment*, Vol. 20, No. 3, pp. 879-886, 2012.

35. Díaz, E., I. Sandonis and M. B. Valle, "In Vitro Degradation of Poly(caprolactone)/nHA Composites", *Journal of Nanomaterials*, Vol. 2014, pp. 185-185, 2014.

36. An, J., C. K. Chua, K. F. Leong, C. -H. Chen, and J. -P. Chen, "Solvent-free fabrication of three dimensionally aligned polycaprolactone microfibers for engineering of anisotropic tissues", *Biomedical Microdevices*, Vol. 14, No. 5, pp. 863–872, 2012.

37. Shao, H. –J., C. –C. Ho, Y. –T. Lee, C. –S. Chen, J. H. Wang and T. -H. Young, "Chondrogenesis of human bone marrow mesenchymal cells by transforming growth factors β1 through cell shape changes on controlled biomaterials", *Journal of Biomedical Materials Research*, Vol. 100A, No. 12, pp. 3344-3352, 2012.

38. Schrieber, R. and H. Gareis, *Gelatine handbook: Theory and industrial practice*, Weinheim, Wiley-VCH, 2007.

39. Rollason, G., J. E. Davies and M. V. Sefton, "Preliminary report on cell culture on a thermally reversible copolymer", *Biomaterials*, Vol. 14, No. 2, pp. 153–155, 1993.

40. Schild, H.G., M. Muthukumar and D.A. Tirrell, "Cononsolvency in mixed aqueous solutions of poly(N-isopropylacrylamide)", *Macromolecules*, Vol. 24, No. 4, pp. 948–952, 1991.

41. Wang, H., O. C. Boerman, K. Sariibrahimoglu, Y. Li, J. A. Jansen and S. C. G Leeuwenburgh, "Comparison of micro- vs. nanostructured colloidal gelatin gels for sustained delivery of osteogenic proteins: Bone morphogenetic protein-2 and alkaline phosphatase", *Biomaterials*, Vol. 33, pp. 8695–8703, 2012.

42. Binulal, N. S., A. Natarajan, D. Menon, V. K. Bhaskaran, U. Mony and S. V. Nair, "PCL-gelatin composite nanofibers electrospun using diluted acetic acid-ethyl acetate solvent system for stem cell-based bone tissue engineering", Journal of Biomaterial Science Polymer Edition, Vol. 25, pp. 325–340, 2014.

43. Righi, T. M., R. S. Almeida and M. A. d'Ávila, "Electrospinning of gelatin/PEO blends: influence of process parameters in the nanofiber properties", *Macromolecular Symposia*, Vol. 319, No. 1, pp. 230–234, 2012.

44. Smith, E. L., R. L. Hill, I. R. Lehman, R. J. Lefkowitz, P. Handler and A. White, *Principles of Biochemistry: Mammalian Biochemistry*, McGraw-Hill Book Company, 7th edition, New York, 1983.

45. Hench, L. L., "The Skeletal System", *Biomaterials, Artificial Organs and Tissue Engineering*, Hench, L. L. and Jones, J. R., (Ed.), Woodhead Publishing Ltd., England, pp. 79-89, 2005.

46. Ipekoglu, M., Effects of Calcination and Particle Size on the Sintering of Natural Hydroxyapatite, M.S. Thesis, Bogazici University, 2004.

47. Gokbayrak, H., Production of Hydroxyapatite Ceramics, M.S. Thesis, Bogazici University, 1996.

48. Ipekoglu, M., Production of Antibacterial Hydroxyapatite, Ph.D. Thesis, Bogazici University, 2011.

49. ICH, "Q3C Guideline for Residual Solvents (R6)", The International Council for Harmonisation of Technical Requirements for Pharmaceuticals for Human Use (ICH), 20 October 2016, http://www.ich.org/fileadmin/Public_Web_Site/ICH_Products/Guidelines/Quality/QC/Q3C__R6___Step_4.pdf, accessed at March 2018.

50. Luo, C. J., E. Stride and M. Edirisinghe, "Mapping the influence of solubility and dielectric constant on electrospinning polycaprolactone solutions", *Macromolecules*, Vol. 45, No. 11, pp. 4669–4680, 2012.

51. Luo, C. J., M. Nangrejo and M. Edirisinghe, "A novel method of selecting solvents for polymer electrospinning", *Polymer*, Vol. 51, pp. 1654−1662, 2010.

52. Scheffler, R., N. Bell and W. Sigmund, "Electrospun Teflon AF fibers for superhydrophobic membranes", *Journal of Materials Research*, Vol. 25, No. 8, pp. 1595−1600, 2010.

53. Human Metabolome Database, "Showing metabocard for Acetic acid (HMDB0000042)", 2018, http://www.hmdb.ca/metabolites/HMDB0000042, accessed at March 2018.

54. National Cancer Institute Thesaurus, "Acetic Acid (Code C61623)", https://ncit.nci.nih.gov/ncitbrowser/ConceptReport.jsp?dictionary=NCI_Thesaurus&ns=NCI_Thesaurus&code=C61623, 2018, accessed at March 2018.

55. "NIOSH Pocket Guide to Chemical Hazards". Department of Health & Human Services, Centers for Disease Prevention & Control, National Institute for Occupational Safety & Health, DHHS (NIOSH) Publication No. 2010-168, 2010, http://www.cdc.gov/niosh/npg/, accessed at March 2018.

56. “EPA/Office of Pollution prevention and toxics; High production Volume (HPV) Challenge program's Robust summaries and Test Plans”, December 2001, http://www.epa.gov/hpv/pubs/hpvrstp.htm, accessed at March 2018.

57. Cooley, J. F., Improved methods of and apparatus for electrically separating the relatively volatile liquid component from the component of relatively fixed substances of composite fluids, UK Pat. 6385, 1900.

58. Morton, W. J., Method of dispersing fluids, US Pat. 705691, 1902.

59. Formhals, A., Production of artificial fibers, US Pat. 2077373, 1937.

60. Hagiwara, K., Process for manufacturing artificial silk, CA Pat 293884, 1929.

61. Formhals, A., Vorrichtung zur Herstellung von Fasern und Faserbaendern aus faserbildenden Loesungen mittels Hochspannungselektrizitaet, DE 746708 C, 1944.

62. How, T.V., Synthetic vascular grafts, and methods of manufacturing such grafts, US Pat. 4552707, 1985.

63. Groitzsch, D. and E. Fahrbach, Microporous multilayer non-woven material for medical applications, US Pat 4618524, 1986.

64. Formhals, A., Process and apparatus for preparing artificial threads, US Pat. 1975504, 1934.

65. Formhals, A., Production of artificial fibers, US Pat. 2077373, 1937.

66. Formhals, A., Artificial fiber construction, US Pat. 2109333, 1938.

67. Ramakrishna, S., K. Fujihara, W. E. Teo, T. C. Lim and Z. Ma, *An Introduction To Electrospinning And Nanofibers*, World Scientific Publishing Company, 2005.

68. Haupt, K. and S.M.A. Bueno, "Affinity Separation: Affinity Membranes", *Reference Module in Chemistry, Molecular Sciences and Chemical Engineering*, 2015.

69. Chong, L. H., M. M. Lim and N. Sultana, "Fabrication and Evaluation of Polycaprolactone/Gelatin-Based Electrospun Nanofibers with Antibacterial Properties", *Journal of Nanomaterials*, Vol. 2015, pp.1-8, 2015.

70. Yao, R., J. He, G. Meng, B. Jiang and F. Wu, "Electrospun PCL/Gelatin composite fibrous scaffolds: mechanical properties and cellular responses", *Journal of Biomaterials Science*, Polymer Edition, Vol. 27, No. 9, pp. 824–838, 2016.

71. Rong, D., P. Chen, Y. Yang, Q. Li, W. Wan, X. Fang and J. Ouyang, "Fabrication of Gelatin/PCL Electrospun Fiber Mat with Bone Powder and the Study of Its Biocompatibility", *Journal of Functional Biomaterials*, Vol. 7, No. 1, pp. 1-6, 2016.

72. Ramakrishna, S., K. Fujihara, W. E. Teo, T. C. Lim, Z. Ma, *An Introduction To Electrospinning And Nanofibers*, World Scientific Publishing Company, 2005.

73. Kameoka, J., R. Orth, Y. Yang, D. Czaplewski, R. Mathers, G. Coates and H. G. Craighead, "A scanning tip electrospinning source for deposition of oriented nanofibres", *Nanotechnology*, Vol. 14, No.10, pp. 1124-1129, 2003.

74. Megelski, S., J. S. Stephens, D. B. Chase and J. F Rabolt, "Micro- and nanostructured surface morphologyon electrospun polymer fibers", *Macromolecules*, Vol. 35, No. 22, pp. 8456-8466, 2002.

75. Fong, H., I. Chun and D. H. Reneker, "Beaded nanofibers formed during electrospinning", *Polymer*, Vol. 40, No.16, pp. 4585-4592, 1999.

76. Zong, X., K. Kim, D. Fang, S. Ran, B. S. Hsiao and B. Chu, "Structure and process relationship of electrospun bioabsorbable nanofiber membranes", *Polymer*, Vol. 43, No.16, pp. 4403- 4412, 2002.

77. Chakrapani, V. Y., A. Gnanamani, V. R. Giridev, M. Madhusoothanan and G. Sekaran, “Electrospinning of type I collagen and PCL nanofibers using acetic acid”, *Journal of Applied Polymer Science*, Vol. 125, No. 4, pp. 3221–3227, 2012.

78. Zhang, Q., S. Lv, J. Lu, S. Jiang and L. Lin, “Characterization of polycaprolactone/collagen fibrous scaffolds by electrospinning and their bioactivity”, International Journal of Biological Macromolecules, Vol. 76, pp. 94–101, 2015.

79. Mit-uppatham, C., M. Nithitanakul and P. Supaphol, “Ultrafme Electrospun Polyarnide-6 Fibers: Effect of Solution Conditions on Morphology and Average Fiber Diameter”, *Macromolecules Chemistry and Physics*, Vol. 205, pp. 2327-2338, 2004.

80. Wang, C., C. –H. Hsu and J. -H.Lin, “Scaling Laws in Electrospinning of Polystyrene Solutions”, *Macromolecules*, Vol. 39, No. 22, pp. 7662-7672, 2006.

81. Sukigara, S., M. Gandhi, J. Ayutsede, M. Micklus and F. Ko, “Regeneration Of Bombyx Mori Silk By Electrospinning—Part 1: Processing Parameters and Geometric Properties”, *Polymer*, Vol. 44, No. 19, pp. 5721–5727, 2003.

82. Fong, H., I. Chun and D. H. Reneker, “Beaded Nanofibers Formed During Electrospinning”, *Polymer*, Vol. 40, No. 16, pp. 4585–4592, 1999.

83. Mckee, M. G., G. L.Wilkes, R. H. Colby and T. E. Long, “Correlations of solution rheology with electrospun fiber formation of linear and branched polyesters”, *Macromolecules*, Vol. 37, No.5, pp. 1760–1767, 2004.

84. Tan, S. H., R. Inai, M. Kotaki and S. Ramakrishna, “Systematic Parameter Study for Ultra-Fine Fiber Fabrication Via Electrospinning Process”, *Polymer*, Vol. 46, No.16, pp. 6128-6134, 2005.

85. Yalcinkaya, F., B. Yalcinkaya and O. Jirsak, "Influence of Salts on Electrospinning of Aqueous and Nonaqueous Polymer Solutions", *Journal of Nanomaterials*, Vol. 2015, No. 5, pp. 12-12, 2015.

86. Spurk, J. H. and N. Aksel, *Fluid Mechanics*, Springer, Berlin Heidelberg, 2nd edition, 2008.

87. Kundu, P. K., I. M. Cohen and H. Hu, *Fluid Mechanics*, Elsevier Academic Press, Amsterdam, Heidelberg, 2006.

88. Yang, Q., Z. Li, Y. Hong, Y. Zhao, S. Qiu, C. Wang and Y. Wei, "Influence Of Solvents on the Formation Of Ultrathin Uniform Poly(Vinyl Pyrrolidone) Nanofibers With Electrospinning", *Journal of Polymer Science Part B: Polymer Physics*, Vol. 42, No. 20, pp. 3721–3726, 2004.

89. Rayleigh, J. W. S., *Scientific Papers: 1887 – 1892*, Primary Source Edition, University Press, 1902.

90. Coles, S.R. and A. Wooldridge, "Optimising Solutions for Electrospinning", *Electrospinning: Principles, Practice and Possibilities*, The Royal Society of Chemistry, pp. 57-70, 2015.

91. Yuan, X., Y. Zhang, C. Dong and J. Sheng, "Morphology of ultrafine polysulfone fibers prepared by electrospinning", *Polymer International*, Vol. 53, No. 11, pp.1704–1710, 2004.

92. Druesedow, C. J., C. Batur, M. Cakmak and B. Yalcin, "Pressure control system for electrospinning process", *Polymer Engineering and Science*, Vol. 50, No.4, pp. 800–810, 2010.

93. Doshi, J. and D. H. J. Reneker, "Electrospinning Process and Applications of Electrospun Fibers", *Journal of Electrostatics*, Vol. 35, pp. 151-160, 1995.

94. Demir, M. M., I. Yilgor, E. Yilgor and B. Erman, "Electrospinning of polyurethane fibers", *Polymer*, Vol. 43, No. 11, pp. 3303–3309, 2002.

95. Coles, S. R., D. K. Jacobs, J. O. Meredith, G. C. Barker, A. J. Clark, K. Kirwan, J. Stanger and N. Tucker, "A design of experiments (DoE) approach to material properties optimization of electrospun nanofibers", *Journal of Applied Polymer Science,* Vol. 117, No.4, pp. 2251-2257, 2010.

96. Reneker, D. H. and I. Chun, "Nanometre diameter fibres of polymer, produced by electrospinning", *Nanotechnology*, Vol. 7, No. 3, pp. 216–223, 1996.

97. Buchko, C. J., L. C. Chen, Y. Shen, D. C. Martin, "Processing and microstructural characterization of porous biocompatible protein polymer thin films", *Polymer*, Vol. 40, No. 26, pp. 7397–7407, 1999.

98. Deitzel, J. M., J. Kleinmeyer, D. Harris and N. C. Beck Tan, "The effect of processing variables on the morphology of electrospun nanofibers and textiles", *Polymer*, Vol. 42, No. 1, pp. 261–272, 2001.

99. Persano, L., A. Camposeo, C. Tekmen and D. Pisignano, "Industrial Upscaling of Electrospinning and applications of polymer nanofibers: A review", *Macromolecular Materials and Engineering*, Vol. 298, pp. 504-520, 2013.

100. Zheng, J., A. He, J. Li, J. Xu and C.C. Han, "Studies On The Controlled Morphology And Wettability Of UHMWPE Surfaces By Electrospinning Or Electrospraying", *Polymer*, Vol. 47, pp. 7095- 7102, 2006.

101. Thompson, C. J., G. G. Chase, A. L. Yarin and D. H. Reneker, "Effects Of Parameters On Nanofiber Diameter Determined From Electrospinning Model", *Polymer*, Vol. 48, No. 23, pp. 6913-6922, 2007.

102. Heikkila, P. and A. Harlin, “Parameter Study Of Electrospinning Of Polyamide-6”, *European Polymer Journal*, Vol. 44, No. 10, pp. 3067-3079, 2008.

103. Macossay, J., A. Marruffo,R. Rincon, T. Eubanks and A. Kuang, “Effect Of Needle Diameter On Nanofiber Diameter And Thermal Properties Of Electrospun Poly(Methyl Methacrylate)”, *Polymers for Advanced Technologies*, Vol.18, pp.180–183, 2007.

104. Casper, C. L., J. S. Stephens, N. G. Tassi, D. B. Chase and J. F. Rabolt, “Controlling surface morphology of electrospun polystyrene fibers: Effect of humidity and molecular weight in the electrospinning process”, *Macromolecules*, Vol. 37, No. 2, pp. 573–578, 2004.

105. Coates, J., *Interpretation of Infrared Spectra, a Practical Approach*, Encyclopedia of Analytical Chemistry, R. A. Meyers, Ed., John Wiley & Sons Ltd, Chichester, pp. 10815-10837, 2000.

106. Rather, H. A., R. Thakore, R. Singh, D. Jhala, S. Singh and R. Vasita, “Antioxidative Study of Cerium Oxide Nanoparticle Functionalised PCL-Gelatin Electrospun Fibers for Wound Healing Application”, *Bioactive Materials*, Vol. 3, No. 2, pp. 201-211, 2018.

107. Callister, W. D. and D. G. Rethwisch, *Fundamentals of Materials Science and Engineering: An Integrated Approach*, Hoboken, NJ: John Wiley & Sons, 2008.

108. ASTM Standard D 638, “Standard Test Method for Tensile Properties of Plastics”, https://www.astm.org/Standards/D638.htm, accessed at March 2018.

109. Huang, Z. M., Y. Z. Zhang, S. Ramakrishna and C. T. Lim, “Electrospinning and mechanical characterization of gelatin nanofibers”, *Polymer*, Vol. 45, pp. 5361–5368, 2004.

110. Radakovic, D., J. Reboredo, M. Helm, T. Weigel, S. Schürlein, E. Kupczyk, R. G. Leyh, H. Walles and J. Hansmann, "A multilayered electrospun graft as vascular access for hemodialysis", *PLoS ONE*, Vol.12, No. 10, 2017.

111. Wang, N., K. Burugapalli, S. Wijesuriya, M. Y. Far, W. Song, F. Moussy, Y. Zheng, Y. Ma, Z. Wu and K. Li, "Electrospun Polyurethane-Core and Gelatin-Shell Coaxial Fibre Coatings for Miniature Implantable Biosensors", *Biofabrication*, Vol. 6, No. 1, 2013.

112. Oroujzadeh, M., S. Mehdipour-Ataei and M. Esfandeh, "Microphase separated sepiolite-based nanocomposite blends of fully sulfonated poly(ether ketone)/non-sulfonated poly(ether sulfone) as proton exchange membranes from dual electrospun mats", *RSC Advances*, Vol. 5, No. 88, pp. 72075-72083, 2015.

113. ASTM Standard D 882, "Standard Test Method for Tensile Properties of Thin Plastic Sheeting", https://www.astm.org/Standards/D882, accessed at March 2018.

114. Mosmann, T., "Rapid colorimetric assay for cellular growth and survival: application to proliferation and cytotoxicity assays", *The Journal of Immunological Methods*, Vol.65, pp. 55-63, 1983.

115. Pautke, C., M. Schieker, T. Tischer, A. Kolk, P. Neth, W. Mutschler and S. Milz, "Characterization of Osteosarcoma Cell Lines MG-63, Saos-2 and U-2 OS in Comparison to Human Osteoblasts", *Anticancer Research*, Vol. 24, pp. 3743-3748, 2004.